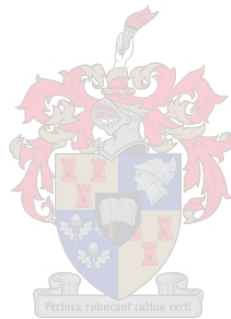


Effect of the Nearshore Profile on Wave Overtopping at a Recurve Seawall

by
F.H. de Bondt



*Thesis presented in fulfilment of the requirements for the degree of
Master of Engineering in the Faculty of Civil Engineering at Stellenbosch
University*

Supervisor: Prof. J.S. Schoonees

March 2020

Declaration

By submitting this thesis electronically, I declare that the entirety of the work contained therein is my own, original work, that I am the sole author thereof (save to the extent explicitly otherwise stated), that reproduction and publication thereof by Stellenbosch University will not infringe any third party rights and that I have not previously in its entirety or in part submitted it for obtaining any qualification.

Date: March 2020

Abstract

Infrastructure located close to the shoreline is generally highly valuable, even though it is often exposed to significant flood risk. With an increased wave attack caused by climate change and the consequent rise in sea levels, the risk of economic damage or loss of life due to violent overtopping is constantly increasing. Reduction of overtopping at coastal defensive structures is therefore crucial in terms of the design, management and adaptation of coastal structures, especially when existing coastal defensive structures are evaluated for suitability in future conditions. In places where space does not allow for the construction of dikes or rubble mound breakwaters, vertical seawalls are often built to decrease the risk of flooding and damage to landward infrastructure, assets and injury to people, especially pedestrians. As some of the existing vertical seawalls are now being exposed to increased wave attack, more sudden, severe overtopping events are taking place which is dangerous to both property and humans. In order to decrease overtopping volumes, often vertical defensive structures incorporate a recurve seawall. The recurve shaped overhang reduces overtopping by deflecting water that is forced upwards by the vertical face of the structure, back seaward. By adding a recurve section onto the crest of a vertical seawall, the crest height of the structure can be reduced. Although recurves are often incorporated into seawall design, literature offers limited guidance for the design of such structures. This study, therefore, investigates the effect that the nearshore profile has on the overtopping of an optimised recurve seawall. A secondary objective was to determine the effect that the nearshore profile has on the increase or reduction of the incoming wave height. In order to achieve the objectives, 2D physical modelling tests were performed in a glass wave flume equipped with a piston type wave paddle that is capable of active wave absorption. The tests were performed on four different nearshore profiles, three which were typical to the Southern African coastline, and the other an average beach profile used in preceding studies. The three typical Southern African profiles included a steep, flat and mild nearshore profile. Tests were performed with 3 different water levels and 5 different wave periods, while the seawall design, crest height and wave height were kept constant. Analysis of the findings indicated that the nearshore profile had a significant influence on the overtopping of a recurve seawall. Results show that wave overtopping increases with a decrease in the steepness of the nearshore profile. Consequently, the gentlest nearshore slope led to the highest overtopping volumes of the recurve seawall. However, the mild profile with an offshore berm also produced large overtopping rates, mostly due to colliding reflected and incident waves causing large individual overtopping events. It is recommended that further model tests be conducted on the effect that beach erosion or accretion has on the overtopping of recurve seawalls. Another possible study can be done on the effect of different wave heights on the overtopping of recurve seawalls. The wave forces caused by different wave conditions should also be

investigated, as forces on a structure is a necessary component for the structural design of recurve seawalls.

Opsomming

Infrastruktuur geleë naby die kuslyn is dikwels uiters waardevol, selfs al is daar 'n groot risiko vir oorstromings as gevolg van stygende seevlakke en verhoogde golfoorslag. Met klimaatsverandering wat lei tot verhoogde seevlakke en meer intense storms, gaan kusverdedigingstrukture gebuk onder 'n verhoogde golfaanval en meer kragtige golfoorslag. Hierdeur neem die risiko vir ekonomiese skade en lewensverlies voortdurend toe. Dit is waarom die vermindering van golfoorslag by kusverdedigingstrukture so uiters belangrik is, vanaf die ontwerpfase, tot die bestuur en aanpassing van bestaande strukture vir hulle geskiktheid in toekomstige seetoestande. In plekke waar spasie vir die konstruksie van dyke en rotsgolfbrekers ontbreek, is vertikale seemure dikwels die beste opsie om die risiko van oorstromings en skade aan landwaartse infrastruktuur, bates en menseleuens te verminder. As gevolg van die verhoogde golfaanval word verskeie bestaande vertikale seemure al meer gereeld blootgestel aan skielike, hewige golfoorslaggebeurtenisse wat gevaarlik vir beide eiendom en mense is. Ten einde hierdie groot volumes golfoorslag te verminder, word vertikale seemure dikwels aangepas om op te tree as terugkaatsseemure. Terugkaatsseemure verlaag golfoorslag deur die opstuwende waterkolom, veroorsaak deur die botsing van inkomende golwe en die vertikale deel van die see muur, terug seewaarts te weerkaats as 'n byna-horisontale waterstraal. Alhoewel terugkaats-oorhange dikwels in die ontwerp van seemure ingesluit word, verskaf literatuur beperkte leiding omtrent die ontwerp van sulke strukture. Daarom ondersoek hierdie studie die effek wat tipiese Suider-Afrikaanse nabystrandse profiele het op die oorslag van terugkaatsseemure, asook die invloed van die nabystrandse profiele op die verandering in die inkomende golfhoogte. Om hierdie doelwitte te bereik, is 2D-fisiese modellering in 'n glas-golfkanaal, toegerus met aktiewe golf-absorpsie, uitgevoer. Toetse is uitgevoer met vier verskillende nabystrandse profiele, waarvan drie van die profiele tipies is aan die Suider-Afrikaanse kus en die ander profiel 'n gemiddelde strandhelling gebruik in voorafgaande studies. Die drie nabystrandse profiele wat tipies is aan die Suider-Afrikaanse kus het 'n steil, plat en gemiddelde helling ingesluit. Toetse is uitgevoer vir 3 verskillende watervlakke en 5 verskillende golfperiodes. Die inkomende golfhoogte, asook die terugkaatsseemuur se ontwerp en -kruinhoogte is egter konstant gehou. Ontleding van die resultate dui daarop dat die nabystrandse profiel 'n groot impak het op die oorslag van 'n terugkaatsseemuur. Resultate wys dat oorslag toeneem met 'n afname in die helling van die nabystrandse profiel. Dus het die nabystrandse profiel met die platste helling gelei tot die grootse golfoorslagvolumes. Die terugkaatsseemuur op die nabystrandse profiel met 'n seewaartse sandbank het egter ook groot oorslag tempo's ervaar, grotendeels as gevolg van die botsing van inkomende en weerkaatste golwe. Daar word aanbeveel dat toekomstige studies oor terugkaatsseemure fokus op die effek wat stranderosie of -opbou op die golfoorslag het, asook die effek wat 'n verandering in golfhoogte op die oorslagvolumes het. Verdere

moontlike navorsing kan ook fokus op die kragte wat inkomende golwe uitoefen op die terugkaatsseemur, aangesien dit 'n belangrike aspek is wat in die ontwerp van nuwe terugkaatsseemure oorweeg moet word.

Acknowledgements

My grateful thanks go to:

- My study leader, Professor Koos Schoonees, for your guidance, knowledge and valuable input in this study.
- Dr André Theron for your advice regarding some aspects of the study.
- Johann Nieuwoudt, Iliyaaz Williams and Jody February, for your time, hard work and willingness to help me during my physical model testing at the Hydraulics Laboratory.
- Esmé Roux, Ross Jarvis and Stewart Walker, for your advice with regards to the setup of the physical model.
- Ms. Christa De Wet for proofreading my thesis.
- My family and friends for your unending support and prayers.
- Our Heavenly Father for the talents and opportunities that he has blessed me with.

Table of Contents

Declaration	i
Abstract	ii
Opsomming	iv
Acknowledgements	vi
List of Figures	xii
List of Tables	xiv
List of Abbreviations	xv
Nomenclature	xvi
1. Introduction	1
1.1. Background	1
1.2. Objectives	2
1.3. Methodology.....	2
1.4. Chapter overview	3
2. Literature review.....	4
2.1. Definitions.....	4
2.1.1. Spatial terms	4
2.1.2. Nearshore transformation processes	5
2.2. Overtopping	8
2.2.1. Overtopping types.....	8
2.2.2. Overtopping limits.....	10
2.2.3. Effect of wind	13
2.3. Types of recurve seawalls	13
2.4. Recurve seawall design	14
2.4.1. Fundamental research	14
2.4.2. EurOtop Artificial Neural Network	18
2.4.3. Japanese wave return wall	22

2.4.4.	Effect of the recurve seawall positioning in reducing wave overtopping	25
2.4.5.	Effect of the parapet angle of a recurve seawall in reducing wave overtopping at smooth dikes.....	27
2.4.6.	Effect of the overhang length of a recurve seawall in reducing wave overtopping.....	29
2.4.7.	Effect of the recurve seawall geometry in reducing wave overtopping	33
2.4.8.	Effect that the addition of a kerb has on overtopping of recurve seawalls	37
2.4.9.	Effect of the beach slope on the overtopping of a recurve seawall	38
2.5.	Typical Southern African nearshore profiles	41
2.6.	Physical modelling in previous wave overtopping studies	46
2.6.1.	Overview	46
2.6.2.	Laboratory and scaling effects.....	46
2.6.3.	Wave spectra	49
2.6.4.	Test duration	49
2.6.5.	Wave generation and overtopping measurement	50
3.	Physical modelling	52
3.1.	Overview	52
3.2.	Model set-up.....	52
3.2.1.	Test facility	52
3.2.2.	Model scale	53
3.2.3.	Nearshore profile design	54
3.2.4.	Recurve seawall design	56
3.3.	Controlled hydraulic parameters	57
3.4.	Experimental procedure	58
3.4.1.	Initial procedure	58
3.4.2.	Shallow water wave measurement	58
3.4.3.	Overtopping test procedure	59
3.5.	Data acquisition	59
3.5.1.	Shallow water wave measurement	59

3.5.2.	Overtopping measurement	61
3.6.	Post-processing	63
3.7.	Test conditions and summary	66
3.8.	Repeatability and accuracy	66
4.	Results.....	68
4.1.	Overview	68
4.2.	Physical model test results.....	68
4.2.1.	Nearshore profile A.....	68
4.2.2.	Nearshore profile B	69
4.2.3.	Nearshore profile C	74
4.2.4.	Nearshore profile D.....	76
4.2.5.	Summary of test results	78
5.	Analysis and discussion	79
5.1.	Overview	79
5.2.	Physical model tests.....	79
5.2.1.	Comparison of overall test results.....	79
5.2.2.	Influence of wave period.....	81
5.2.3.	Influence of water depth.....	84
5.2.4.	Influence of the nearshore profile.....	85
5.2.5.	Influence of wave height	88
5.3.	Comparison with previous studies	91
5.3.1.	Walker (2018) and Kretschmer (2017)	91
5.4.	Repeatability and accuracy of tests performed.....	93
5.5.	Additional aspects to consider	95
5.5.1.	Safety limitations related to allowable overtopping rates	95
6.	Conclusions and recommendations	97
6.1.	General.....	97
6.2.	Findings from physical model tests	97

6.2.1.	Effect of the nearshore profile	97
6.2.2.	Effect of water level	98
6.2.3.	Effect of wave period	98
6.2.4.	Effect of wave height	98
6.3.	Comparison with previous research.....	99
6.4.	Recommendations for further research.....	99
References	100
List of Appendices	105
Appendix A: Recurve seawall designs from previous studies.....		1
A.1.	Schoonees (2014) model recurve seawall designs	1
A.2.	Swart (2016) model recurve seawall designs	2
A.3.	Kretschmer (2017) model recurve seawall designs	4
Appendix B: Long-sections of the wave flume, built-in profiles.....		5
B.1.	Wave flume long section: Existing nearshore profile	5
B.2.	Wave flume long section: Walvis Bay nearshore profile	6
B.3.	Wave flume long section: Richards Bay nearshore profile	7
B.4.	Wave flume long section: False Bay nearshore profile	8
Appendix C: Physical model results		9
C.1.	Profile A: Existing nearshore profile.....	9
C.2.	Profile B: Walvis Bay nearshore profile	15
C.3.	Profile C: Richards Bay nearshore profile	21
C.4.	Profile D: False Bay nearshore profile	27
Appendix D: Influence of wave period on overtopping		33
D.1.	Overtopping rate as a function of wave period for a 1.6 m water depth.....	33
D.2.	Overtopping rate as a function of wave period for a 2.0 m water depth	33
D.3.	Overtopping rate as a function of wave period for a 2.4 m water depth	34
Appendix E: Influence of water level on overtopping		35
E.1.	Overtopping rate as a function of water depth for a 6 s wave period	35

E.2.	Overtopping rate as a function of water depth for an 8 s wave period	35
E.3.	Overtopping rate as a function of water depth for a 10 s wave period	36
E.4.	Overtopping rate as a function of water depth for a 12 s wave period	36
E.5.	Overtopping rate as a function of water depth for a 14 s wave period	37
Appendix F: Influence of the nearshore slope on overtopping		38
F.1.	Overtopping rate as a function of wave period for nearshore profile A	38
F.2.	Overtopping rate as a function of wave period for nearshore profile B.....	38
F.3.	Overtopping rate as a function of wave period for nearshore profile C.....	39
F.4.	Overtopping rate as a function of wave period for nearshore profile D	39
Appendix G: Influence of the nearshore slope on wave height		40
G.1.	Change in wave height for the 1.6 m water level.....	40
G.2.	Change in wave height for the 2.0 m water level.....	40
G.3.	Change in wave height for the 2.4 m water level.....	41
Appendix H: Probe spacings.....		42
H.1.	Nearshore profile A deep water probe spacings.....	42
H.2.	Nearshore profile A shallow water probe spacings.....	43
H.3.	Nearshore profile B deep water probe spacings	44
H.4.	Nearshore profile B shallow water probe spacings	45
H.5.	Nearshore profile C deep water probe spacings	46
H.6.	Nearshore profile C shallow water probe spacings	47
H.7.	Nearshore profile D deep water probe spacings.....	48
H.8.	Nearshore profile D shallow water probe spacings.....	49

List of Figures

Figure 2-1: Definition of coastal terms.....	4
Figure 2-2: Primary types of waves, as classified by EurOtop (2018).....	7
Figure 2-3: Types of wave overtopping.....	8
Figure 2-4: Non-impulsive wave condition resulting in “green water” overtopping (Bruce <i>et al.</i> , 2009)	9
Figure 2-5: Impulsive wave condition resulting in white water overtopping (Bruce <i>et al.</i> , 2009).....	9
Figure 2-6: Broken wave overtopping (Bruce <i>et al.</i> , 2009).....	10
Figure 2-7: Recurve seawall types.....	14
Figure 2-8: Wave return wall profile (Owen and Steele, 1993).....	15
Figure 2-9: Definition parameters for bullnose and wave return walls used by EurOtop (2018).....	18
Figure 2-10: Decision chart to calculate overtopping at bullnose/wave return walls (EurOtop, 2018)	19
Figure 2-11: Possible structural configurations for EurOtop ANN (EurOtop, 2018).....	21
Figure 2-12: Seawalls used in the studies by Murakami <i>et al.</i> (1996) and Kamikubo <i>et al.</i> (2003).....	22
Figure 2-13: FSS countermeasures against sea level rise, as proposed by Murakami <i>et al.</i> (2008).....	23
Figure 2-14: Plan view of the seawall arrangements used by Murakami <i>et al.</i> (2011) for Series A and B	25
Figure 2-15: Design seawall profiles tested by Allsop <i>et al.</i> (2007).....	26
Figure 2-16 Parapet wall definition sketch and model parameters (Van Doorslaer and De Rouck, 2011)	28
Figure 2-17: Dimensionless discharge versus relative crest freeboard for the 50 mm model wall (Van Doorslaer and De Rouck, 2011).....	28
Figure 2-18: Prototype test conditions for the recurve seawalls tested by Schoonees (2014).....	29
Figure 2-19: Effect of overhang length on the mean overtopping rate (Schoonees, 2014).....	30
Figure 2-20: Prototype test conditions for the recurve seawalls tested by Swart (2016).....	31
Figure 2-21: Overtopping comparison of overhang lengths tested (Swart, 2016).....	32
Figure 2-22: Wall profiles tested by Veale <i>et al.</i> (2012).....	33
Figure 2-23: Recurve shapes tested by Kretschmer (2017).....	34
Figure 2-24: Overtopping comparison of overhang shapes tested (Kretschmer, 2017).....	36
Figure 2-25: Prototype test conditions for the square edged, concave shaped recurve overhang tested by Kretschmer (2017).....	36
Figure 2-26: Recurve wall set-ups and dimensions tested by Walker (2018).....	37
Figure 2-27: Model recurve seawall design tested by Roux (2013).....	39

Figure 2-28: Beach slopes tested by Roux (2013)	40
Figure 2-29: Influence of different beach slopes on recurve seawall overtopping (Roux, 2013)	40
Figure 2-30: Locations of typical nearshore profiles of Southern Africa (US Department of State Geographer, 2018).....	42
Figure 2-31: Typical Southern African nearshore profiles	45
Figure 3-1: Physical modelling equipment	53
Figure 3-2: Nearshore profiles tested	55
Figure 3-3: Recurve seawall design (Walker, 2018)	56
Figure 3-4: Probe spacing for shallow water wave tests	60
Figure 3-5: Resistance probes in the physical model	61
Figure 3-6: Probe spacing for overtopping tests	62
Figure 3-7: Overtopping bin, funnel boards and splash screens	63
Figure 3-8: Reflection Analysis valid frequency range.....	65
Figure 3-9: Reflection Analysis bulk reflection coefficient calculator.....	65
Figure 4-1: Wave reflection at nearshore profile A ($WL_{toe} = 1.6$ m, $T_p = 10$ s)	70
Figure 4-2: Wave overtopping at nearshore profile A ($WL_{toe} = 2.0$ m, $T_p = 14$ s).....	70
Figure 4-3: Wave overtopping at nearshore profile A ($WL_{toe} = 2.4$ m, $T_p = 14$ s).....	71
Figure 4-4: Wave reflection at nearshore profile B ($WL_{toe} = 1.6$ m, $T_p = 14$ s)	71
Figure 4-5: Wave reflection at nearshore profile B ($WL_{toe} = 2.0$ m, $T_p = 12$ s)	73
Figure 4-6: Wave overtopping at nearshore profile B ($WL_{toe} = 2.4$ m, $T_p = 14$ s).....	73
Figure 4-7: Wave overtopping at nearshore profile C ($WL_{toe} = 2.0$ m, $T_p = 8$ s)	75
Figure 4-8: Wave overtopping at nearshore profile C ($WL_{toe} = 2.4$ m, $T_p = 14$ s).....	75
Figure 4-9: Wave overtopping at nearshore profile D ($WL_{toe} = 2.4$ m, $T_p = 14$ s).....	77
Figure 4-10: Wave overtopping at nearshore profile D ($WL_{toe} = 1.6$ m, $T_p = 14$ s).....	77
Figure 4-11: Complete overtopping data set	78
Figure 5-1: Comparison of test results obtained from all nearshore profiles	79
Figure 5-2: Overtopping rate as a function of wave period for a 2.4 m water depth.....	81
Figure 5-3: Overtopping rate as a function of water level for a 14 s wave period	84
Figure 5-4: Decision chart to aid recurve seawall design	86
Figure 5-5: Wave steepness on nearshore profiles B (left) and D (right) ($WL_{toe} = 2.4$ m, $T_p = 14$ s) ..	89
Figure 5-6: Wave steepness on nearshore profiles B (left) and C (right) ($WL_{toe} = 2.0$ m, $T_p = 10$ s) ..	89
Figure 5-7: Influence of the wave period on wave height factors for 1.6 m toe water level.....	90

List of Tables

Table 2-1: Typical wave reflection coefficients (Chadwick et al., 2013)	7
Table 2-2: Overtopping limits for people and vehicles, set by EurOtop (2018).....	12
Table 2-3: Tidal levels (SA Navy, 2018)	44
Table 2-4: Similitude ratios for Froude and Reynolds scaling laws, after Hughes (1993).....	48
Table 3-1: Model scale factors	53
Table 3-2: Physical modelling test breakdown.....	57
Table 5-1: Wave height factors (H_t/H_i)	90
Table 5-2: Comparison of overtopping from previous studies with overtopping experienced over nearshore profile A	92
Table 5-3: Accuracy of tests D15 evaluated by CoV ($WL_{toe} = 2.4$ m; $T_p = 14$ s)	94
Table 5-4: Accuracy of tests WD15 evaluated by CoV ($WL_{toe} = 2.4$ m; $T_p = 14$ s)	95
Table 5-5: Summary of critical overtopping rates for each nearshore profile	96

List of Abbreviations

2D	-	Two-dimensional
3D	-	Three-dimensional
CLASH	-	Crest Level Assessment of Coastal structures and Hazard analysis on permissible wave overtopping
DWA	-	Dynamic Wave Absorption
EPP	-	Equivalent Paddle Position
FSS	-	Flaring Shaped Seawall
JONSWAP	-	Joint North Sea Wave Project
LLD	-	Land Levelling Datum
MSL	-	Mean Sea Level
PM	-	Pierson Moskowitz
PVC	-	Polyvinyl chloride
RMS	-	Root Mean Square
SLR	-	Sea Level Rise
SWL	-	Still water level
WL	-	Water level

Nomenclature

α	-	Angle of recurve (°)
γ	-	JONSWAP peak enhancement factor
σ	-	Standard deviation of overtopping rates
μ	-	Average of overtopping rates
\emptyset	-	Wave return angle (°)
B_r	-	Horizontal recurve overhang length (m)
g	-	Gravitational acceleration (m/s^2)
h^*	-	Wave breaking parameter
H_{max}	-	Maximum wave height (m)
H_i	-	Incident wave height (m)
H_{m0}	-	Incident spectral significant wave height (m)
H_r	-	Reflected wave height (m)
H_s	-	Significant wave height at the toe of the structure (m)
H_t	-	Incident wave height at the toe of the structure (m)
h_r	-	Vertical dimension of recurve (m)
k-factor	-	Reduction factor for wave overtopping
K_r	-	Bulk reflection coefficient
L_o	-	Deep water wavelength (m)
N_x	-	Scale ratio between prototype and model values
P_c	-	Height of vertical part of wall above SWL (m)
ρ_w	-	Fluid density

q	-	Mean overtopping discharge per meter of seawall (L/s/m)
$R_{2\%}$	-	Wave run-up height for top 2% of waves in a sequence (m)
R_c	-	Freeboard (m)
T	-	Wave period (s)
T_m	-	Nominal mean wave period, JONSWAP spectrum (s)
$T_{m-1.0}$	-	Spectral wave period (s)
T_p	-	Peak wave period (s)
WL_{paddle}	-	Water level at wave paddle (m)
WL_{toe}	-	Water level at toe of structure (m)
X_m	-	Dimensional value in model
X_p	-	Dimensional value in prototype

1. Introduction

1.1. Background

Infrastructure located close to the shoreline (coastal, estuarial or lakefront) is generally highly valuable, even though they are often exposed to significant flood risk. Due to climate change, the consequent rise in sea level and stronger wind speeds, the flooding risks at coastal properties are increasing. Other factors that are adding to the flood risk is the ever-increasing value of assets in areas prone to high flood risk, as well as an increase in the population living and working in high-risk areas.

Understanding the future changes in flood risk due to wave overtopping at seawalls is a crucial component in ensuring effective management of coastal infrastructure. With an increased wave attack caused by the rising sea levels, the risk of economic damage or loss of life due to violent overtopping is constantly increasing. Reduction of overtopping at coastal defensive structures is therefore crucial in terms of the design, management and adaptation of coastal structures, especially when existing coastal defensive structures are evaluated for suitability in future conditions.

In places where space did not allow for the construction of dikes or rubble mound breakwaters, vertical seawalls were often built to decrease the risk of flooding and damage of landward infrastructure (buildings, roads, railways and walkways) as well as injury to people, especially pedestrians. As some of the existing vertical seawalls are now being exposed to increased wave attack, more sudden, severe overtopping events are taking place which is dangerous to both property and humans.

In order to decrease overtopping volumes, often vertical defensive structures are converted to recurve seawalls by constructing a recurve shaped overhang, pointing seawards, on top of a new or existing vertical seawall. The recurve shaped overhang reduces overtopping by deflecting water that is forced upwards by the vertical face of the structure, back seaward. By adding a recurve section onto the crest of a vertical seawall, the crest height of the structure can be reduced. The lowering of the seawall crest is one of the main reasons for converting vertical seawalls to recurve seawalls.

Although recurves are often incorporated into seawall design, literature offers limited guidance for the design of such structures. The most popular source providing guidance on the analysis of wave overtopping at bullnose or wave return walls is the EurOtop Manual (2018). Some additional research on

recurve seawalls was, however, done at Stellenbosch University by Schoonees (2014), Swart (2016), Kretschmer (2017) and Walker (2018).

In 2014, Schoonees finished her research on the use of a recurve section at the top of a vertical seawall. Swart (2016) continued from Schoonees' (2014) research to determine the effect that the overhang length has on the overtopping of a recurve seawall. Kretschmer (2017) investigated the effect that the recurve shape has on the overtopping of a recurve seawall. Walker (2018) determined the effect that a kerb on top of an existing recurve seawall has on the reduction of wave overtopping at the structure. Walker (2018) also investigated the effect that chamfering of the recurve overhang has on overtopping of the seawall. This study will primarily build on the four abovementioned studies and determine the effect the nearshore profile has on the overtopping of a recurve seawall.

1.2. Objectives

The main objectives of this study are to determine the effect that different nearshore profiles have on the overtopping of a recurve seawall by determining the:

- Effect that the nearshore profile has on the increase or reduction of the incoming wave height.
- Effect that different Southern African nearshore profiles have on the overtopping of a recurve seawall.
- Influence that the wave period has on the overtopping of recurve seawalls over different nearshore profiles.
- Effect that the water- and freeboard levels have on the overtopping of recurve seawalls over different nearshore profiles.

1.3. Methodology

A literature review was conducted to gain a comprehensive understanding of previous research on the reduction of wave overtopping at different seawalls, but mainly recurve seawalls. Nearshore profiles of Southern Africa were also studied to find a range of different profiles to test in the physical modelling study. Existing profiles were used instead of simplified slopes, to ensure the results of the physical modelling are realistic and relevant.

Two-dimensional physical model tests were undertaken in a wave flume at the Hydraulic Laboratory of Stellenbosch University's Civil Engineering Faculty. A set of experiments were done to test the influence of the nearshore profile on the overtopping rates of a recurve seawall. The experiments were done for a range of maritime conditions, during which the wall height, crest height, recurve shape and wave height were kept constant. The water level, wave period and nearshore profile were varied.

As the recurve seawall structure is relatively impermeable to wave action, it will reflect a large amount of the incident wave energy, causing unwanted wave disturbance, which complicates the wave height measurement process (EurOtop, 2018). Therefore, before testing the overtopping of the recurve seawall for the different maritime conditions, the wave height at the toe of the structure and at one peak wavelength away from the structure was measured for each nearshore profile, without the recurve wall in place. The wave heights were then compared, to determine the effect that the nearshore profile has on the increase or reduction of the incoming wave height. In order to reduce the effect of reflected waves on the wave height measurements close to the structure during overtopping tests, the wave height was only measured at one peak wavelength away from the structure, as recommended by Mansard and Funke (1980).

To ensure the accuracy and reliability of the physical modelling tests, some of the tests were repeated. From the experiments, the overtopping of the model was measured to determine the effect that the nearshore profile has on the wave overtopping of a recurve seawall. The results were also compared to previous research, to see whether the results can add value to previous research.

1.4. Chapter overview

The thesis consists of six chapters, including Chapter 1, which gives a brief background, the objectives and a brief methodology used to conduct the research. Chapter 2, the literature review, aims to obtain a comprehensive understanding of existing research on wave overtopping, recurve seawall design and Southern African nearshore profiles. In Chapter 3, the scope and a detailed methodology of the physical model tests are given. Chapter 4 is used to summarise the results obtained from the physical model tests, whereas Chapter 5 analyses the results and presents the results as graphs, which are also interpreted and discussed. The conclusion of the project, along with recommendations for future research, is given in Chapter 6.

2. Literature review

2.1. Definitions

2.1.1. Spatial terms

Figure 2-1 below shows a typical cross-section of the coastal zone with some of the important terminology used in this study. The definitions of the applicable terms are discussed below Figure 2-1.

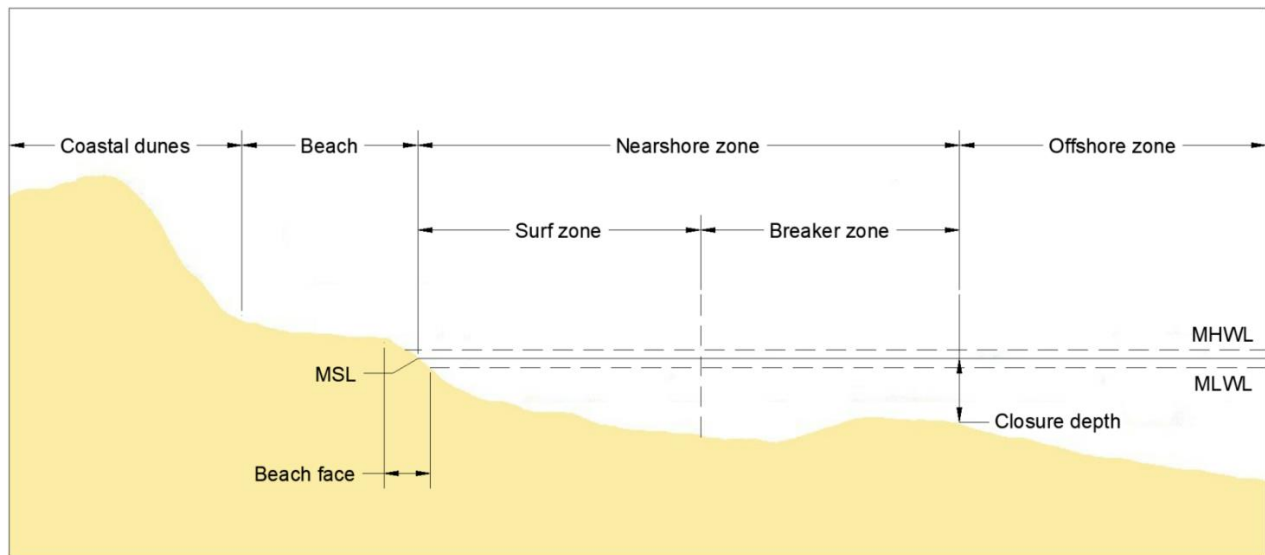


Figure 2-1: Definition of coastal terms

From Figure 2-1 it can be seen that the nearshore zone extends from the low water line to beyond the breaker line, where the bathymetry is no longer influenced by the longshore and cross-shore sediment transport. On the seaward boundary of the nearshore zone, the depth is defined as the closure depth, since this is the depth beyond which no significant longshore or cross-shore sediment transport takes place. The offshore zone therefore starts at the seaward boundary of the nearshore zone (closure depth) and continues into deep water. In the offshore zone, the effects of longshore sediment transport are negligible. Deep water is defined as water that is too deep for the waves to be influenced by the seafloor bathymetry. The deep-water boundary is usually taken as half the deep-water wavelength.

The surf zone is defined as the area within the nearshore zone which gets affected by the depth-induced breaking waves. The surf zone is located within the nearshore zone, between the breaker line and the beach. It is also within the surf zone that most of the longshore sediment transport tends to take place.

Longshore sediment transport is made possible by the longshore current, which transports sediment parallel to the shore in the nearshore zone, but primarily in the surf zone. The current is usually generated by oblique incoming waves, which breaks and creates a shore-parallel energy component, i.e. the longshore current.

2.1.2. Nearshore transformation processes

As swell- or wind waves approach the coast, they are affected by changes in the nearshore bathymetry. Shoaling occurs as waves enter shallower water, where the waves start to interact with the nearshore bathymetry. Interaction with the sea bed leads to a decreased wave celerity and wavelength, while the wave period remains constant. For a steady-state, the energy flux, which is the rate of change at which energy is transferred by the waves, remains constant. The conservation of energy can be described mathematically by Equation 2.1.

$$E c_{g0} = E c_g \quad (2.1)$$

Where:

E	=	wave energy
c_{g0}	=	wave group celerity
c_g	=	deep-water wave group celerity

Therefore, if the wave group celerity decreases, the wave energy has to increase for the energy flux to remain constant. And since the wave energy is proportional to the wave height squared (H^2), the wave height increases as the waves start to shoal.

Following the process of shoaling is wave breaking. Waves may break due to the interaction between waves and currents, due to the presence of natural or artificial barriers, or the relationship between water depth and wave height, which produces an inherently unstable waveform, leading to wave breaking (Chadwick *et al.*, 2013).

According to Chadwick *et al.* (2013), waves will break due to the waves becoming too steep, or because the wave height over water depth ratio becomes too large. In order to determine whether the waves will break and in what manner, the surf similarity parameter, or Iribarren number can be calculated with Equation 2.2.

$$\xi_{m-1.0} = \frac{\tan \alpha}{\sqrt{H_{m0}/L_{m-1.0}}} \quad (2.2)$$

Where:

- $\xi_{m-1.0}$ = Iribarren number, or surf similarity parameter
- $\tan \alpha$ = beach slope
- H_{m0} = spectral significant wave height
- $L_{m-1.0}$ = spectral wavelength in deep water.

Figure 2-2 displays the different beach slopes and their associated types of wave breaking. Waves on a flat foreshore tend to break as spilling waves. Spilling breakers break slowly from the top of the wave, with turbulent water “spilling” down the wave face. Usually, more than one breaker line can be found on such slopes. Plunging waves occur on mild to steep slopes, breaking with a steep, overhanging wave face and a curling crest. Falling in the spectrum between plunging and surging waves is collapsing waves, which break onto the beach face in a collapsing motion. Surging waves occur on very steep beach slopes. Surging waves do not break, but surge up the slope and then reflect back offshore (EurOtop, 2018).

Waves that collide with a solid object like a breakwater, a seawall or even a sloping beach will be reflected to some extent. When waves collide with a solid vertical structure, such as a seawall, the resulting energy from reflected waves can be large. On the other hand, if the waves collide with permeable structures or gentle slopes, much less wave energy will be reflected. Typical wave reflection coefficients (K_r) are summarised Table 2-1 .

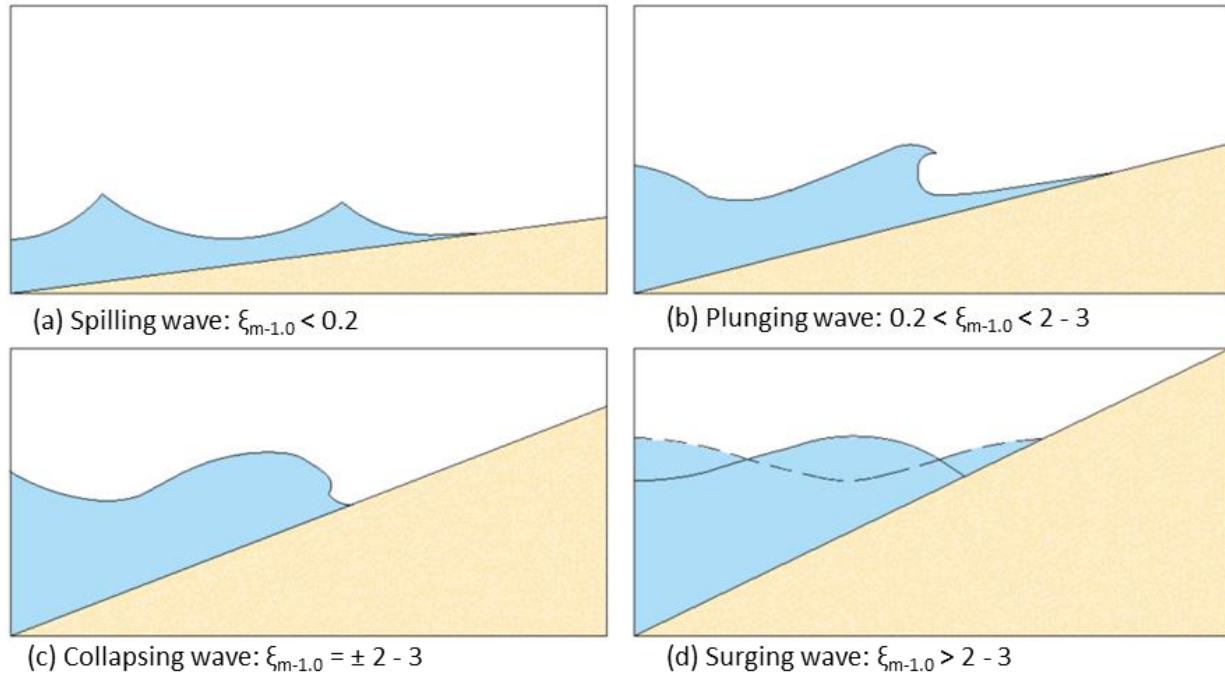


Figure 2-2: Primary types of waves, as classified by EurOtop (2018)

Table 2-1: Typical wave reflection coefficients (Chadwick et al., 2013)

Reflection barrier	Reflection coefficient (K_r)
Concrete seawalls	0.70 – 1.00
Rock breakwaters	0.40 – 0.70
Beaches	0.05 – 0.20

2.2. Overtopping

Wave overtopping occurs when incoming waves colliding with a marine structure cause water to be discharged over the crest of the structure. The three types of overtopping are discussed in Section 2.2.1.

2.2.1. Overtopping types

Wave overtopping can be partitioned into three types, as shown in Figure 2-3. The first type of wave overtopping occurs when waves run up the face, and over the crest of the seawall in a coherent water mass, known as 'green water' overtopping.

Another type of wave overtopping occurs when waves break in front of a vertical defensive structure or on the face of the structure, producing high localised overtopping along certain parts of the structure, with significant volumes of spray. This type of overtopping is often called 'white water' overtopping and is considered to be the most common overtopping.

The third type of overtopping is overtopping 'spray', which is carried over the crest of the seawall by its own momentum or by onshore wind. The spray is produced by waves breaking in front or on the face of a vertical structure. Without the help of a strong onshore wind, spray does not contribute much to the total overtopping, but it may still cause local hazards. Spray overtopping will not be considered, as the influence of wind on spray overtopping is not yet completely understood.

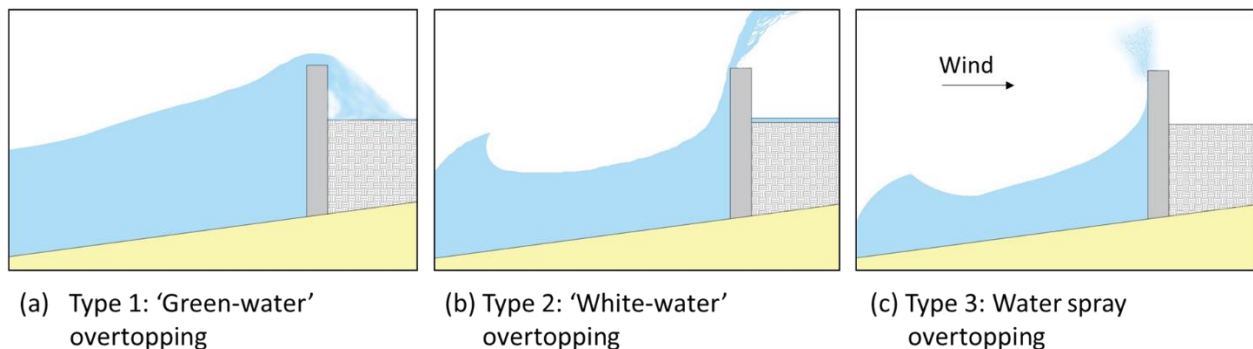


Figure 2-3: Types of wave overtopping

'Non-impulsive' or 'pulsating' wave conditions occur at vertical seawalls when the waves are rather small compared to the water depth at the toe of the structure. Because of the deep water, the waves are not critically influenced by the approach slope, or structure. Overtopping waves run up the face and over the crest of the seawall as a coherent mass of water, called 'green-water'. A 'green-water' overtopping event can be seen in Figure 2-4 (Bruce *et al.*, 2009)

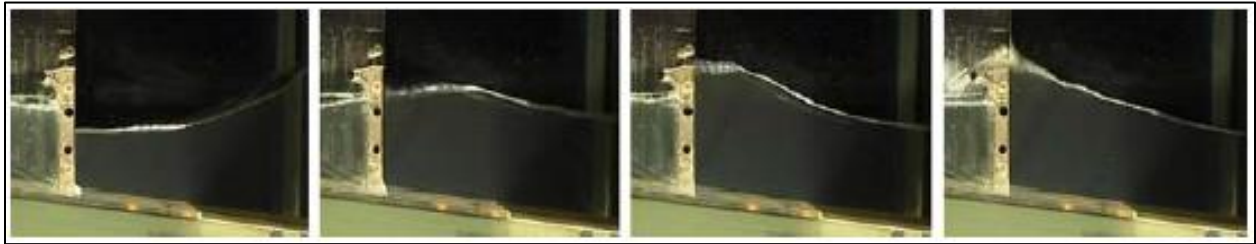


Figure 2-4: Non-impulsive wave condition resulting in "green water" overtopping (Bruce *et al.*, 2009)

'Impulsive' wave conditions occur at vertical seawalls when incoming waves are high in comparison to the water depth at the structure. During 'impulsive' wave conditions, incoming waves may shoal over the nearshore slope or on the defensive structure's toe, causing waves to break violently against the face of the vertical seawall. At the vertical defensive structures, overtopping occurring during 'impulsive' wave conditions can be denoted by a violent up-rushing water jet, as shown in Figure 2-5. The impact forces on the wall can be as much as 10 to 40 times larger than that of pulsating wave conditions (Bruce *et al.*, 2009).

Falling in the spectrum between 'pulsating' and 'impulsive' wave conditions are the 'near-breaking' wave conditions. For 'near-breaking' waves, overtopping is denoted by a rapid water jet that rushes up the wall face at a near vertical angle. As 'near-breaking' wave conditions result in similar overtopping to 'impulsive' wave conditions, 'near-breaking' waves are categorised as a type of 'impulsive' wave condition.



Figure 2-5: Impulsive wave condition resulting in white water overtopping (Bruce *et al.*, 2009)

During 'broken' wave conditions, waves typically collide with the seawall as a highly aerated water mass, resulting in short-duration pressure loadings similar to impulsive wave conditions, just less significant, as a result of the waves' high level of aeration. A broken wave condition can be seen in Figure 2-6.

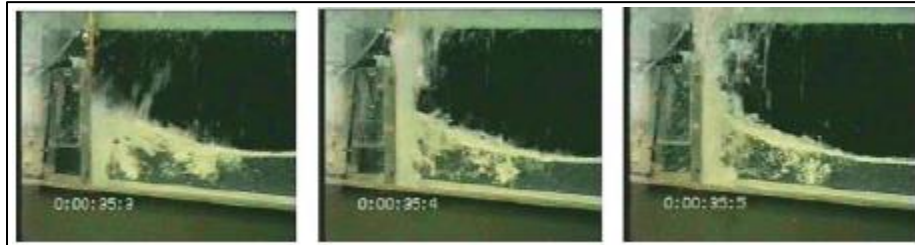


Figure 2-6: Broken wave overtopping (Bruce *et al.*, 2009)

2.2.2. Overtopping limits

Coastal defensive structures are primarily constructed to prevent wave overtopping, which could lead to death, injury, property damage or transport disruptions on the landward side of the structure. Owners and designers of coastal defensive structures, therefore, have to be mindful of the potential risks during a wave overtopping event, enabling them to bring these risks into consideration during the design of the structure. It is therefore helpful to categorise the dangerous effects of waves and overtopping (EurOtop, 2018):

- Damage to coastal defensive structure (long- and short-term), with possible breaching leading to flooding behind the structure.
- Risk of people behind the defensive structure being seriously injured or possibly dying (pedestrians, cyclists, motorists).
- Damage to assets, infrastructure or operations behind the defensive structure (loss of economic- and/or environmental resources, or disruption to the local economy).
- Shallow water flooding.

EurOtop (2018) found that a strong relationship exists between the wave height that causes overtopping and the tolerable overtopping volumes, as tolerable overtopping events relies strongly on individual overtopping events. For example, large incident waves can cause large individual overtopping events, while for the same event, the mean overtopping discharge is low.

At some locations, assets or equipment might be situated behind the seawall. The equipment or assets are, however, rarely designed to resist significant overtopping, so the equipment has to be protected either by revising the seawall design or by protecting the equipment and/or assets with a coastal defensive structure. For a case with an incident wave height of $H_{mo} = 4 - 5$ m, where the equipment and/or assets are unprotected, the mean overtopping discharge should be kept below 1 L/s/m (EurOtop, 2018). Because the equipment/property failure will be sudden, designers should apply the limit to the overload condition, which is assumed to be 10 – 20 percent above the design condition (EurOtop, 2018).

In coastal cities and towns, buildings and other structures may be located directly landward of the coastal defensive structures, with just a promenade or road separating them. The promenade, which is located directly behind the defensive structure may be protected, but the overtopping discharge could still travel across the promenade and damage doors and windows of buildings located behind the promenade, which are not designed to withstand the impact of overtopping water. EurOtop (2018), therefore, advises that mean wave overtopping discharges in such cases be kept below $q = 1$ L/s/m.

Due to human curiosity, some people may take risks, to the extent of possibly being injured or drowned. Unfortunately, human curiosity cannot be avoided by governing authorities or operators of coastal facilities. Some coastal defensive facilities can, however, be blocked off to the public, but where not possible, people should be warned of the possible dangers. For waves larger than 3 m, conditions are too dangerous to let any people onto the defensive structure. For wave heights smaller than 3 m, the overtopping generally flows over the crest horizontally, resulting in overtopping values around 500 L/m (EurOtop, 2018). If the wave height is just above 2 m, the allowable mean discharge should be kept below 1 L/s/m. If the waves are even smaller, tolerable mean discharges should be less than 5 L/s/m. For waves smaller than 0.5 m, no overtopping limits are specified (EurOtop, 2018).

Driving vehicles on roads located behind coastal defensive structures during overtopping conditions can become very dangerous, especially when the flow is strong enough to ‘float’ the vehicle. Large overtopping jet velocities or overtopping volumes can also cause vehicles to start sliding on the roadway. Overtopping events that endangers road users can be expected when wave overtopping volumes reach about 1000 to 2000 litre per meter, with a 3 m mean wave height and a mean discharge of 5 L/s/m (EurOtop, 2018). For a mean wave height of 2 m, a tolerable mean discharge of 10 to 20 L/s/m is advised, and for 1 m waves, 75 L/s/m, given the flow depth is less than 0.3 m (EurOtop, 2018).

When driving vehicles at high speed on unprotected causeways, behind coastal defensive structures, any overtopping is dangerous. Strong onshore winds worsen white water overtopping, which may carry debris and/or beach material, making conditions very dangerous to traffic. Roads should, therefore, be closed well before the actual overtopping events (EurOtop, 2018).

In some places, railways are located behind coastal defensive structures, where trains can be affected by wave overtopping. Trains are, however, more stable than road-going vehicles, primarily because of their weight, making them more difficult to float. They however still need to travel at a low speed as beach material and/or debris can be carried onto the tracks by water. Tolerable overtopping volumes for railways are specified to be lower than 2000 L/m, but varies depending on the overtopping violence and how far behind the defensive structure the tracks are located. Table 2-2 summarises the overtopping limits given by EurOtop (2018) to ensure the safety of people and vehicles at coastal defensive structures.

Table 2-2: Overtopping limits for people and vehicles, set by EurOtop (2018)

Hazard type and reason	Mean discharge q (L/s/m)	Maximum volume (L/m)
Unprotected property or equipment behind the defensive structure. $H_{m0} = 4 - 5$ m	≤ 1	-
People at structures with possible violent overtopping, mostly vertical structures.	No access for any predicted overtopping.	No access for any predicted overtopping.
People at seawall/dike crest. Clear view of the sea. $H_{m0} = 3$ m $H_{m0} = 2$ m $H_{m0} = 1$ m $H_{m0} < 0.5$ m	0.3 1 10 - 20 No limit	600 600 600 No limit
Cars on seawall/dike crest, or railway close behind crest. $H_{m0} = 3$ m $H_{m0} = 2$ m $H_{m0} = 1$ m	< 5 10 - 20 < 75	2000 2000 2000
Highways and roads, fast traffic.	Close before debris in spray becomes dangerous.	Close before debris in spray becomes dangerous.

2.2.3. Effect of wind

According to EurOtop (2018), wind could influence wave overtopping and overtopping discharges in the following ways:

- Wind can change the crest shape of incident waves approaching a defensive structure, thereby resulting in modification of the governing waveform colliding with the seawall.
- An onshore wind can blow up-rushing water over the structure crest, while an offshore wind blows up-rushing water back seawards. Both onshore and offshore winds, therefore, affect the mean overtopping discharges and volumes at a structure.
- Wind can change the physical form of an overtopping jet, of which the primary concerns are the change in the jet's aeration and post-overtopping characteristics, such as a change in overtopping trajectory and velocity, landward distribution of discharge and post-overtopping force loadings.

To model the effects of wind in a small-scale physical model can be extremely difficult, due to the simultaneous scaling that has to be used for wave-structure and water-air interaction processes. Very limited research is available which offers assistance in how to reshape the incident waves, and therefore, the effect of wind on overtopping was omitted from this study.

2.3. Types of recurve seawalls

Recurve seawalls are coastal defence structures that are built to reduce or prevent overtopping and flooding of the landward side of the structure. Recurve seawalls operate by redirecting the up-rushing water jet, which arises when a wave collides with the vertical face of a seawall, back seaward. In the past, recurve seawall designs has proven to be more feasible in stopping a wave mass than a plain vertical defensive structure.

Various types of recurve seawalls can be found all around the world today, all working in the same basic principle. Although recurve seawalls are often used as coastal defensive structures, little research has been done to provide guidance on the design of recurve walls. Schoonees (2014) classified recurve seawalls into the following three categories:

- Type 1: Large recurve seawalls.
- Type 2: Recurve seawalls on top of coastal defensive structures, as part of a composite structure.
- Type 3: Recurve seawalls on top of vertical seawalls.

Examples of the three types of recurve seawalls, as classified by Schoonees (2014), can be seen in Figure 2-7. Recurve seawalls can also be referred to in literature as wave return walls, bullnose walls or parapet walls. Parapet walls have a straight seaward overhang, which is angled upward to an angle larger than zero with the vertical part of the wall. Bullnose walls have a more rounded seaward overhang. Their purpose, however, remains the same, regardless of their shape.

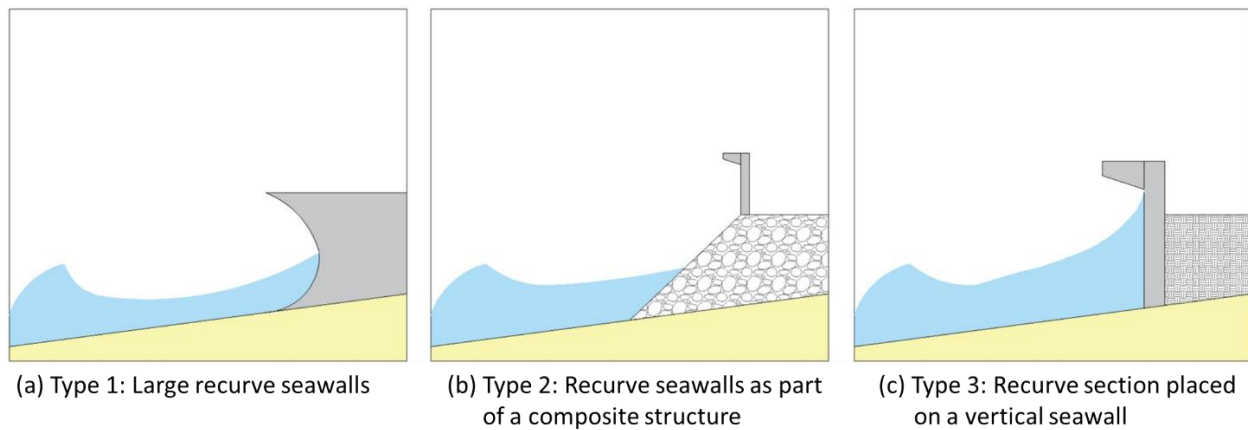


Figure 2-7: Recurve seawall types

2.4. Recurve seawall design

2.4.1. Fundamental research

Physical modelling of the seawall at Northern Kent in South East England, was completed during research done by Berkeley-Thorn and Roberts (1981). In the study, Berkeley-Thorn and Roberts (1981) proposed a recurve seawall design (Figure 2-8) to be constructed on top of the existing sloped seawall crest. Physical modelling tests were conducted for severe wave conditions, where the wave crest heights exceeded the crest height of the recurve profile. In such severe conditions, the recurve profile proved to be ineffective. However, for less severe conditions, the recurve profile was found to be more effective, especially when compared to vertical seawalls (Berkeley-Thorn and Roberts, 1981).

Research by the US Army Corps of Engineers (1991), found that a recurve seawall considerably lowers wave overtopping when placed on an existing embankment. The physical model study investigated whether placing a recurve structure on top of a riprap embankment would be effective in reducing wave overtopping at the structure. A recurve profile, as well as vertical seawalls of different heights was tested during physical modelling. In conclusion, the US Army Corps of Engineers (1991) states that the recurve

structure proved to be very efficient in reducing wave overtopping, as the overtopping rates were about 91 percent less than the overtopping measured for a vertical wall. The effectiveness is partially attributed to the riprap considerably reducing the force and velocity of the wave uprush toward the recurve/vertical wall structure (USACE, 1991).

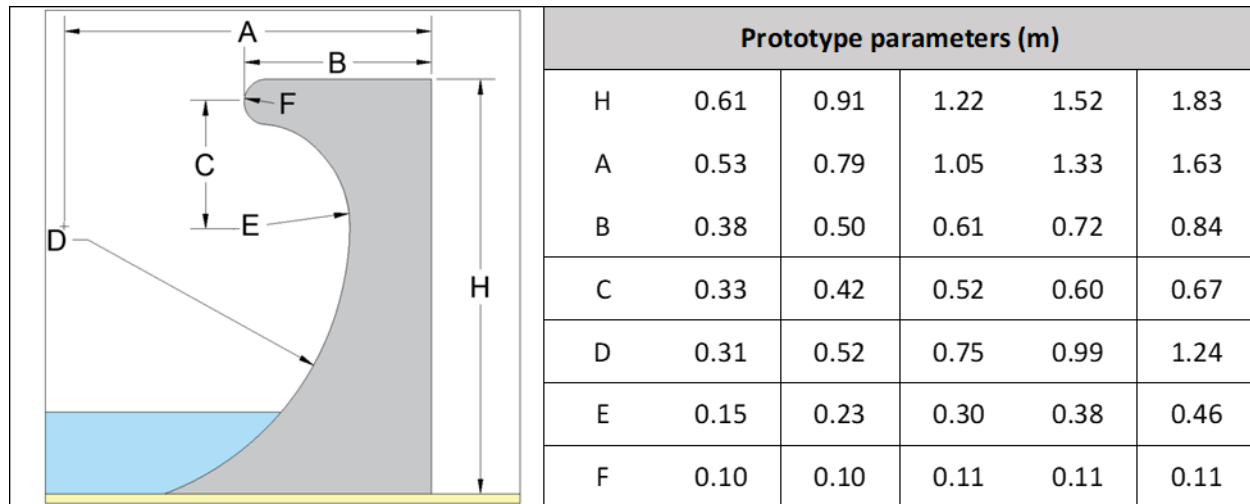


Figure 2-8: Wave return wall profile (Owen and Steele, 1993)

Owen and Steele (1993) studied the effectiveness of wave return walls on the crests of 1:2 and 1:4 simply sloping seawalls. The physical model tests were performed with the wave return wall designed by Berkeley-Thorn and Roberts (1981), as shown in Figure 2-8. The aims of the study were to investigate the effectiveness of different sizes of wave return walls on both permeable and impermeable sloped seawalls, while also varying the space between the recurve wall and the crest of the seaward slope. To achieve the objectives, Owen and Steele (1993) conducted random wave physical model tests, from which empirical equations to predict wave overtopping discharges were derived. The performance of the wave return walls were quantified with a discharge factor, D_f , which is the ratio of discharge overtopping of the composite recurve structure to the discharge overtopping of plain embankment seawalls, as calculated in previous studies by Owen (1980). On the effectiveness of the return wall profile, Owen and Steele (1993) suggested that the recurve structure designed by Berkeley-Thorn and Roberts (1981), had undoubtedly a very effective recurve profile, primarily because of the near horizontal angle at which the waves are returned back seaward.

In terms of overtopping discharge, it was found to be more effective to build a wave return wall on top of an existing embankment seawall than to raise the crest level of the embankment with the required

amount. The permeability of the structure, particularly that of the crest, as well as the shape of the recurve wall was found to be important factors influencing the effectiveness of the wave return wall. Results show that a wall placed on top of a permeable crest is more effective at reducing overtopping than a wall placed on top of an impermeable crest. Owen and Steele (1993), however, found that the primary factor influencing the effectiveness of a wave return wall was the height of the wall relative to its position above the still water line.

Franco *et al.* (1994) conducted research on overtopping experienced at vertical and composite breakwaters, which included vertical- and recurve parapets on top of caisson breakwaters. During physical modelling, Franco *et al.* (1994) discovered that in order to get the same reduction in overtopping, the recurve seawall could be about 30 percent lower than the vertical seawall tested under the same conditions. The finding is however only applicable to relatively low overtopping volumes (Franco *et al.*, 1994).

Banyard and Herbert (1995) studied the effectiveness of recurve seawalls under oblique wave attack, building on the study by Owen and Steele (1993). Physical model studies show that under oblique wave attack, overtopping discharges increased significantly and that whether the sea conditions were short or long-crested did not make a difference. The largest increase in overtopping was over six times that of the normal overtopping for perpendicular incident waves. In conclusion, Banyard and Herbert (1995), found that the discharge factor, D_f , and not the angle of wave attack, was the factor which had the biggest influence on the overtopping ratio.

As mentioned by Kortenhaus *et al.* (2003), abundant data is available in the form of systematic- and case studies on the overtopping of vertical seawalls. On the other hand, not much research exists on the overtopping of vertical seawalls with recurve or parapet overhangs. Therefore, Kortenhaus *et al.* (2003) decided to focus their research on finding a possible overtopping reduction factor for recurve and parapet seawalls, based on their geometry, shape and size.

Physical model studies proved that for recurve seawalls with a relatively high freeboard ($R_c/H_s = 1.5$), no wave overtopping was experienced as the incoming wave was completely deflected. However, for lower freeboards and high wave conditions, overtopping did occur, as the recurve overhang could not contain the incoming wave, consequently leading to green water overtopping.

Kortenhaus *et al.* (2003) performed a range of overtopping tests on conventional vertical walls ($q_{no\ recurve}$) and also on vertical walls with recurve profiles ($q_{recurve}$), with both walls being exactly the same height. The k-factor, which is an effectiveness parameter measuring the effectiveness in reducing the overtopping rate was defined by Kortenhaus *et al.* (2003), as:

$$k_r = \frac{q_{recurve}}{q_{no\ recurve}} \quad (2.3)$$

Where: $q_{recurve}$ = Overtopping rate experienced at the recurve seawall.
 $q_{no\ recurve}$ = Overtopping rate experienced at the vertical seawall.

After further analysis of the test data, Kortenhaus *et al.* (2003) developed an approach for predicting the overtopping rate reduction (k-factor) for recurve- and parapet walls. However, because the overtopping rate reduction (k-factor) from the overtopping tests showed a scatter for the large reductions in overtopping, Pearson *et al.* (2004) decided to develop an improved approach to decrease the scatter in results. An adjusted k-factor (k'), along with a decision chart to give some guidance for the design of recurve seawalls was consequently developed.

The research of Kortenhaus *et al.* (2003) and Pearson *et al.* (2004) eventually led to the design methodology for recurve and bullnose walls, outlined in EurOtop (2018). The design parameters used in EurOtop (2018), can be found in Figure 2-9, whereas the decision chart, summarising the design methodology for recurve and bullnose walls can be found in Figure 2-10. From the chart, the adjusted recurve effectiveness parameter, k , can be calculated. The effectiveness parameter is used to calculate the expected overtopping at a recurve seawall, given the overtopping at a vertical seawall of the same height and metocean conditions are known. However, because of the scatter in the original data and the fact that the approach is not based on detailed physical mechanisms or processes, it is advised that reductions in mean discharges greater than 20 percent should not be predicted. Rather, a detailed physical model study should be undertaken (EurOtop, 2018).

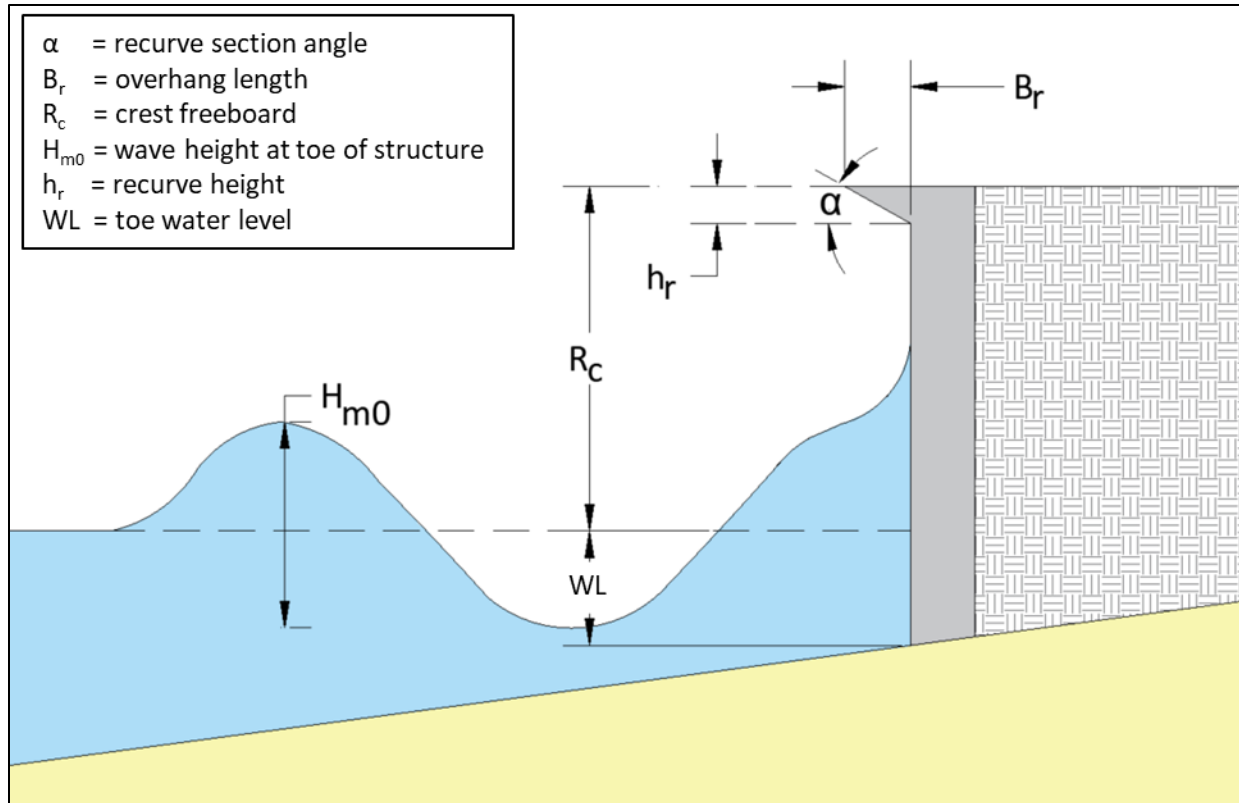


Figure 2-9: Definition parameters for bullnose and wave return walls used by EurOtop (2018)

2.4.2. EurOtop Artificial Neural Network

EurOtop (2018) is the second edition of the world-renowned manual and benchmark on wave overtopping of sea defences and related structures. The manual is compiled from the work of various researchers, to assist and guide government, consultants and businesses worldwide on the analysis and/or design of coastal defensive structures, which protect property and people from flooding due to wave attack. The methods set out within the manual is applicable for performance assessments of current structures, as well as for long-term design calculations.

In parallel with the EurOtop (2018) Manual, an Artificial Neural Network, known as the EurOtop ANN, was developed to assist the prediction of mean overtopping discharges for various different structure geometries, using a number of hydraulic and geometrical parameters as input. The ANN is made up of a large database, which was extended from the original CLASH database.

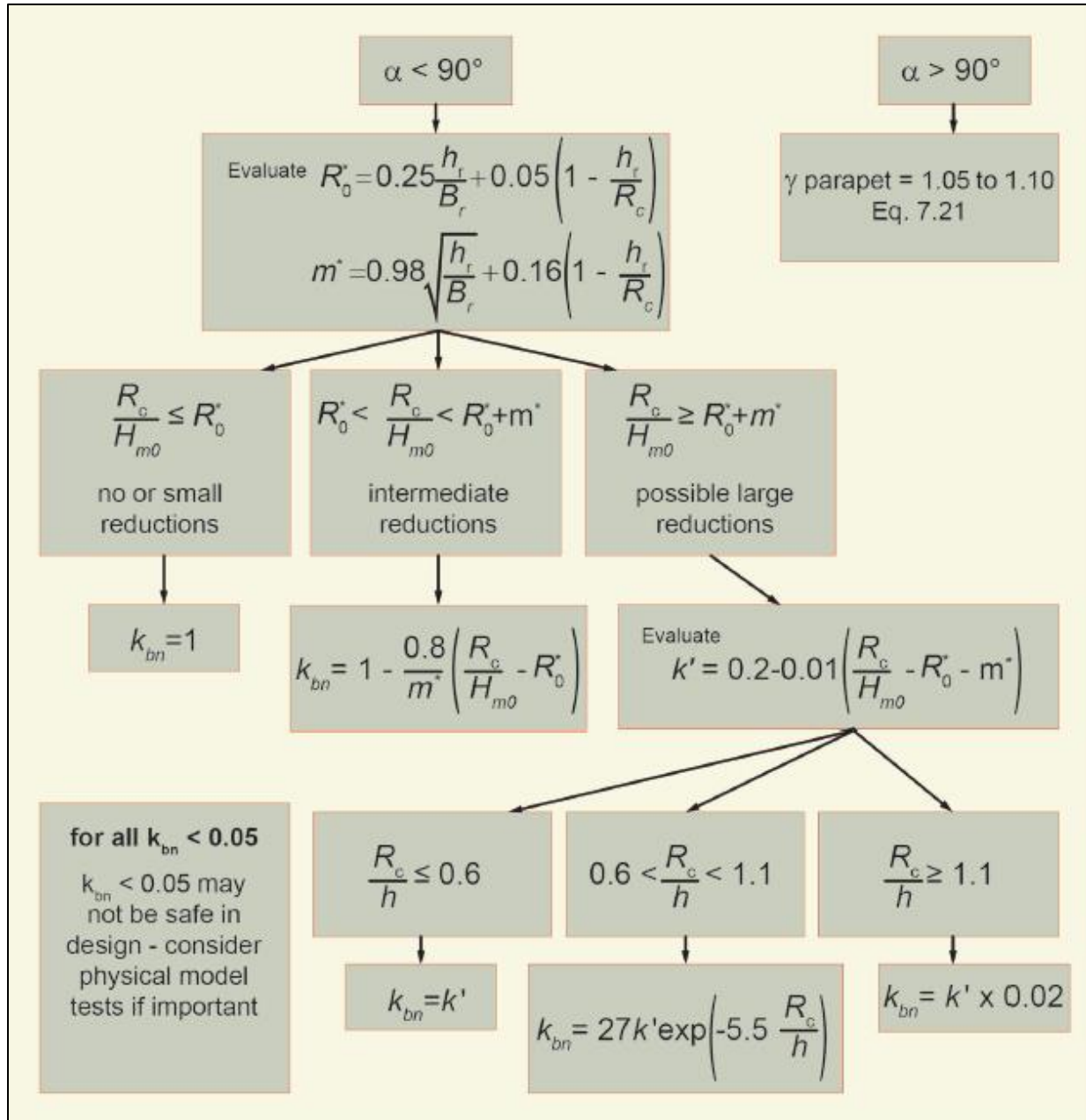


Figure 2-10: Decision chart to calculate overtopping at bullnose/wave return walls (EurOtop, 2018)

The Crest Level Assessment of coastal Structures by full-scale monitoring, neural network prediction and Hazard analysis on permissible wave overtopping (CLASH) was launched by the European Union as a project to gather more information on wave overtopping at different types of coastal structures. The objectives were to firstly measure wave overtopping in reality, from which scale effects could be defined and secondly to create an extensive homogeneous database, from which an ANN could be trained to predict wave overtopping for various kinds of structure geometries (EurOtop, 2018).

The new and improved EurOtop ANN is made up of a larger database than the original CLASH database, with the capability of predicting small overtopping events more accurately. The EurOtop ANN encompasses more than 17 000 tests, of which 13 500 are for overtopping only. The types of structures included in the tests are berm breakwaters, rubble mound breakwaters, dikes, caissons, vertical seawalls and other composite structures. Before entering any tests into the database, every test first was screened and given a reliability factor, RF, depending on the reliability and availability of data. A complexity factor, CF, was also given, based on the complexity of schematising the structure's geometry by a number of geometrical parameters. The geometries that can be schematised are shown in Figure 2-11 (EurOtop, 2018).

The EurOtop database consists of 11 hydraulic parameters, characterising the wave conditions, 23 structural parameters, 5 general parameters and 3 output parameters (q , K_r , K_t). The extended database can be characterised into 7 sections, namely: straight permeable rock slopes, straight impermeable rock slopes, straight slopes with armour units, straight smooth slopes, structures with combined slopes and berms, vertical walls and oblique wave attack or 3D wave basin tests (EurOtop, 2018).

The new EurOtop ANN makes use of dimensionless parameters, as opposed to principle dimensions which were used in CLASH. Using dimensionless parameters has proved to give more accurate output predictions than methods making use of principle dimensions. The ANNs can, therefore, be used to predict overtopping for a range of structures and hydraulic parameters. The development and of such ANNs are especially helpful when dealing with complicated structure geometries and/or when variable wave conditions are present. It is, however, very important that the database which is used to train the ANN is accurate and large enough, otherwise results can be unreliable. Both the EurOtop and CLASH databases are available on the EurOtop website.

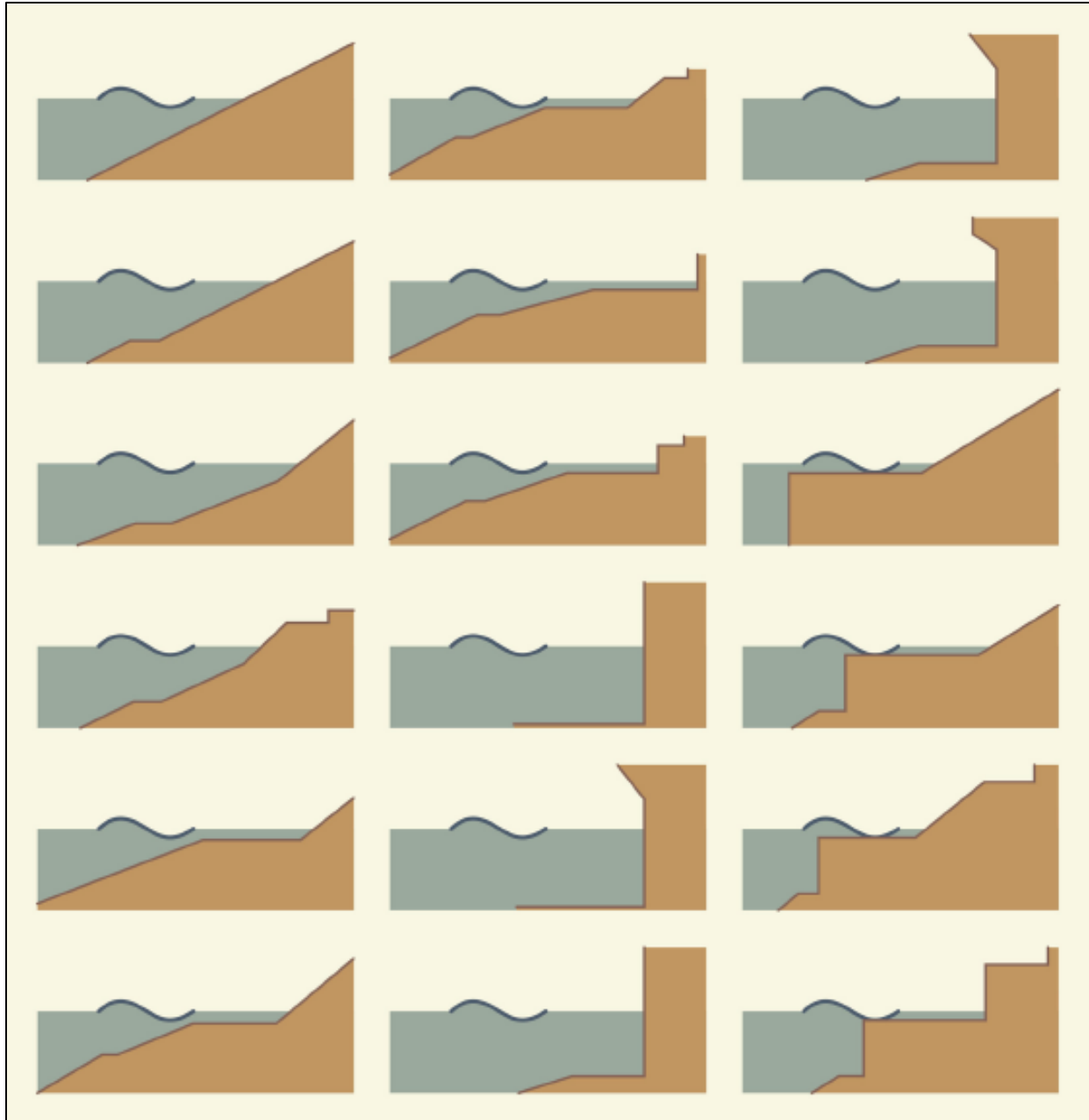


Figure 2-11: Possible structural configurations for EurOtop ANN (EurOtop, 2018)

2.4.3. Japanese wave return wall

Murakami *et al.* (1996) proposed a seawall profile, called the Flaring Shaped Seawall (FSS). The aim of the FSS design was to limit wave overtopping to zero, while still retaining a relatively low wall height. The wall was designed with a deep circular arc cross-section, as shown in

Figure 2-12 (a). The critical crest height was taken as the crest height at which zero overtopping was measured. In the study, the critical crest height, wave pressures and wave forces acting on the wall were investigated with 2D physical model tests.

Murakami *et al.* (1996) found that an increase in the relative water depth (h/H_0) caused the critical crest elevation of the FSS to decrease. They also found that an increase in the relative circular arc depth (D/B) reduced wave overtopping at the FSS. Therefore, the crest height of the FSS could be considerably lower than that of a conventional vertical seawall. As expected, the decrease in crest height brought other benefits, such as less obstruction of the sea view and more space behind and on top of the wall for recreational usage (Murakami *et al.*, 1996).

Kamikubo *et al.* (2003) extended the research on the FSS. The aim was to find a dual solution to reduce both wave overtopping and water spray behind FSSs. Physical and numerical modelling were undertaken to determine the optimum FSS cross-section. Figure 2-12 (a) shows the optimum cross-section, which is to be built with a continuous radius of curvature, a smaller curvature at the top of the wall and a larger curvature at the bottom. Kamikubo *et al.* (2003) also advised that the wall should be built with a footing, to prevent scour at the toe of the structure.

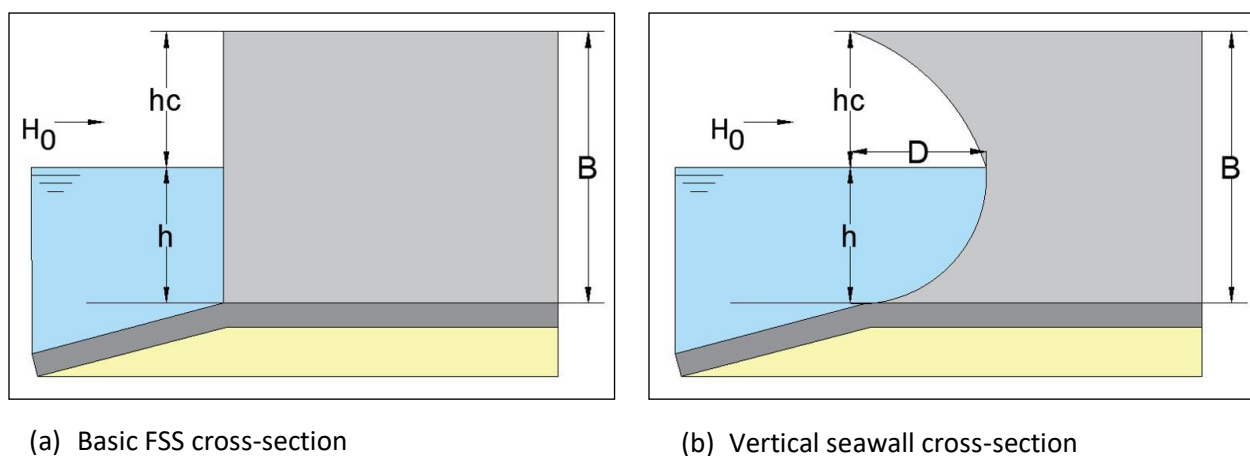


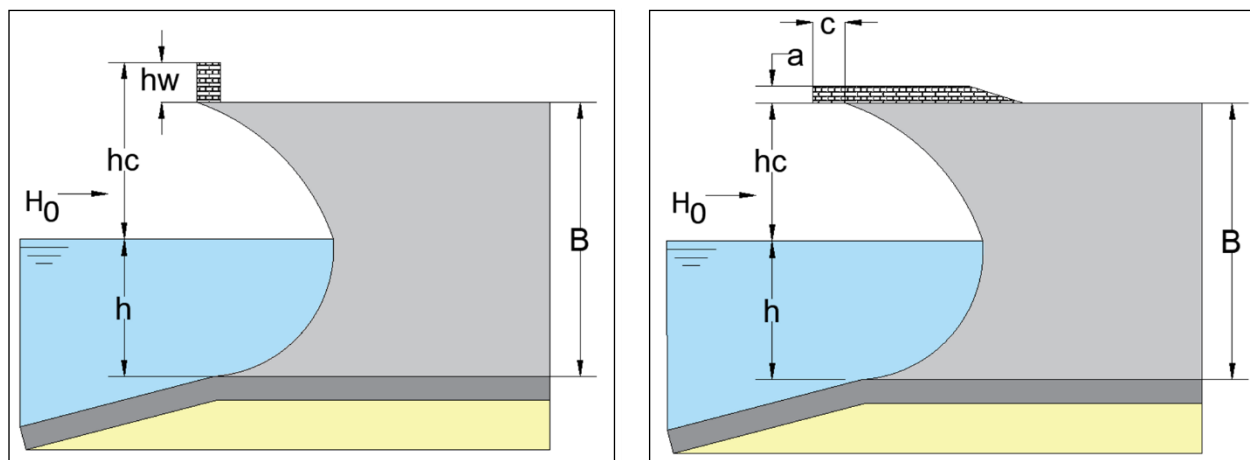
Figure 2-12: Seawalls used in the studies by Murakami *et al.* (1996) and Kamikubo *et al.* (2003)

Kamikubo *et al.* (2003) proposed that a low vertical wall be attached to the tip of the FSS, as shown in Figure 2-13 (a). By physically modelling the FSS and vertical seawall with the low vertical wall on top, they found that the extra low vertical wall was efficient and effective in reducing wave overtopping and water spray behind the FSS (Kamikubo *et al.*, 2003).

Murakami *et al.* (2004) performed an experimental study to determine the critical wave height for a FSS with a mound. During the tests, the water depth and mound height were kept constant, while the sea bottom slope, mound length and wave period were varied. Every time a critical wave height reflected from the seawall, the reflection coefficient and wave pressures at the wall were measured.

Murakami *et al.* (2004) found that a FSS with a mound has a 10 to 20 percent higher relative crest elevation than a FSS without a mound. However, if the mound is inadequately designed, it may cause impulsive wave breaking, which then results in high pressures on the seawall. The mound design, therefore, has to be based on local site conditions, such as the topography and soil type in the vicinity of the seawall (Murakami *et al.*, 2004).

The reflection coefficient was found to decrease with an increasing relative mound length and a decreasing bottom slope, as the breaker type, breaker height and breaking point are all dependant on the specific bed slope (Murakami *et al.*, 2004).



(a) FSS with low vertical crest wall

(b) FSS with extended overhang

Figure 2-13: FSS countermeasures against sea level rise, as proposed by Murakami *et al.* (2008)

Murakami *et al.* (2008) studied the influence that sea-level rise has on hydraulic characteristics like the wave overtopping rate, wave reflection rate, wave pressure distributions and the ability to return a wave offshore, specifically for the FSS.

In order to effectively redirect a wave seaward, the design sea level of the FSS has to be set to the same level as the deepest location on its curved section. If the sea level rises above the design water level for the FSS, its ability to restrict wave overtopping might be reduced, as the space of the curved section, which redirects the wave seaward, is reduced. The wave overtopping rate then gradually increases over time due to the constant rise in sea level (Murakami *et al.*, 2008).

Murakami *et al.* (2008) therefore decided to propose countermeasures to extend the service lifetime of FSSs against the rise in sea levels and subsequent rise in overtopping volumes. The first was to raise the crest by constructing a vertical wall on the FSS's crest. The second countermeasure was to extend the crest's overhang lip seaward. Design drawings of both countermeasures can be seen in Figure 2-13. Performing physical modelling to test the countermeasures, Murakami *et al.* (2008) found that the extended overhang (Figure 2-13 (b)) performed excellently in reducing overtopping, almost recovering the original performance of the FSS. The first countermeasure, shown in Figure 2-13 (a), did not perform suitably, as the vertical wall would have to be raised more than three times the sea level rise.

Murakami *et al.* (2011) then decided to investigate wave overtopping at Flaring Shaped Seawalls due to obliquely incident waves. They performed physical model tests using two different seawall arrangements, which can be seen in Figure 2-14.

Analysis of the results found that the incident wave angle with respect to the seawall clearly influenced the overtopping volume. Under obliquely incident waves, waves ran along the seawall before being reflected seaward. By increasing the incident wave angle, the reflected wave component was decreased, causing the overtopping rate to increase. Under oblique wave attack, the FSS, however, still outperformed the vertical seawall by allowing fewer waves to overtop. Lower overtopping was also experienced for shorter wave periods, while for both seawall arrangements, the overtopping rate was distributed evenly along the seawall. For Series B, which is the second arrangement tested, shown in Figure 2-14, no excess overtopping was experienced around the bend (Murakami *et al.*, 2011).

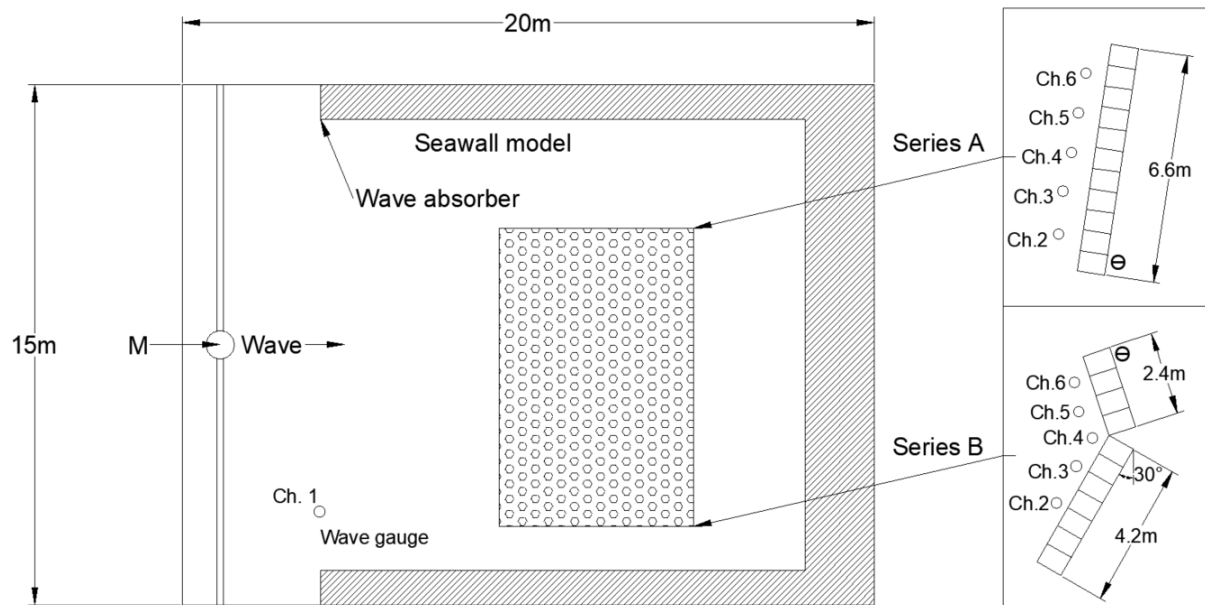


Figure 2-14: Plan view of the seawall arrangements used by Murakami *et al.* (2011) for Series A and B

2.4.4. Effect of the recurve seawall positioning in reducing wave overtopping

Allsop *et al.* (2007) conducted a research study on innovative solutions that could manage overtopping hazards at space-restricted residential and commercial developments along the United Kingdom and Mediterranean coast. In the case study, residential and commercial developments were located close to the harbour edge, besides parts of the coast where the wave attack was worsened by steep foreshore slopes shoaling up longer waves. Occasionally, incident waves at the site were also reinforced by local wind waves.

Four coastal defensive structures, including two vertical and two recurve seawalls, were investigated and compared to achieve the best possible solution. Design drawings of the structures can be found in Figure 2-15 (a) to (d). The preferred strategy was to locate the seawalls as far as possible seaward of the shoreline, thereby creating more space behind the wall to manage the overtopped water. Locating the defensive structures more seaward also simplified the construction of approach slopes to control the wave breaking. Uncertainty, however, existed on whether local authorities would allow the seawall to be built seaward of the high-water line at that time. Therefore, wave overtopping was also measured for seawalls placed on the shoreline (Allsop *et al.*, 2007).

Results from the physical model study proved that in both cases, a recurve wall would be more effective at reducing overtopping than a vertical wall. The recurve wall in Figure 2-15 (c) performed especially well in physical model tests, reducing overtopping by 2 to 9 times more than the corresponding vertical wall. Allsop *et al.* (2007) also observed that when the incoming wave hits the recurve seawall in Figure 2-15 (c), water fills the recurve and then gets redirected back seaward (Allsop *et al.*, 2007).

For the recurve wall placed seaward, as in Figure 2-15 (d), the vertical step at the toe of the wall started acting as a vertical wall during high freeboard conditions. Water was, therefore, projected upwards instead of filling the recurve, thereby essentially losing the beneficial effect of the recurve. The problem was solved by installing an angled fillet at the toe of the wall, which helped guide the waves into the recurve section of the wall (Allsop *et al.*, 2007).

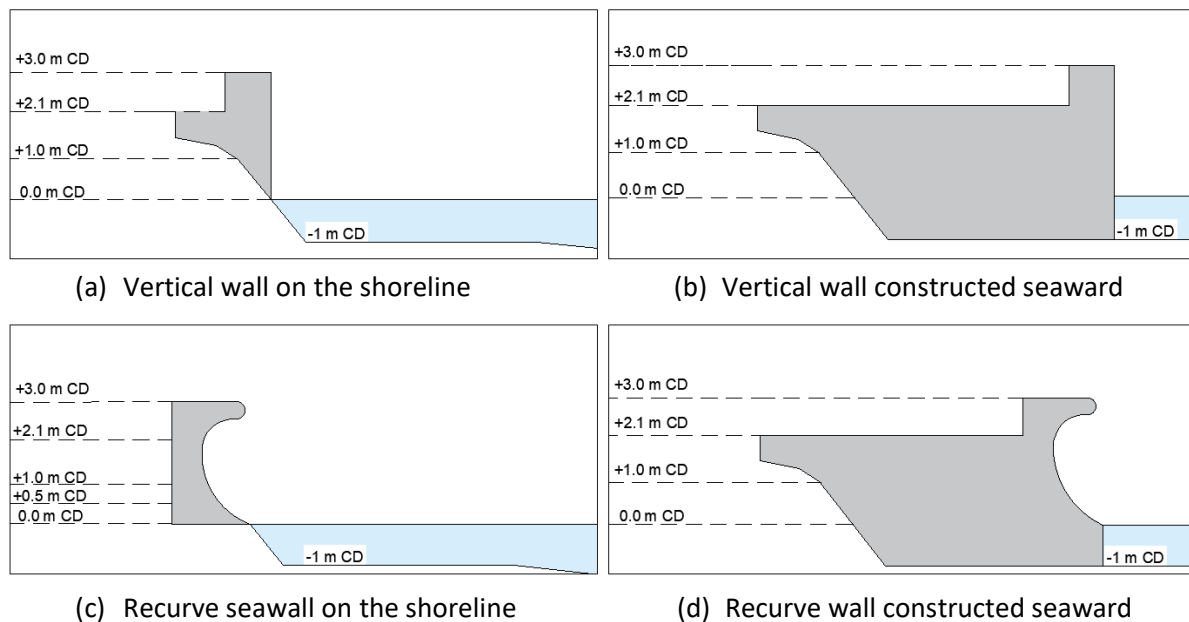


Figure 2-15: Design seawall profiles tested by Allsop *et al.* (2007)

Allsop *et al.* (2007) advised that whenever recurve walls are constructed on the shoreline, the return jet has to be projected past the point of wave breaking, to prevent the projected water from being trapped in the breaking waves, which leads to unwanted air pockets being formed. Also, for very steep shorelines, the recurve section needs to be extended seaward past the wave breaking point. The recurve seawall also had to be designed and constructed as smooth as possible to ensure the most effective return of waves, even at angled shorelines and that if no overtopping was required, both recurve seawall types had to be fitted with additional splash guards (Allsop *et al.*, 2007). A splash guard can be defined as a secondary defensive structure, usually a wall, built landward of a seawall, to protect people, property, vehicles and equipment from flooding imposed by wave overtopping of the coastal defensive structure.

2.4.5. Effect of the parapet angle of a recurve seawall in reducing wave overtopping at smooth dikes

Van Doorslaer and De Rouck (2011) studied the effectiveness of parapet and vertical walls in reducing wave overtopping of smooth dikes. Only non-breaking waves were generated during physical modelling. One of the most important objectives was to determine the optimal parapet geometry.

Van Doorslaer and De Rouck (2011), therefore, decided to look at the influence that the parapet angle (β) and height ratio ($\lambda = h_n/h_t$) have on the reduction of wave overtopping, specifically for the case where a parapet is built into a smooth dike with a 1:2 (V: H) slope. The range of geometrical properties that were tested can be seen in Figure 2-16. Ninety-two tests were performed with several β , h_t and λ combinations.

Figure 2-17 displays the results of the physical model studies for the 50 mm high parapet walls, grouped according to the different parapet nose angles. In the graph, the dimensionless freeboard is plotted against the dimensionless overtopping rate. On the top part of the figure, the correlation coefficient for each parapet nose angle is given.

Figure 2-17 shows that the 45 and 30-degree nose angles provide a similar reduction in wave overtopping. By comparing the reduction factor obtained for the different parapet nose angles, it can be seen that the parapet wall starts performing the same as a vertical wall when the nose angle is increased above 40°.

Van Doorslaer and De Rouck (2011) found that by constructing a parapet at the same crest height as the original smooth dike, a significant reduction in wave overtopping can be achieved. Finally, for design, they recommended that the parapet nose angle should be equal to or smaller than 45° and that the nose height should be approximately a third of the total wall height ($\lambda = 1/3$).

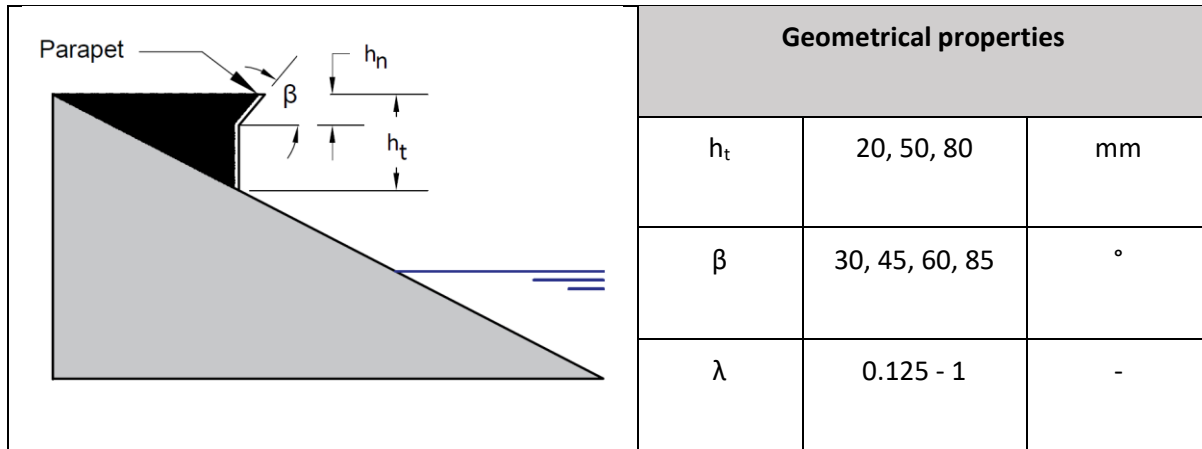


Figure 2-16 Parapet wall definition sketch and model parameters (Van Doorslaer and De Rouck, 2011)

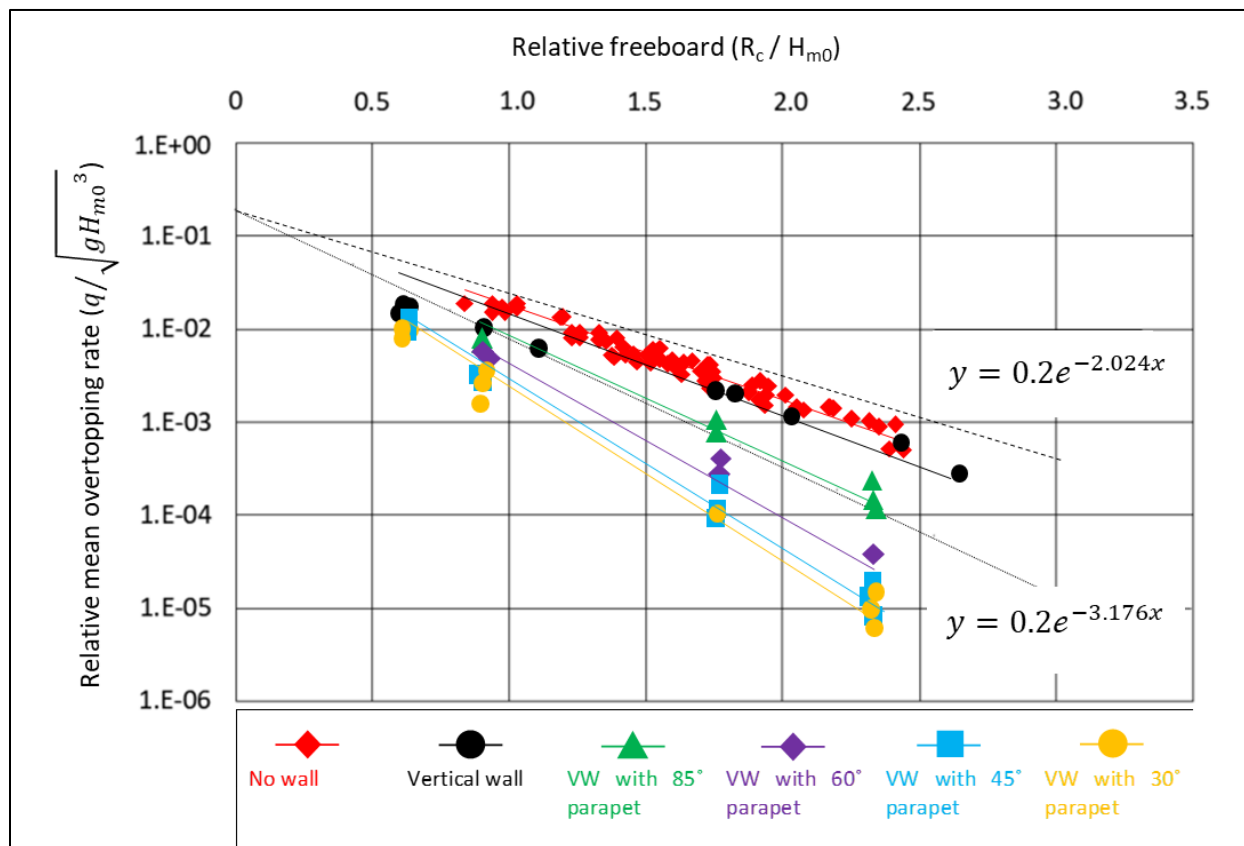


Figure 2-17: Dimensionless discharge versus relative crest freeboard for the 50 mm model wall (Van Doorslaer and De Rouck, 2011)

2.4.6. Effect of the overhang length of a recurve seawall in reducing wave overtopping

Schoonees (2014) classified recurve seawalls into three categories (see Section 2.3) and then went on to study the effectiveness of recurve seawalls, classified as Type 3, which is recurved seawalls where the recurve section is placed on top of a vertical wall. The aim of the research was to determine how effective a recurve seawall, placed at the back of the beach, would be in reducing wave overtopping and to see by how much the recurve wall could be lowered to provide the same reduction in overtopping as a vertical seawall.

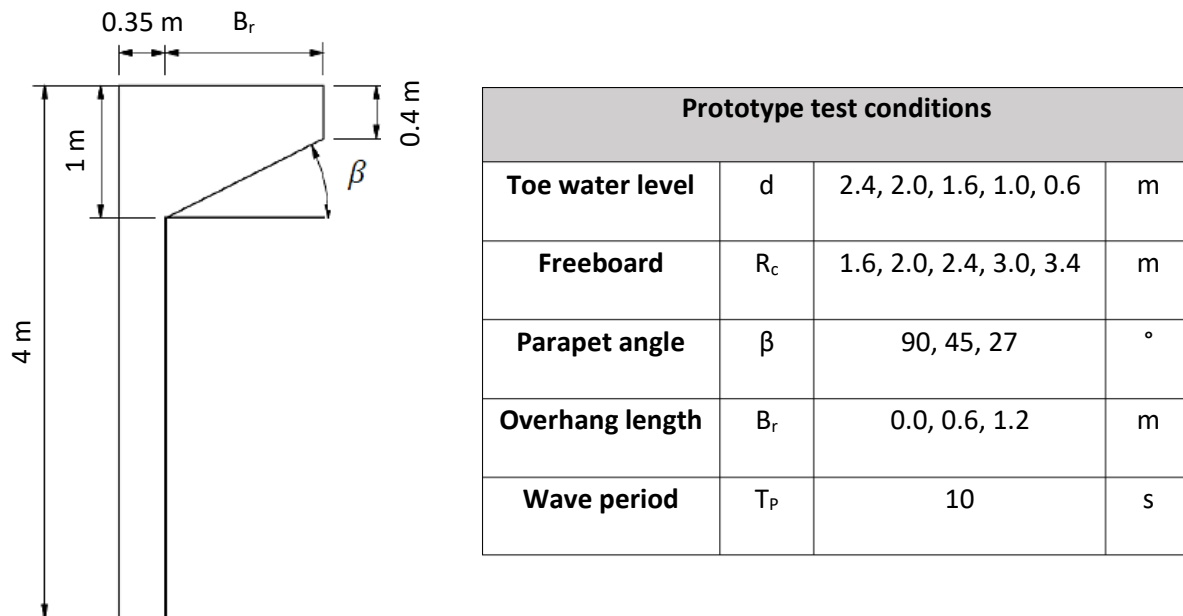


Figure 2-18: Prototype test conditions for the recurve seawalls tested by Schoonees (2014)

Schoonees (2014) performed physical model tests to compare the overtopping at recurve seawalls with conventional vertical seawalls and to determine how the overhang length influenced the reduction of wave overtopping. Two-dimensional physical modelling was done for breaking and non-breaking waves, with a constant prototype wave height of 1 m, a 4 m wall height, a 10 s peak wave period and a bed slope of 1:18.6. The variables were the water- and freeboard levels, the recurve angle and the overhang length. The vertical and recurve seawall designs, with their geometrical properties, are summarised in Figure 2-18.

Comparing the test results, Schoonees (2014), found that both the recurve walls were more effective at reducing wave overtopping than a vertical wall. Recurve seawalls with longer overhangs were found to be better at reducing wave overtopping than seawalls with shorter overhangs. Figure 2-19 visually displays the effect that the overhang length has on the mean overtopping rate. Figure 2-19 also shows that the

overtopping rate typically decreases as the overhang length increases. The overhang length thus has a significant effect on the overtopping reduction provided by recurve seawalls.

At high freeboard levels, where $\frac{R_C}{H_{m0}} > 2.2$, the overtopping for both recurve walls were found to be similar, as both walls reflected all the water from the reflecting waves back seaward. For a decrease in relative freeboard, overtopping increased and the difference in overtopping between the two recurve profiles became more apparent. Although the functionality of the recurve overhang becomes less during lower freeboard conditions, where $\frac{R_C}{H_{m0}} \leq 1.4$, both recurve seawalls still proved to be much better at reducing wave overtopping compared to the vertical seawall.

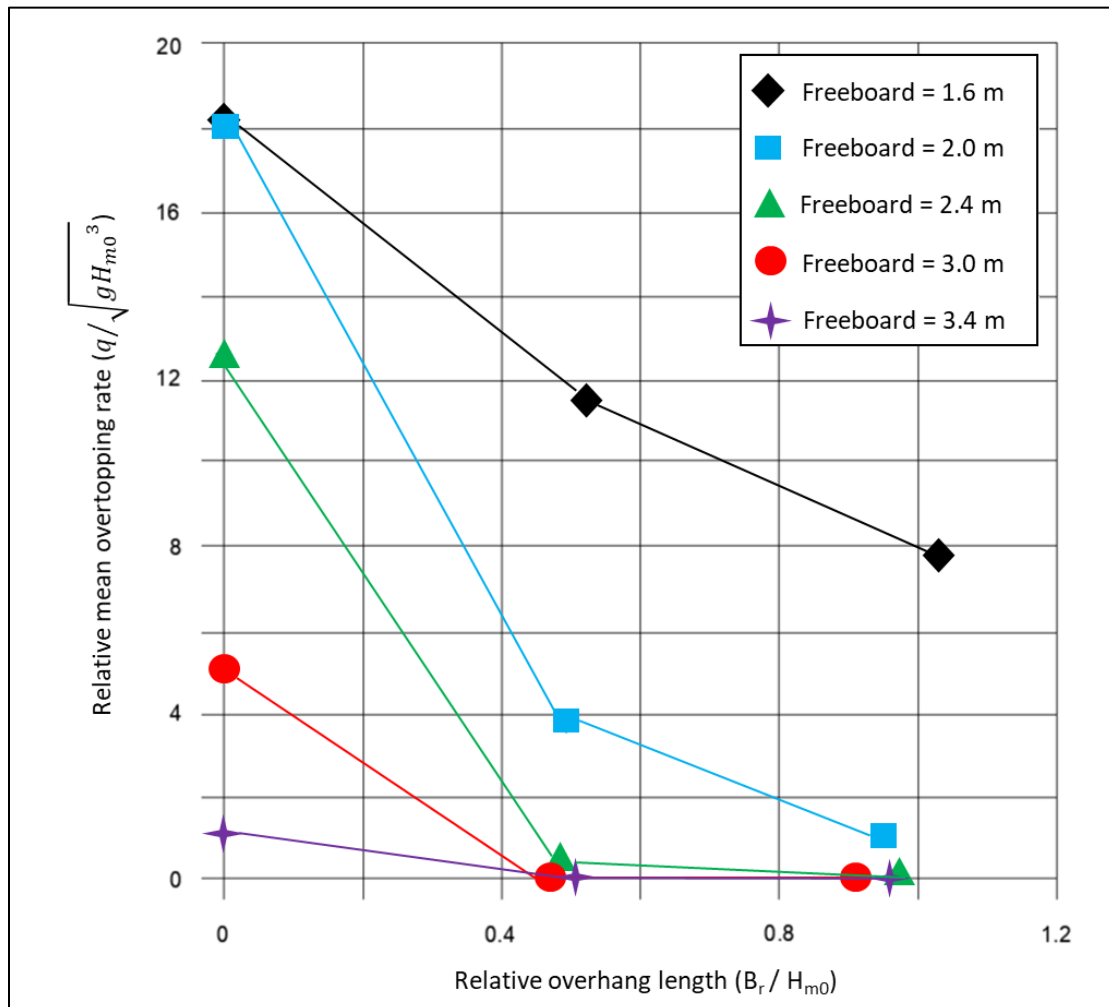


Figure 2-19: Effect of overhang length on the mean overtopping rate (Schoonees, 2014)

Schoonees (2014) repeated a test with the same wall design and water level, but with different peak periods, to find that the overtopping rate was sensitive to an alteration in the peak wave period. However, she suggested that more tests are necessary to validate the results and to research other possible factors that could have an influence on wave overtopping at recurve seawalls.

Swart (2016) continued on the work done by Schoonees (2014) by investigating the influence that the overhang length and freeboard height has on reducing wave overtopping at recurve seawalls. To determine the impact that the overhang length and freeboard have on wave overtopping, physical modelling was done in the 2D wave flume at Stellenbosch University. Tests were done for breaking and non-breaking waves, with a constant prototype wave height of 1 m, a wall height of 4 m and a bed slope of 1:18.6. The variables were the water- and freeboard levels, the wave period, parapet angle and the overhang length. The recurve seawall profile, along with the test variables can be found in Figure 2-20.

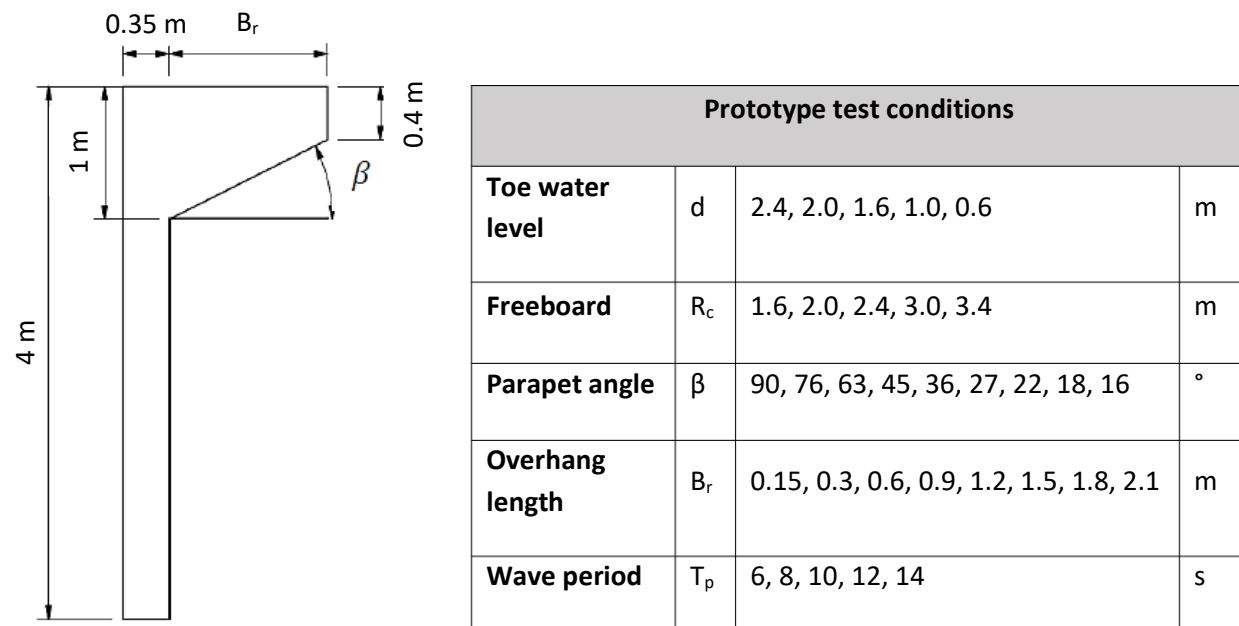


Figure 2-20: Prototype test conditions for the recurve seawalls tested by Swart (2016)

Figure 2-21 visually displays the results of the study as the overtopping discharge ($q/(gH_{m0}^3)^{0.5}$) against the relative crest freeboard (R_c/H_{m0}). From the results, Swart (2016) found that with an increase in overhang length, the overtopping reduction increased, but only up to a specific overhang length, from where the increase in overhang length didn't lead to any further reduction in overtopping. The overhang length was different for each water level and wave period. Swart (2016) also found that under some conditions, the

0.15 m and 0.30 m overhang lengths experienced more overtopping than a vertical wall. Recurve walls with parapet angles larger than 50° also did not provide any better reduction in wave overtopping, compared to vertical seawalls.

It was also established that the crest- and freeboard levels are the most critical parameters to consider when designing a recurve seawall. Results showed that an increase in water depth (decrease in freeboard) led to an increase in wave overtopping. At low freeboard levels, the 0.15 m, 0.30 m and 0.60 m overhangs were found to be the most sensitive to changes in the wave period. For tests in which the incident wave heights were larger than the water level, the wave period had a minimal impact on the overtopping rate. For shorter wavelengths, the volume of water caught up in the waves is less and therefore they were easily reflected. For some of the larger wavelengths, however, the first wave is reflected seaward after which the reflected wave superimposes with the next incoming wave, creating a large single overtopping event (Swart, 2016).

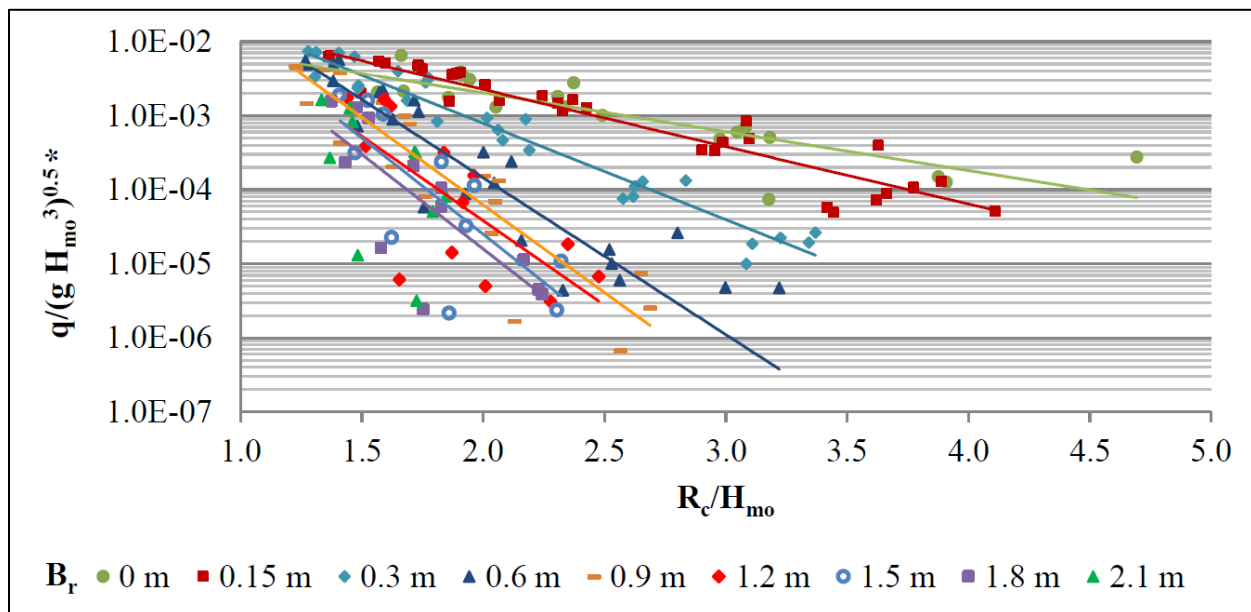


Figure 2-21: Overtopping comparison of overhang lengths tested (Swart, 2016)

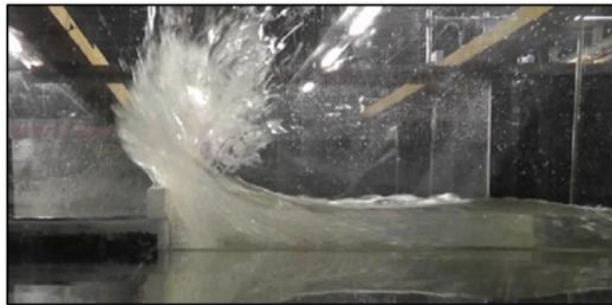
*Note the overtopping rate is in $\text{m}^3/\text{s}/\text{m}$.

In conclusion, Swart (2016) recommended that the recurve seawall's freeboard should be large enough for incoming waves to collide with the vertical part of the wall, thereby ensuring that the wall does not become submerged, which would cause the recurve section to become ineffective. A properly designed recurve seawall, with a high freeboard and low toe water level can produce overtopping reduction up to 100 percent.

2.4.7. Effect of the recurve seawall geometry in reducing wave overtopping

Veale *et al.* (2012) performed research to find the optimum geometry for the design of a new wave return wall which was to be built on top of the existing sea dike at Wenduine, Belgium. Research objectives were to find a return wall design that would integrate aspects of engineering safety, architectural design, urban planning and community requirements. The crest level needed to be kept as low as possible as per community requirements but also needed to restrict overtopping to acceptable limits.

In the study by Veale *et al.* (2012), a parapet wall refers to a triangle shape fitted to a vertical wall, as shown in Figure 2-22(b). The parapet design chosen were based on the geometry outlined in a report by Van Doorslaer and De Rouck (2011). The parapet nose angle (β) was chosen as 50° , while the λ ratio was varied with sea water level. On the other hand, a recurve wall has a curved seaward face, as shown in Figure 2-22(c). Figure 2-22 shows the three wall profiles that were tested, along with their response to wave impact during the largest overtopping event. All the walls have a prototype height of 1.2 m (Veale *et al.*, 2012).



(a) Plain vertical wall
 $q = 8.2 \text{ l/s/m}$



b) Vertical wall with parapet overhang
 $q = 5.0 \text{ l/s/m}$



b) Vertical wall with recurve overhang
 $q = 5.0 \text{ l/s/m}$

Figure 2-22: Wall profiles tested by Veale *et al.* (2012)

The mean overtopping rate for each wall profile, as determined from physical model study, is included below its respective figure. Veale *et al.* (2012) found that the parapet- and recurve wall provided about the same reduction in overtopping, both performing better than the vertical wall. Figure 2-22 shows the reason for the effectiveness of the recurve and parapet walls, namely that they reflected the incoming waves seaward, instead of upwards, like the vertical wall in Figure 2-22(a).

Kretschmer (2017) investigated the effectiveness of different overhang shapes on the reduction of wave overtopping at recurve seawalls. Through 2D physical modelling, the effectiveness of the different shapes was determined by comparing the reduction in overtopping delivered by each overhang shape. Figure 2-23 shows the five overhang forms that were tested during physical modelling, at different water levels and wave periods. The schematizations for all the recurve walls tested are included in Appendix A.3.

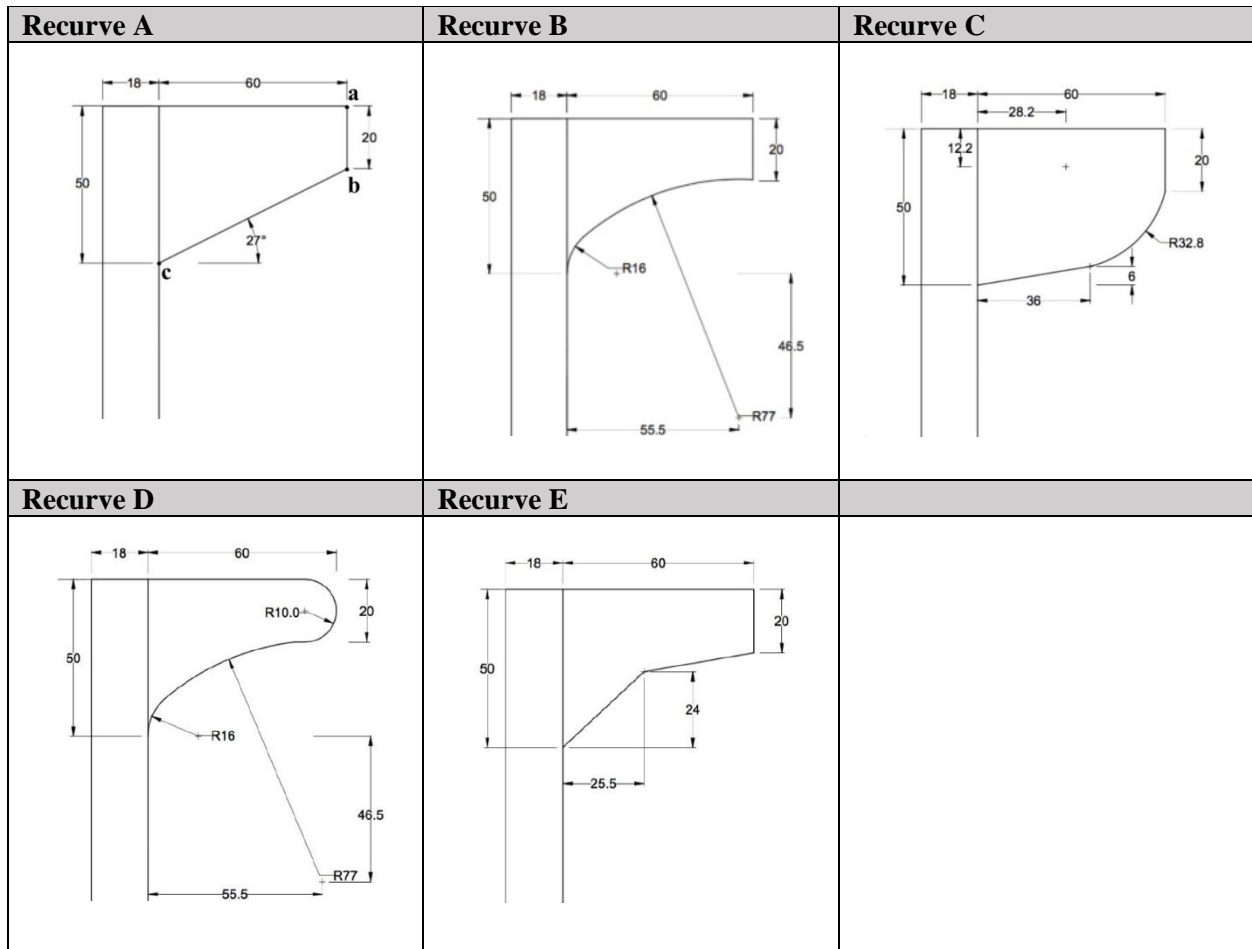


Figure 2-23: Recurve shapes tested by Kretschmer (2017)

The coordinates of the three points marked a, b and c, in Figure 2-23, were kept the same for all the recurve shapes, to maintain a constant overhang length and height for all the recurves. The principal dimensions, along with the prototype test conditions can be seen in Figure 2-25.

Kretschmer (2017) confirmed the finding of Swart (2016) stating that the rate of overtopping is particularly sensitive to a change in freeboard- and water level. For most recurves, a gradual increase in overtopping occurred between the water depths of 0.6 m and 2.0 m. A significant increase in overtopping occurred between the water depths of 2.0 m and 2.4 m, as the incident waves started to submerge the wall regularly, which lead to a reduction in the wall's reflective capacity and consequently to more green water overtopping. At high freeboard levels, small volumes of overtopping were observed due to the colliding incident and reflected waves close to the toe of the structure. Overtopping at high freeboard levels mostly occurred as white-water spray, which was negligibly small but could increase considerably with the presence of onshore wind (Kretschmer, 2017).

In contrast with Roux (2013), results showed that overtopping increased with an increase in wave period, up to a peak period of 14 s, whereas Roux (2013) found that the overtopping increased with an increase in wave period, but only up to a peak period of 12 s, after which overtopping started to reduce (Kretschmer, 2017).

After analysis of the test results in Figure 2-24, Kretschmer (2017) concluded that the shape of the overhang has a significant impact on the overtopping reduction capabilities of recurve seawalls. Results showed that overtopping generally increased with an increase in the wave return angle of the recurve seawall, that being the angle at which the reflected water jet leaves the recurve section. By comparing the performance of the two concave-shaped overhangs, Kretschmer (2017) discovered that the concave overhang with the rounded edge (Recurve D) produced up to fifty per cent more overtopping than the recurve with the squared overhang edge (Recurve B). The increased overtopping at Recurve D was ascribed to the strong adhesion forces of water on the rounded edge of the overhang, which helped water travel along the face of the recurve, still adhered to the surface until it overtopped the crest of the structure.

Kretschmer (2017) therefore concluded that the square-edged, concave-shaped overhang, shown in Figure 2-25, was the most effective recurve shape in reducing wave overtopping and that apart from the overhang length, the overhang shape also significantly influences the reduction in overtopping at recurve seawalls.

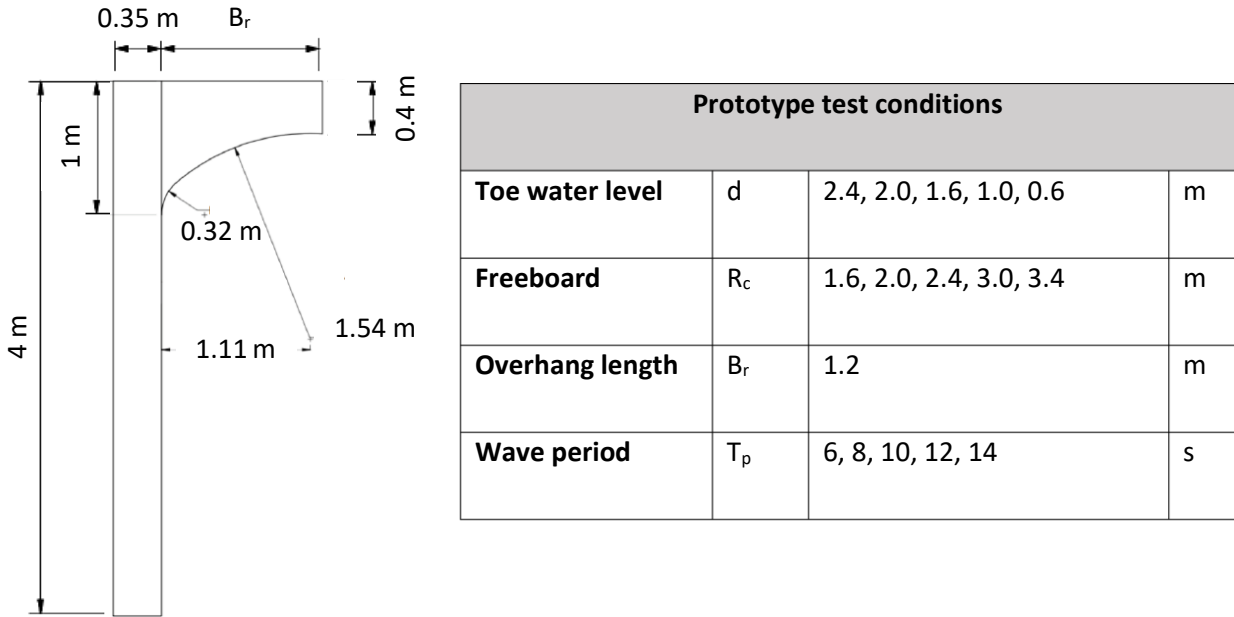


Figure 2-25: Prototype test conditions for the square edged, concave shaped recurve overhang tested by Kretschmer (2017)

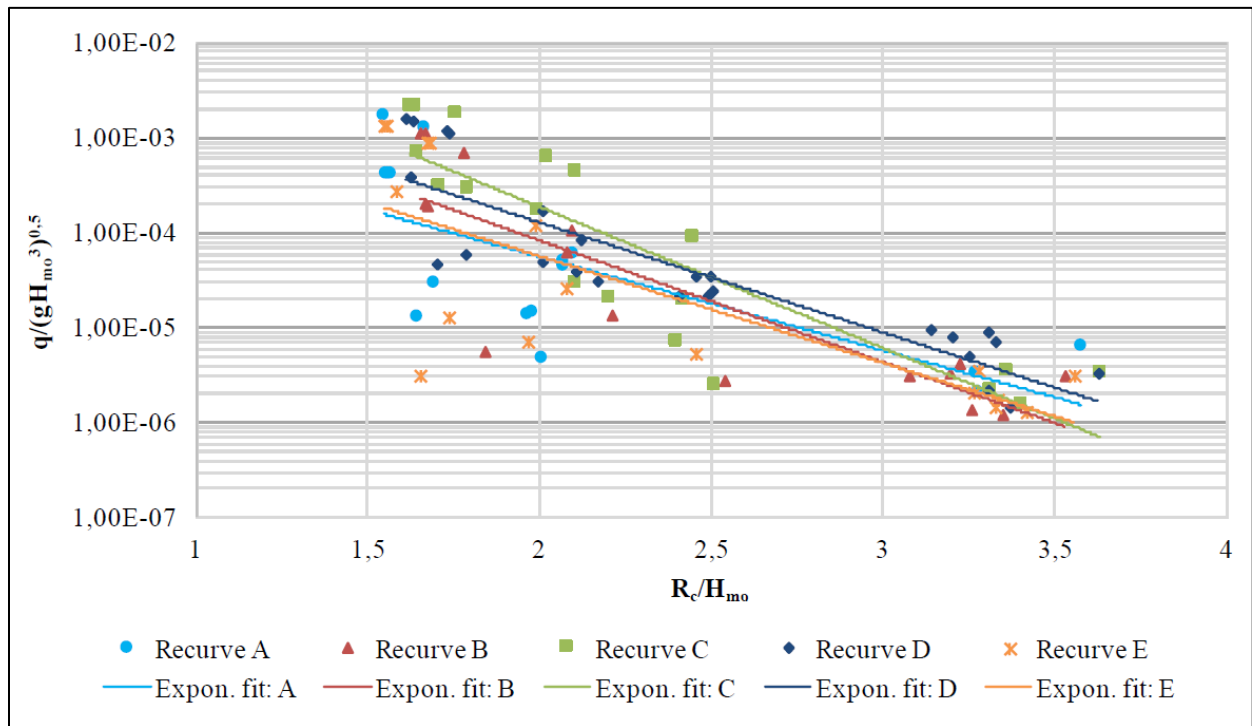


Figure 2-24: Overtopping comparison of overhang shapes tested (Kretschmer, 2017)

*Note the overtopping rate is in $m^3/s/m$.

2.4.8. Effect that the addition of a kerb has on overtopping of recurve seawalls

Walker (2018) studied the effect that a kerb on top of a recurve seawall will have on the reduction of overtopping at the wall. A secondary objective was to determine the effect that chamfering has on the overtopping of a recurve seawall. To achieve the objectives, Walker (2018) conducted 2D physical modelling tests in the same wave flume and on the same bed slope as Schoonees (2014), Swart (2016) and Kretschmer (2017). The seawall configurations that were tested are shown in Figure 2-26.

Results proved that placing a kerb on top of the recurve wall could provide a significant reduction in overtopping, especially at low freeboards. At high freeboards, the extra reduction in overtopping provided by the kerb was found to be minimal. The type of overtopping, governed partly by the freeboard level, therefore had a significant impact on the effectiveness of the kerb. At low freeboard levels, where green water overtopping is the primary form of overtopping, the kerb proved to be very effective. At high freeboard levels, where white water overtopping dominated, the kerb proved to be less effective. The wave period was, however, found to have a minimal impact on the effectiveness of the kerb (Walker, 2018).

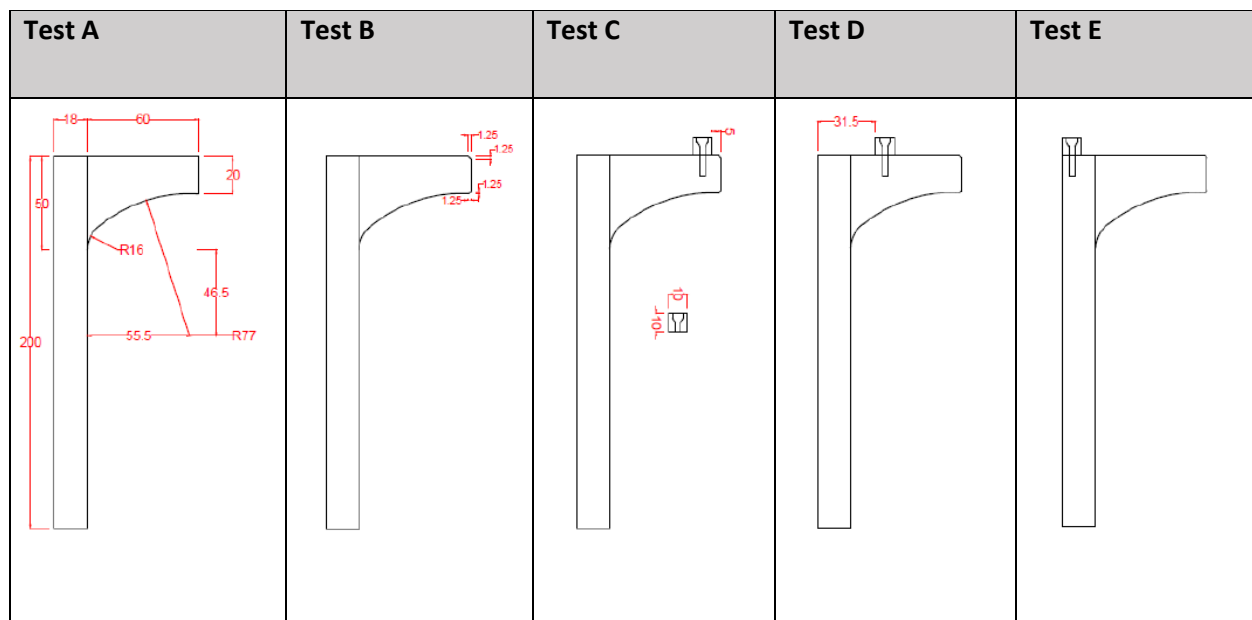


Figure 2-26: Recurve wall set-ups and dimensions tested by Walker (2018)

Results indicated that chamfering of the overhang edges resulted in a significant lowering of the overtopping reduction capabilities of the recurve seawall. Like Kretschmer (2017), Walker (2018) ascribed the increase in overtopping to the strong adhesion of water to the chamfered edge, which helped water to travel along the face of the recurve until it overtopped the crest of the structure (Walker, 2018).

Because an irregular wave spectrum was generated by the wave paddle, small variations in the wave heights were inevitable. By comparing the wave height variations and the accompanying overtopping rates, Walker (2018) found that a small change in wave height had a significant impact on the overtopping rate. Just as Kretschmer (2017), but contradictory to Roux (2013), Walker (2018) found that an increase in wave period led to an increase in overtopping. Like the previous studies by Schoonees (2014), Swart (2016) and Kretschmer (2017), Walker (2018) also found that irrespective of the wave period, the overtopping rate increased with an increase in water level.

Walker (2018), therefore, recommended that wherever green water overtopping presents a danger for pedestrians, traffic and structures, a kerb should be fitted flush with the back of the recurve seawall, thereby providing a simple and cost-effective solution to reduce overtopping and also extending the service life of the structure. Secondly, Walker (2018) recommended that the chamfering be kept as small as possible during construction.

2.4.9. Effect of the beach slope on the overtopping of a recurve seawall

In 2013, Roux extended a study performed by a private company, whose aim was to find a solution to the overtopping experienced at the Strand seawall on the False Bay coast in South Africa. The company conducted 2D physical modelling tests to determine the effectiveness of their proposed solution, which was to install a recurve seawall (Figure 2-27) at the back of the beach. Roux (2013) focused his study on the following factors:

1. The effect that changes to the beach slope has on the overtopping of the proposed recurve seawall. Factors changed include the beach slope, beach width and beach level.
2. The effectiveness of the proposed recurve seawall in terms of overtopping reduction capability, compared to the performance of a vertical seawall.
3. The influence that the wave period has on the overtopping rate.

Through numerical modelling, Roux (2013) discovered that incoming waves at Strand were depth limited and very susceptible to changes in the water depth. By changing the beach level in the model, Roux (2013)

discovered that the wave height at the toe of the seawall also changed. The different beach slopes tested can be seen in Figure 2-28. Physical modelling proved that for pulsating wave conditions, gently sloped beach slopes (1:50) had a higher overtopping rate than the steeper beach slopes (1:10), as displayed in Figure 2-29. Impulsive wave conditions were also found to be much more sensitive to a change in freeboard and toe water level than the pulsating wave conditions (Roux, 2013).

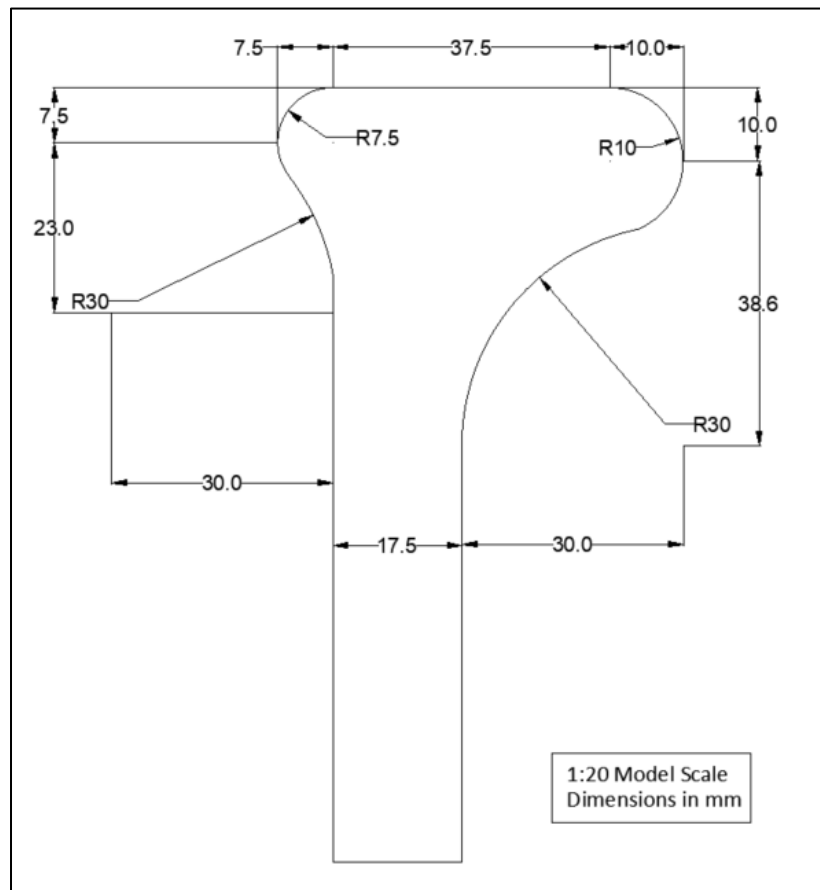


Figure 2-27: Model recurve seawall design tested by Roux (2013)

To reduce overtopping, the beach level had to be increased to a level where the water depth was shallow enough to induce wave breaking before reaching the seawall. When the beach level was increased, but the water was not shallow enough to induce wave breaking, the overtopping rate increased, as the waves, enlarged by shoaling, were allowed to reach the back of the beach without breaking (Roux, 2013).

The recurve seawall reduced overtopping by about 50 percent compared to a vertical wall, with the reduction factor dependent on the specific wall height. Overtopping was found to increase with wave

period up to a prototype period of about 12 s, after which the wavelength became too long, resulting in the waves breaking offshore and thereby reducing the overtopping rate.

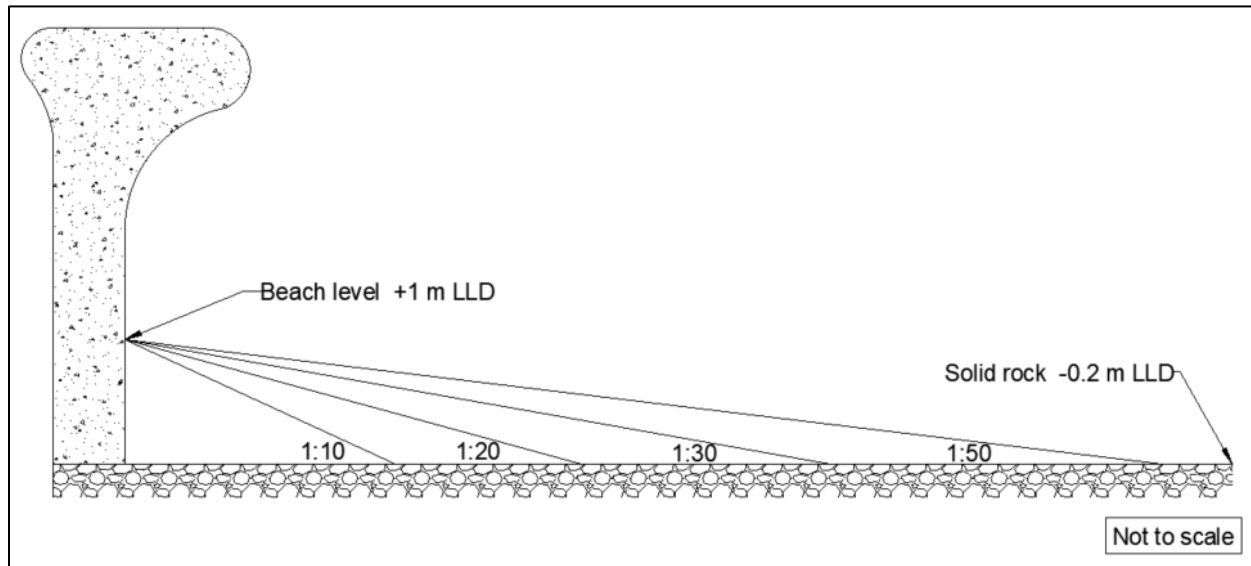


Figure 2-28: Beach slopes tested by Roux (2013)

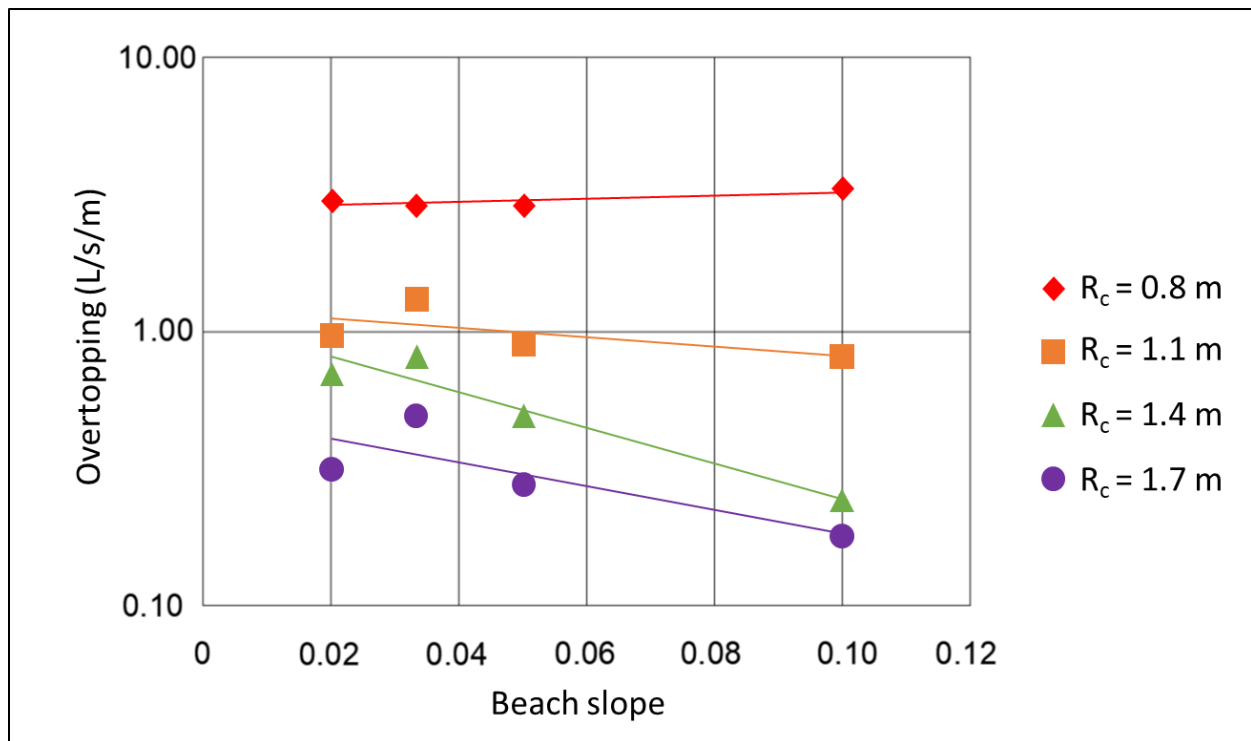


Figure 2-29: Influence of different beach slopes on recurve seawall overtopping (Roux, 2013)

2.5. Typical Southern African nearshore profiles

As the influence of the nearshore profile on wave overtopping at recurve seawalls had to be studied, a number of nearshore profiles around the Southern African coast was collected. Nearshore profiles chosen were to have as little as possible influence from coastal features such as islands, rocky outcrops, rocky shores or pebble beaches. However, due to the difficulty of surveying in the surf zone, not many documented nearshore profiles of Southern Africa exist. But because the nearshore profiles collected are realistic, and not simplified, profiles measured 50 years ago is still valid to be used for modelling today.

Due to the highly dynamic nature of the nearshore zone, any changes made to the profile dimensions for simplification of the physical modelling, would lead to unrealistic nearshore profiles that does not exist in nature. For example, if the profile dimensions would be altered in practice, the altered profile would simply be converted back to its natural state by the local wave environment. Therefore, nearshore profiles were chosen to represent certain typical Southern African nearshore profiles. The locations of the nearshore profiles chosen are shown in Figure 2-30.

A small-craft harbour development was proposed for Swakopmund in 2005. CSIR was approached to investigate the technical feasibility of the proposed harbour with regards to sedimentation. The study made use of several bathymetric surveys done from 1970 to 1972. Surveys for profiles 42, 43, 44, 45 and 46 were completed in November 1970, February 1971, May 1971, August 1971, November 1971, February 1972 and July 1972 (Schoonees *et al.*, 2005). The average of all the nearshore profiles measured at the 46th marker, included in Figure 2-31, was chosen as a representative of the Swakopmund nearshore, as it is located on an exposed part of the coast, with minimal anthropogenic influences, and because the marker is located more than 5 km away from the Swakop River Mouth the profile will not be variable due to fluctuations in the longshore sediment transport volumes.

The Walvis Bay nearshore profiles were measured in 1999, when Schoonees *et al.* (1999) studied the possibility of the Walvis Bay sand spit being breached at Donkey Bay. Modelling of the changes in the beach profiles before and after storms were done and conceptual measures proposed to prevent breaching. As the nearshore profile measured before the storm is representative for a larger part of the year, the profile shown in Figure 2-31 was chosen as a representative nearshore profile for Walvis Bay.

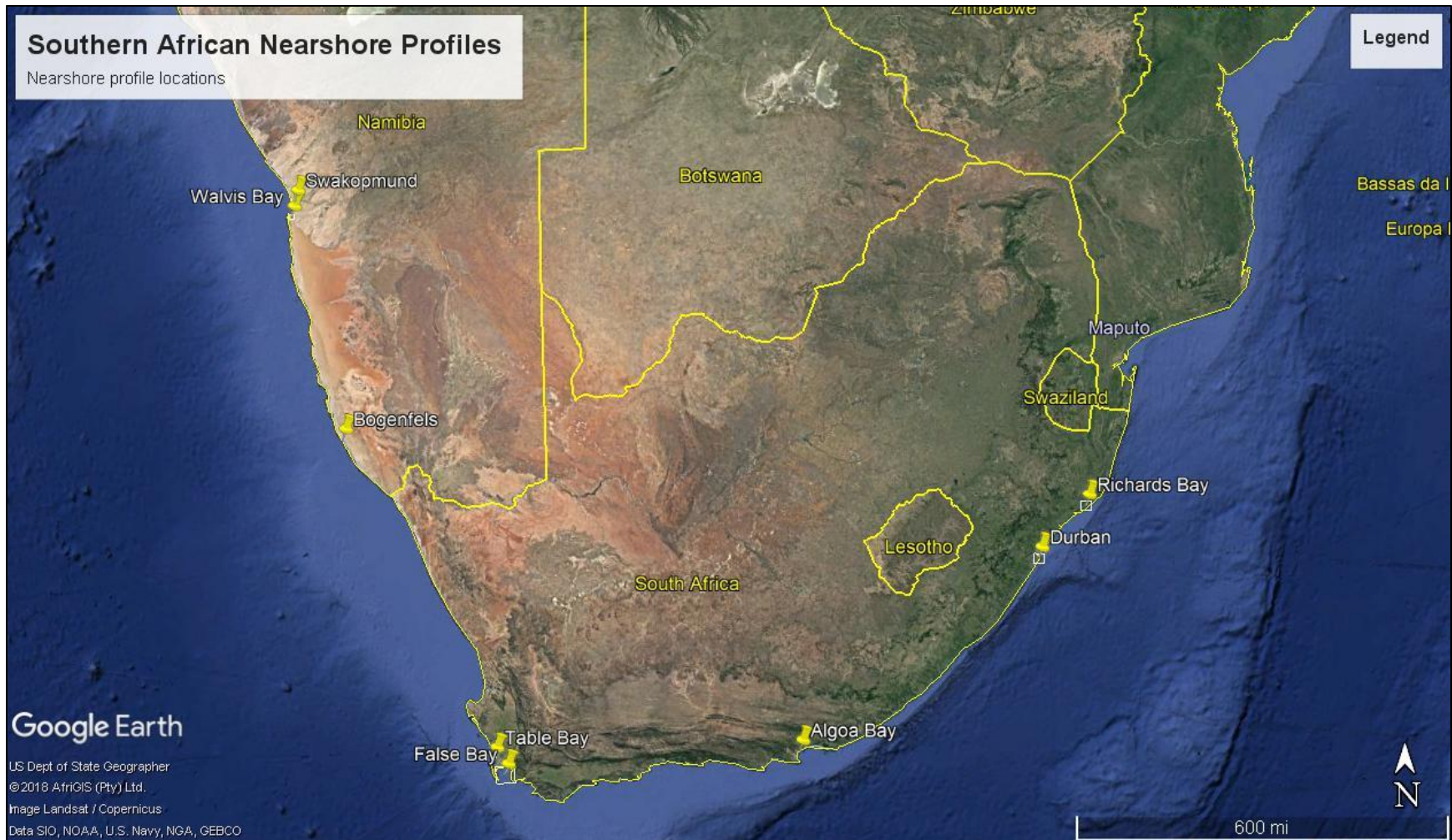


Figure 2-30: Locations of typical nearshore profiles of Southern Africa (US Department of State Geographer, 2018)

Soltau (2009) studied the cross-shore distribution of the sediment grain size in the longshore transport zone at Bogenfels. Bogenfels is located in southern Namibia, a coastline which is exposed to severe wave conditions throughout the year. The area is known for its series of sandy beaches with some rocky headlands. Some limited bathymetric surveys were obtained during the research study, which was done for mining in the area. A representative nearshore profile obtained from a survey in May 2002, is shown in Figure 2-31.

Soltau (2009) also conducted field measurements at four locations along Table Bay between September 2005 and September 2006. Table Bay is located on the northern edge of the Cape Peninsula, facing westward towards the Atlantic Ocean. The bay is sheltered from the main southwest swell in the southern corner, but opens up to the north. The nearshore profiles for the northern beaches in Table Bay (Lines A and B), which is the more exposed part of the coastline, were considered as possible nearshore profiles to be tested. Line A is an exposed beach with powerful collapsing and surging waves breaking on the beach step. Line B represents a partly exposed beach with plunging and collapsing waves typically experienced. Nearshore profiles A and B are shown in Figure 2-31.

The CSIR was approached by the consulting firm O'Connel, Manthé and Associates to carry out a study regarding the possibility of improving the bathing conditions at some locations in False Bay. A detailed bathymetric survey was subsequently done for the False Bay coast. Of the 36 locations surveyed, profile T14, included in Figure 2-31, was chosen to be a representative nearshore profile for False Bay. Profile T14 is located slightly west of the halfway mark between Kapteinsklip and the Strandfontein tidal pool, meaning the wave dynamics and beach accretion or erosion due to anthropogenic influences would be low. No rock were present in the area of the nearshore profile (Swart *et al.*, 1983).

In September 2002, prior to the construction of the Port of Ngqura in South Africa, beach monitoring surveys were done to obtain the pre-construction beach profiles. To obtain a pre-construction profile, Rutherford (2015) calculated an average nearshore profile from those measured by PRDW and Gibb Consulting (PRDW *et al.*, 1997). Both profiles were measured close to the Ngqura sand bypass system. The profiles above and below mean sea level were combined to form a representative nearshore profile pre-construction of the port. The final profile is included in Figure 2-31.

Durban nearshore profiles were obtained from bathymetric surveys done by the CSIR while looking at restoration schemes for the Durban beaches between 2006 and 2009. Several nearshore profiles were available, but the profile at marker CD, north of the Bight was chosen, as the nearshore profile had the least amount of anthropogenic influences. The sediment transported by the Mgeni River was also assumed to be minimal, as the five large dams in the river trapped 87% to 100% of the sand load in the river between 1965 to 1988. In addition, the primary longshore sediment transport direction was to the north and away from profile CD (Theron, 2016). The nearshore profile at marker CD is shown included in Figure 2-31.

In a study by Schoonees *et al.* (2008), storm induced beach profile changes were modelled at stations SB10 and SB26, south-west of the Richards Bay harbour. Profile SB10 is included in Figure 2-31. Another Richards Bay nearshore profile was obtained from Theron (2016). The profile, shown in Figure 2-31, is an averaged profile which was calculated from the available beach and bathymetric surveys done for the Richards Bay coast. In the study, Theron (2016) numerically simulated a September 1990 storm event to calculate the maximum horizontal erosion, from which the coastal setback lines were developed.

Figure 2-31 summarises the 11 nearshore profiles that were collected. For the graph, all the profiles had to be moved relative to mean sea level (MSL). To move the profiles that were measured relative to chart datum (CD), the tide tables, compiled by the South African Navy, were used. The MSL relative to CD of Durban and Richards Bay is included in Table 2-3 (SA Navy, 2018).

Table 2-3: Tidal levels (SA Navy, 2018)

Place	LAT	MSL
Durban	0.00	1.11
Richards Bay	0.00	1.20

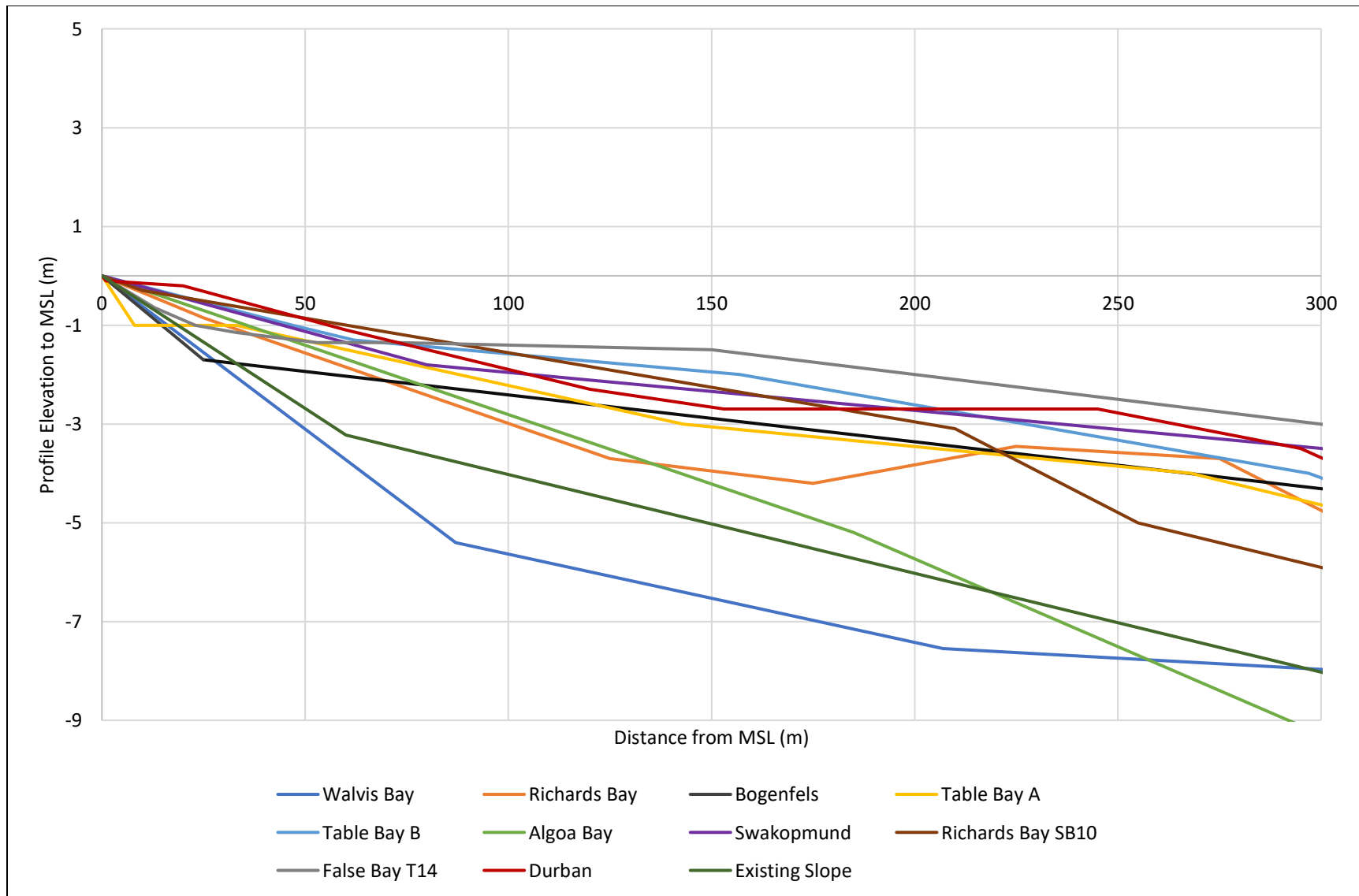


Figure 2-31: Typical Southern African nearshore profiles

2.6. Physical modelling in previous wave overtopping studies

2.6.1. Overview

Physical modelling is the reproduction of a physical system, usually at a reduced scale, with the purpose of reproducing the major dominant forces acting on the system in correct proportion to the actual physical system. It gives the researcher the opportunity to develop a complete, all-inclusive view of the nearshore processes of the modelled area, without too much simplification (Hughes, 1993).

Physical models provide a good alternative to large scale field measurements, as their small scale permits easier and cheaper data collection, while still incorporating all the important factors necessary for accurate decision making. Numerical and analytical models, on the other hand, require many simplifying assumptions, causing the researcher to lose the holistic view needed especially in nearshore modelling. The researcher should nonetheless take into account all possible laboratory and scale effects when designing a physical model (Hughes, 1993).

2.6.2. Laboratory and scaling effects

Due to limiting factors, such as laboratory and scale effects, physical model studies are unlikely to ever exactly replicate a field study. Scale effects arise due to the impossibility of having similitude of all the relevant forces in the physical model. Laboratory effects arise due to the impossibility of simulating all the prototype conditions in a physical model. Examples of laboratory effects include the effect of solid model boundaries or the inability to accurately simulate the effect of wind and currents in a physical model (Hughes, 1993).

When describing scaling relationships in physical modelling, the terms similitude and similarity are often used. Similitude criteria, also referred to as scale laws, describe the mathematical relationships between a parameter in the prototype to the same parameter in the model. Similarity refers to the way in which the prototype and physical models behave in the same way, irrespective of their adherence to similitude criteria (Hughes, 1993).

As the purpose of this study is to model the overtopping of recurve seawalls over different nearshore profiles, the dominant forces influencing the waves and the overtopping behaviour will be gravitational and inertial forces. Therefore, Froude's criterion of similitude will be used as scaling law, as the Froude criterion is primarily intended for model studies where inertial and gravitational forces dominate.

Hughes (1993) substantiated the choice of using the Froude criterion of similitude by suggesting that vertical-wall structures should be designed and operated according to the Froude criterion of similitude.

The Reynolds law is used in physical modelling where dynamic similarity of inertial and frictional forces is required. But because the similarity requirements posed by the Froude and Reynolds laws can typically not be satisfied simultaneously, only Froude scaling will be used. The general Froude scaling ratio is provided in Equation 2.4.

$$N_x = \frac{X_p}{X_m} = \frac{\text{Value of } X \text{ in prototype}}{\text{Value of } X \text{ in model}} \quad (2.4)$$

A summary of the Froude and Reynolds scale ratios are provided in Table 2-4. According to Hughes (1993), the primary laboratory effects experienced in short-wave modelling are caused by:

- Physical limitations placed on the flow by the model boundaries.
- Using a mechanical wave generator, which causes unintentional nonlinear effects.
- The simplification of natural processes and forces.

Hughes (1993) also found that generating waves in a two-dimensional wave flume can lead to the development of unintended raised amplitudes, groups of waves, cross waves or unintended long waves.

Another laboratory effect experienced in a two-dimensional wave tank is the re-reflection of waves from the wave paddle (Hughes, 1993). In real-life circumstances, incident waves moving toward a beach or structure would be reflected by the structure, causing the reflected waves to travel into the ocean indefinitely. However, in a two-dimensional wave tank, the incident waves are reflected off the structure only to be re-reflected from the wave paddle back towards the structure. The most effective mitigation against the re-reflection of waves was found to be a wave generator fitted with active wave absorption which detects and then absorbs any reflected wave (Hughes, 1993). As the wavemaker at Stellenbosch University's Hydraulic Laboratory is equipped with active wave absorption, no other mitigation measure against the re-reflection of waves were required.

Table 2-4: Similitude ratios for Froude and Reynolds scaling laws, after Hughes (1993)

Characteristic	Froude	Reynolds	Dimension
Geometric			
Length	N_L	N_L	[L]
Area	N_L^2	N_L^2	[L ²]
Volume	N_L^3	N_L^3	[L ³]
Kinematic			
Time	$N_L^{1/2} N_P^{1/2} N_Y^{-1/2}$	$N_L^2 N_P N_U^{-1}$	[T]
Velocity	$N_L^{1/2} N_P^{-1/2} N_Y^{1/2}$	$N_L^{-1} N_P^{-1} N_U$	[LT ⁻¹]
Acceleration	$N_P^{-1} N_Y$	$N_L^{-3} N_P^{-2} N_U^2$	[LT ⁻²]
Discharge	$N_L^{5/2} N_P^{-1/2} N_Y^{1/2}$	$N_L N_P^{-1} N_U$	[L ³ T ⁻¹]
Dynamic			
Mass	$N_L^3 N_P$	$N_L^3 N_P$	[M]
Force	$N_L^3 N_Y$	$N_P^{-1} N_U^2$	[MLT ⁻²]
Mass Density	N_P	N_P	[ML ⁻³]
Specific Weight	N_Y	$N_L^{-3} N_P^{-1} N_U^2$	[ML ⁻² T ⁻²]

Hughes (1993) also found that tests that were done on a fixed-bed in a two-dimensional wave tank generally provided acceptable results, as the scale effects for fixed-bed models are well understood.

Pearson *et al.* (2002) conducted a study on violent wave overtopping at small and large-scale physical models, as studies often suggested that wave overtopping measured in physical model studies could possibly include scale effects which could negatively influence the reliability of predictions to full scale. Overtopping tests were done for a battered seawall structure at a variety of wave conditions, at both large- and small-scale. After analysis of the results, Pearson *et al.* (2002) found that the influence of scale effects on mean and peak overtopping volumes were insignificant for both impulsive and non-impulsive

wave conditions. Pearson *et al.* (2002) therefore came to the conclusion that overtopping measurements from small-scale studies can be used with confidence to predict overtopping in the prototype.

Pearson *et al.* (2002) also found that the inability to simulate wind and the use of fresh instead of salt water were the most apparent laboratory effects experienced during physical model testing. The wind was predicted to have a significant effect on small overtopping discharges, especially when violent breaking occurs. The effect of wind on large overtopping discharges was, however, predicted to be minimal. The use of fresh water instead of salt water has not been found to have any influence on wave overtopping and no evidence exists proving otherwise (Pearson *et al.*, 2002).

2.6.3. Wave spectra

For a given wind speed, the characteristics of the waves created will depend on the duration and fetch. A bigger duration or fetch will thus result in larger waves. Since the wind only has a limited amount of energy, the wave heights will reach an upper limit for the particular fetch and duration, referred to as a fully developed sea state (Chadwick *et al.*, 2013).

Parametric spectrum models can be used to describe the elevation of the sea surface for a given sea-state (USACE, 2006). The single-parameter Pierson-Moskowitz (PM) spectrum model, which describes a fully developed sea state, was one of the first spectrum models. The PM spectrum was developed in 1964 from measurements of ocean waves taken by weather ships in the North Atlantic (Chadwick *et al.*, 2013).

More recent research on wave energy spectra, based on wave readings in the North Sea, resulted in the development of the Joint North Sea Wave Project (JONSWAP) spectrum model. The JONSWAP spectrum was derived from the PM spectrum to describe a fetch-limited or growing sea-state. JONSWAP spectrum waves are used for the majority of wave overtopping studies worldwide, but also in South Africa, as Rossouw (1989) found that the spectrum also closely resembles the wave spectrum along the Southern African coast.

2.6.4. Test duration

When studying wave overtopping of coastal structures in physical model studies, the test duration and number of waves are crucial factors to be considered prior to the execution of any physical model tests. Therefore, in order to optimise the test duration, it is crucially important to find the correct balance between the required accuracy of measurements and the total number of tests (Reis *et al.*, 2008).

Reis *et al.* (2008) therefore set out to investigate the required duration of physical model tests with the aim of identifying a minimum test duration and number of test repetitions required to accurately measure mean overtopping discharges. A total of 87 physical model tests were done with varying test durations. From the results, Reis *et al.* (2008) pointed out that the measured mean discharge mostly decreased with an increasing number of waves, but only up to about 1100 to 1400 waves, after which only small reductions in mean overtopping discharge were found.

Analysis of the test results, however, failed to provide a constant test duration for which the mean overtopping discharges remained constant. Reis *et al.* (2008) therefore concluded that information obtained from a single test with a long duration still provided limited information on the expected mean overtopping discharge, as the mean overtopping discharge varies even for the same structure and wave characteristics. Reis *et al.* (2008), therefore, recommended that several tests of shorter duration should rather be done, as opposed to one long-duration test. Also, in studies where active wave absorption is unavailable or ineffective, several short duration tests should be done, as shorter duration tests would minimise any build-up of wave energy due to the re-reflection of waves (Reis *et al.*, 2008).

2.6.5. Wave generation and overtopping measurement

Numerous methods exist to determine the volume of wave overtopping in a physical model study. Owen and Steele (1993) published a physical model study where the overtopping discharge for embankment type seawalls was measured by collecting the overtopping water in calibrated tanks behind the seawall. To improve the accuracy of the measurements, the mean discharge and standard deviations were calculated for every test by using the results of five overtopping intervals for the same test conditions. An overtopping interval was taken as $100T_m$, where T_m is the nominal mean wave period for the JONSWAP spectrum.

The volume of overtopping was calculated by using a float which helped indicate the water level in the tank. After every overtopping interval, the water was first allowed to settle, after which the water level was read from the overtopping container. After the measurement of the water level, the overtopped water was then pumped back into the wave flume to re-establish the desired water level for testing (Owen and Steele, 1993).

Pearson *et al.* (2002) conducted a physical model study on wave overtopping to compare the accuracy of large- and small-scale models. During the study, overtopping measurements were taken by directing

individual overtopping discharges via a chute into a container suspended from a load cell. Individual overtopping events were identified by two metal strips which were placed parallel to each other, along the width of the structure, thereby acting as a switch when closed by overtopping water. Each individual wave overtopping volume was then determined by calculating the incremental water mass in the overtopping container after every wave overtopping (Pearson *et al.*, 2002).

Pearson *et al.* (2002) calibrated the measurement system by simulating overtopping events by adding known volumes of water into the overtopping container, after which the results from the load cell were processed by an algorithm to identify the individual overtopping events. The method of overtopping measurement was found to be extremely accurate, as the difference between derived and actual overtopping volumes was limited to less than 0.7 percent.

For the study, Pearson *et al.* (2002) generated waves with a flap-type wave maker, equipped with active wave absorption. The active wave absorption technology reduced the effect that re-reflection of waves had on the incident wave height measurements in the flume. Uncertainties regarding the difference between the incident wave height and the wave height at the toe of the structure was reduced by repeating all the tests with wave gauges at the location where the structure would have been.

3. Physical modelling

3.1. Overview

In order to empirically analyse the effect that the nearshore profile has on the overtopping of recurve seawalls, a physical model study was undertaken. Tests were conducted at the Stellenbosch University Hydraulics Laboratory. This study, therefore, made use of the same facility and mostly the same methodology and equipment that was used by Schoonees (2014), Swart (2016), Kretschmer (2017) and Walker (2018), which enabled the comparison and validation of test results.

During the study, two types of tests were done. The first set of tests was done to determine the difference between the wave height above the recurve seawall's location and at one peak wavelength away from the structure. The second set of tests consisted of the actual wave overtopping tests, which examined the effect of the nearshore profile on wave overtopping at recurve seawalls. The detailed test procedures and data acquisition methods are discussed in Sections 3.4 and 3.5 respectively.

3.2. Model set-up

3.2.1. Test facility

The Stellenbosch University Hydraulics Laboratory is equipped with a two-dimensional glass wave flume which is 50 m long, 1.0 m wide and has a maximum operational depth of 0.8 m. The glass wave flume is fitted with a piston-type wave generator, which can generate both regular and irregular wave sequences. The wave generator is also equipped with built-in wave-absorption technology, which reduces the unwanted effects of wave reflection in the flume (HR Wallingford, 2010). Figure 3-1 shows the glass wave flume and wave generator that were used for the physical model tests.

The height of the generated waves was measured by resistance probes, which measures the electric potential difference (volts) from one electrical wire to another wire which is at a fixed distance away. The voltage measurements were analysed by HR-DAQ data acquisition and analysis software, developed by HR Wallingford, which converted the voltage measurements to water-level readings. Resistance probes were calibrated at least three times per day, as the probes are particularly sensitive to changes in the water salinity and temperature. HR Wallingford recommends that the probes should be calibrated at least twice daily (HR Wallingford, 2010).

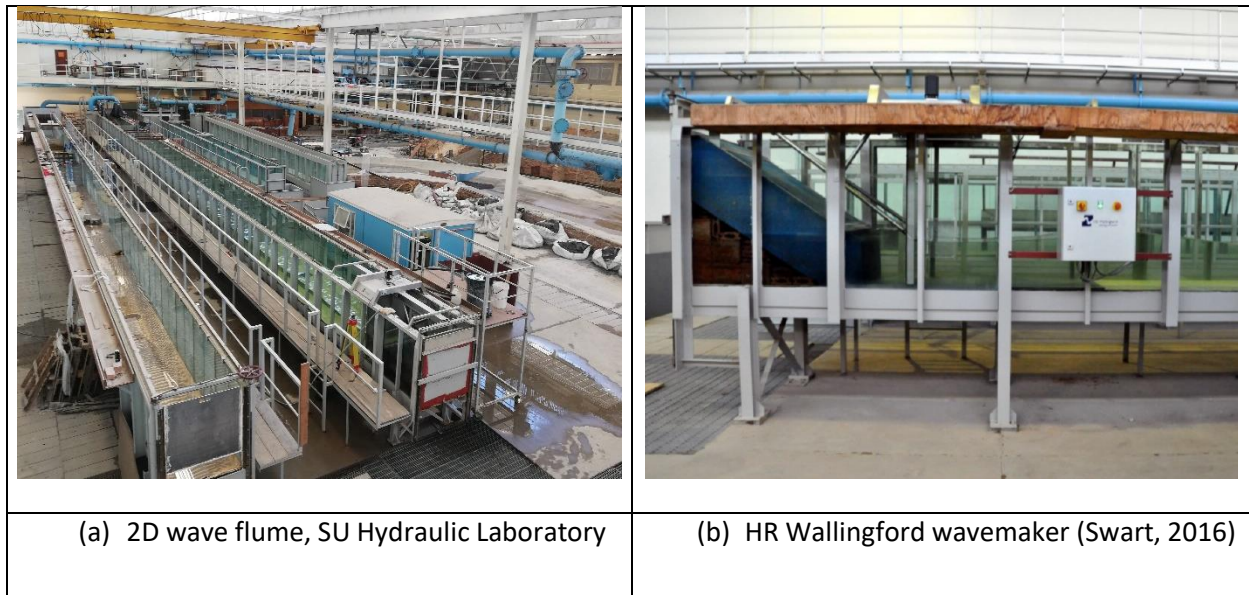


Figure 3-1: Physical modelling equipment

3.2.2. Model scale

In order to minimise scale effects in the physical model, the largest possible scale had to be chosen. A 1:20 length scale was chosen for the physical model, applying the Froude similitude scale law as discussed in Section 2.6.2. The scale was chosen by firstly taking into consideration the wave generating capacity of the wave generator and secondly the seawall height used by recent studies on wave return walls by Schoonees (2014), Swart (2016), Kretschmer (2017) and Walker (2018). A summary of the scale factors is included in Table 3-1.

Table 3-1: Model scale factors

Scale type	Parameters	Froude equation	Scale
Linear scale	Wave height, water depth, wall and slope dimensions	1: 20	1:20
Volume scale	Overtopping volumes	1: 20 ³	1: 8000
Time scale	Wave period, test duration	1: $\sqrt{20}$	1: 4.472

The flume was filled with fresh water, therefore a density of 1000 kg/m³ was assumed for calculations.

3.2.3. Nearshore profile design

Of the typical Southern African nearshore profiles collected and summarised in Figure 2-31, it was decided that overtopping tests would be done on steep and flat nearshore profiles, as well as on a mild profile with an offshore berm. The Walvis Bay profile was chosen to be used as the steep profile, False Bay as the flat profile and Richards Bay as the mild profile with an offshore berm. The existing profile that was used in overtopping tests by Schoonees (2014), Swart (2016), Kretschmer (2017) and Walker (2018), also had to be tested to be able to compare the results of this study with those of the previous studies.

As mentioned in Section 2.5, due to the highly dynamic nature of the nearshore zone, any changes made to the profile dimensions for simplification of the physical modelling, would lead to unrealistic nearshore profiles that does not exist in nature. Therefore, in order to keep the results as realistic as possible, nearshore profiles were kept as close as possible to the original measured profile. Figure 3-2 summarises the four nearshore profiles that were tested during physical modelling.

As Schoonees (2014), Swart (2016), Kretschmer (2017) and Walker (2018) tested the overtopping of recurve seawalls with toe water levels between 0.6 m and 2.4 m, the mean sea level was assumed to be at 1.5 m above the toe of the seawall.

For the first set of tests, where the wave heights were measured above the recurve seawall location, and at one peak wavelength seaward of the recurve seawall toe, the nearshore profile was extended to the maximum run-up height that a wave set with a significant wave height (H_s) of 2 m would reach.

For the overtopping tests, the recurve seawall, along with the overtopping measurement equipment, was installed 30 m from the wavemaker. Design sketches of the nearshore profiles, showing the planned and as-built drawings, along with the location of the recurve seawall and probes, are shown in Appendix B.

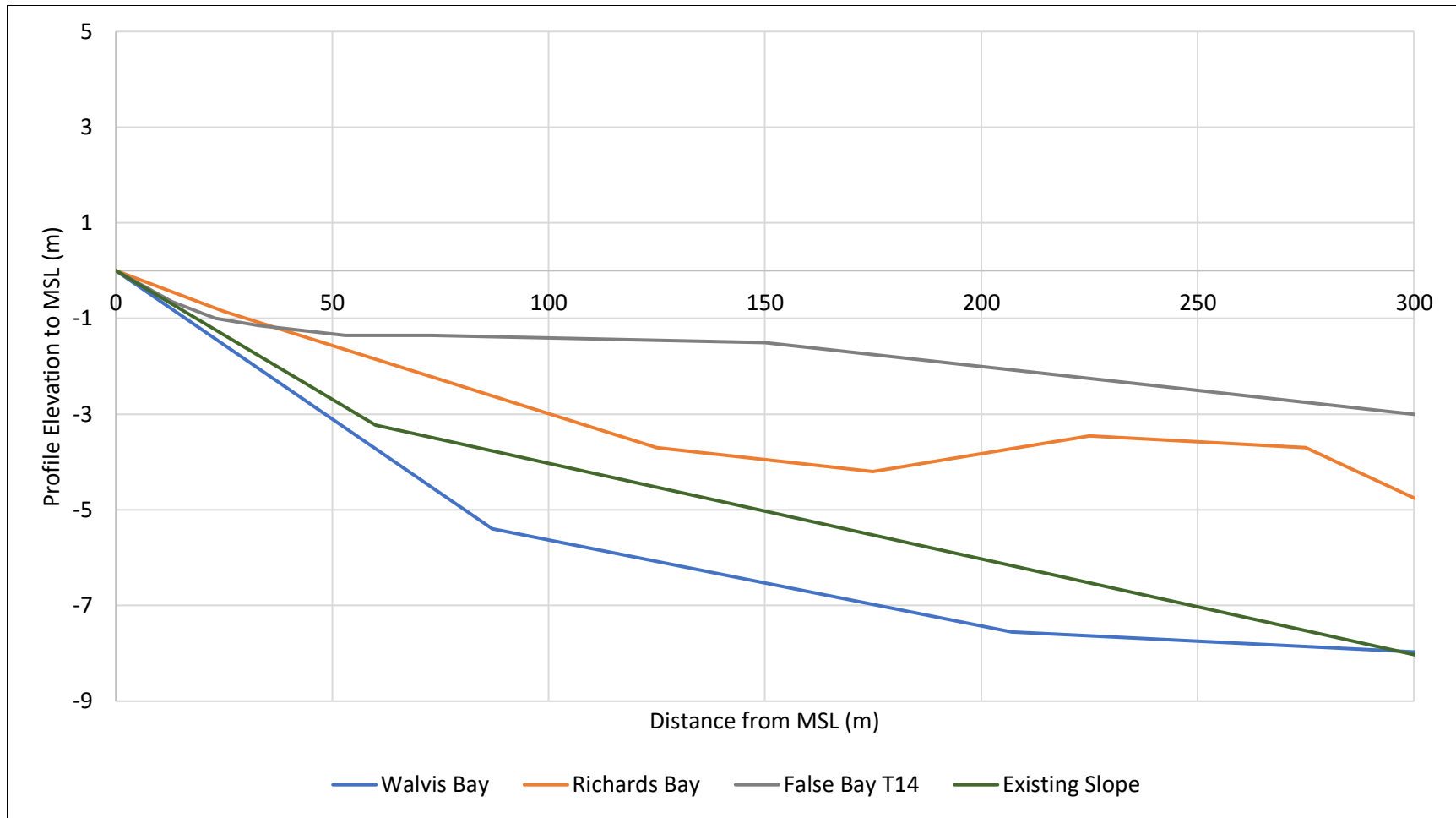


Figure 3-2: Nearshore profiles tested

3.2.4. Recurve seawall design

A type 3 recurve seawall, consisting of a vertical wall with a recurve section on top, was constructed on the one end of the wave flume (Schoonees, 2014). The vertical part of the wall was made from 18 mm thick PVC plate, onto which the recurve section was bolted. The recurve section was constructed of meranti hardwood, which had to be painted to prevent absorption and swelling of the wood.

The shape of the recurve section was based on the optimum design to prevent wave overtopping according to Kretschmer (2017). However, because the formation of a sharp rectangular edge during construction is practically difficult, a similar design to that of Kretschmer (2017), but with chamfered edges was suggested by Walker (2018). Therefore, the design by Walker (2018) was chosen, as the design is the most effective in terms of overtopping reduction, but also practically constructible. The design drawing of the wall is included in Figure 3-3.

In order to ensure accurate overtopping measurement, the wall in the physical model had to be impermeable to water. Therefore, the wall was made to span the entire width of the wave flume and then sealed with a silicone sealant.

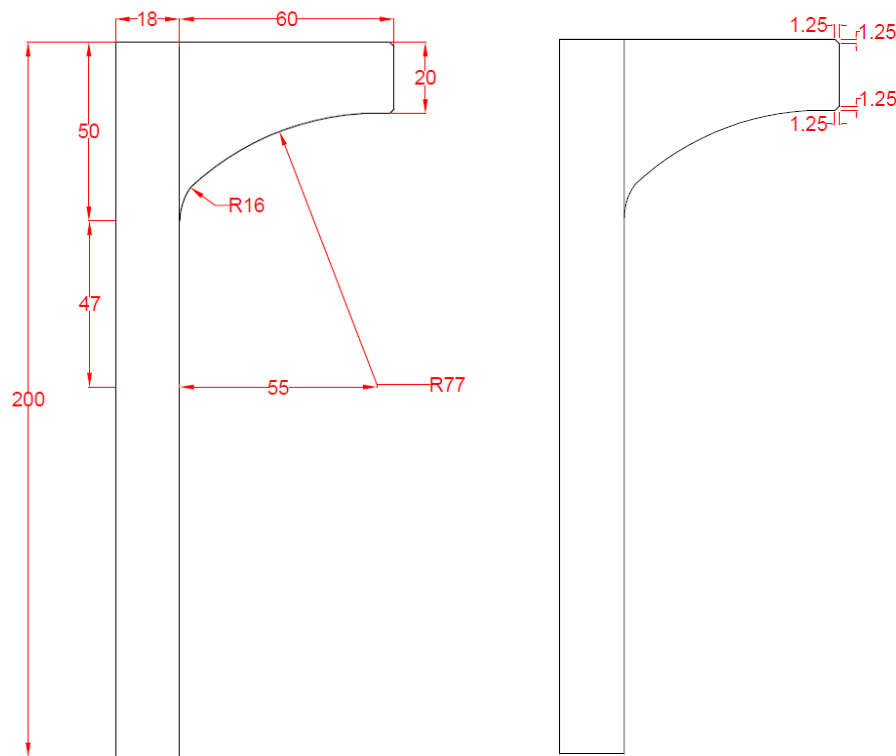


Figure 3-3: Recurve seawall design (Walker, 2018)

3.3. Controlled hydraulic parameters

The water level, wave period and nearshore profiles were chosen to be the variable parameters for this study. The four nearshore profiles were tested against the three water levels that resulted in the most overtopping in the previous studies by Swart (2016), Kretschmer (2017) and Walker (2018). The three prototype toe water levels were 2.4 m, 2.0 m and 1.6 m respectively. Because different profiles have different locations of wave breaking, the study included both breaking and non-breaking waves.

As the wave periods around the South African coast typically range from 8 to 12 s, wave periods between 8 and 12 s had to be tested during physical modelling. However, in order to include the effect of wind waves and storm sea conditions, wave periods of 6 and 14 s were also added. Tests were thus done with peak wave periods of 6, 8, 10, 12 and 14 s. The exact same wave periods were also used by both Kretschmer (2017) and Walker (2018), and wave periods between 8 and 12 s plus a 16 wave period by Swart (2016). Like in the studies by Schoonees (2014), Swart (2016), Kretschmer (2017) and Walker (2018), a total of 1000 waves were run for each physical modelling test.

In order to limit the number of variables, the design wave height, H_i , was fixed at 1 m prototype height, the same wave height used in previous studies by Schoonees (2014), Swart (2016), Kretschmer (2017) and Walker (2018). Other fixed parameters were the recurve seawall design and crest height. The benefit of using the same recurve seawall, water levels and wave heights is that it enables the results of this study to be compared to the results obtained by Walker (2018) especially, but also to a lesser extent to the results of Kretschmer (2017). A breakdown of the physical model parameters is included in Table 3-2.

Table 3-2: Physical modelling test breakdown

Model		Prototype		
Test series	Nearshore profile	Significant wave height H_s (m)	Toe water level (m)	Peak wave period T_p (s)
A	Existing profile	1	1.6, 2.0, 2.4	6, 8, 10, 12, 14
B	Walvis Bay	1	1.6, 2.0, 2.4	6, 8, 10, 12, 14
C	Richards Bay	1	1.6, 2.0, 2.4	6, 8, 10, 12, 14
D	False Bay	1	1.6, 2.0, 2.4	6, 8, 10, 12, 14

3.4. Experimental procedure

Section 3.4 is subdivided into three sections; the initial or start-up procedure and the test procedures for the two different types of tests; the shallow water wave height and wave overtopping tests. Each subsection then explains the exact procedure that was followed for each test.

3.4.1. Initial procedure

Every day, before any testing was to be done, the start-up procedure was done to ensure that the conditions were optimal before commencing with tests. The concern was that the equipment in the laboratory could accidentally have been moved or altered by the lab staff or any of the other researchers.

The initial procedure was as follows:

1. Ensure the initial water level is correct.
2. Turn on wave gauge system, wavemaker and control computers.
3. Check the placement and spacing of the probes.
4. Run a wave sequence for at least 10 minutes to destratify the water, to avoid probe readings being affected by temperature variations due to stratification of the water.
5. Wait 10 minutes until the water surface is calm.
6. Ensure overtopping container is set on zero for overtopping tests.
7. Adjust the water level on the wavemaker control unit to 0.
8. Start the test procedure.

3.4.2. Shallow water wave measurement

The test procedure was as follows:

1. Calibrate the wave probes.
2. Set the water level, wave period and wave height on the wavemaker control computer.
3. Record the initial water level to ensure that the water level is correct for the upcoming test.
4. Start the wave sequence from the control computer (test duration of $1000 T_p$).
5. Adjust absorption gain to the appropriate value for the wave sequence.
6. Start probe reading on HR DAQ Suite.
7. After the wavemaker has run for the required test duration, stop the wave sequence.
8. Commence with post-processing.

3.4.3. Overtopping test procedure

The test procedure was as follows:

1. Calibrate the wave probes.
2. Set the water level, wave period and wave height on the wavemaker control computer.
3. Record the initial water level to ensure that the water level is correct for the upcoming test.
4. Start the wave sequence from the control computer (duration of $1000 T_p$).
5. Adjust absorption gain to the appropriate value for the wave sequence.
6. Start probe reading on HR DAQ Suite.
7. Monitor wave overtopping.
 - 7.1. If 20 litres of water has overtopped, 20 litres are added back behind the wavemaker in 5-litre increments.
 - 7.2. If the overtopped water nears the overtopping bin's capacity, pump the water into the bin behind wavemaker to be weighed.
8. Record the weight of the overtopped water only, subtracting the weight of the bin.
9. After the wavemaker has run for the required test duration, stop the wave sequence.
10. Record the total volume of overtopping.
11. Record the water level. If the water level is not within 2mm of the starting water level, discard the test.
12. Empty the overtopping bin.
13. Commence with post-processing.

3.5. Data acquisition

3.5.1. Shallow water wave measurement

The shallow water wave measurement tests were done to determine the difference between the wave heights measured above the recurve seawall's location and at one peak wavelength away from the structure, a parameter that was specified by Mansard and Funke (1980) to minimise the effect of reflected waves on the wave height measurements, but also to ensure that the waves did not break in the vicinity of the probes.

For the shallow water wave measurement tests, the nearshore profile was extended to the run-up height that 2 percent of waves with a height of 2 m would reach. For a wave sequence with a significant wave

height of 1 m, the maximum wave height was found to be about 2 m. Figure 3-4 shows the probe spacings for the first set of tests. The HR DAQ software requires four resistance probes to perform a reflection analysis. Therefore, in order to measure the wave heights at two locations, two sets of probes needed to be used.

As shown in Figure 3-4, the first set of probes was spaced with the fourth probe positioned above the planned seawall's toe and the second set of probes placed at one peak wavelength offshore of the recurve seawall's location, which is the same probe location used for the overtopping tests. The spacing within a set of probes were done according to the method by Mansard and Funke (1980). By measuring the wave heights at two different locations, the shallow water wave height tests could be used to predict the exact wave height arriving at the seawall's toe during overtopping tests.

The resistance probes, attached to their custom-made brackets is shown in Figure 3-5. The probe spacings are shown in Appendix H.

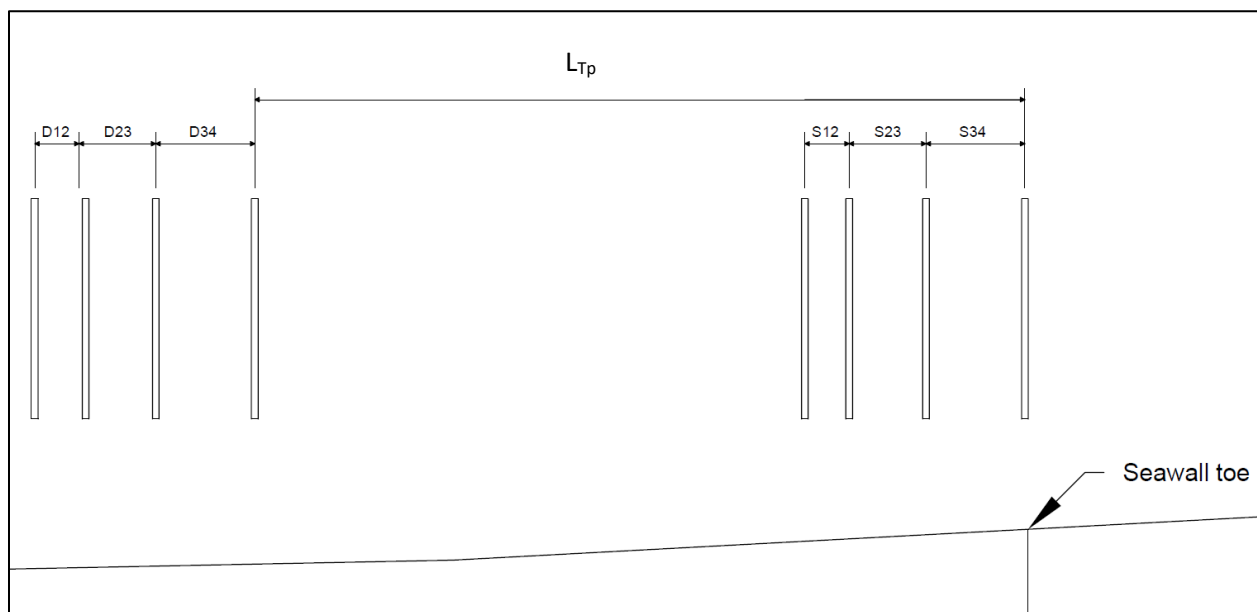


Figure 3-4: Probe spacing for shallow water wave tests

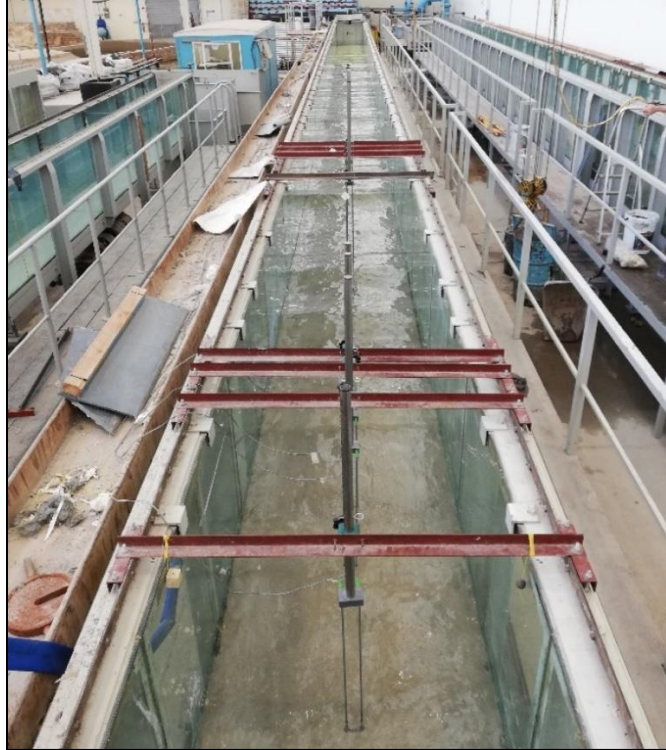


Figure 3-5: Resistance probes in the physical model

3.5.2. Overtopping measurement

During the overtopping tests, the wave heights were measured at one peak wavelength away from the structure, to ensure that the effect of reflected and breaking waves were minimal at the location of wave height measurement. For the overtopping tests, the fourth probe (closest to the seawall) was placed at one peak wavelength away from the reflective structure, with the other three probes spaced according to the method developed by Mansard and Funke (1980). The probe spacing for the overtopping tests is shown in Figure 3-6.

As the wave overtopping tests investigated the effect that the nearshore profile has on wave overtopping at a recurve seawall, space had to be made for the installation of the recurve seawall, overtopping bin and other measurement equipment. To capture any water overtopping the recurve seawall, a steel bin was placed behind the wall. The bin was equipped with a ruler and a see-through Perspex slot on one side, from where the water level before and after every test could be recorded. The ruler was calibrated with predetermined volumes so that the volume of overtopping could be monitored during an overtopping test.

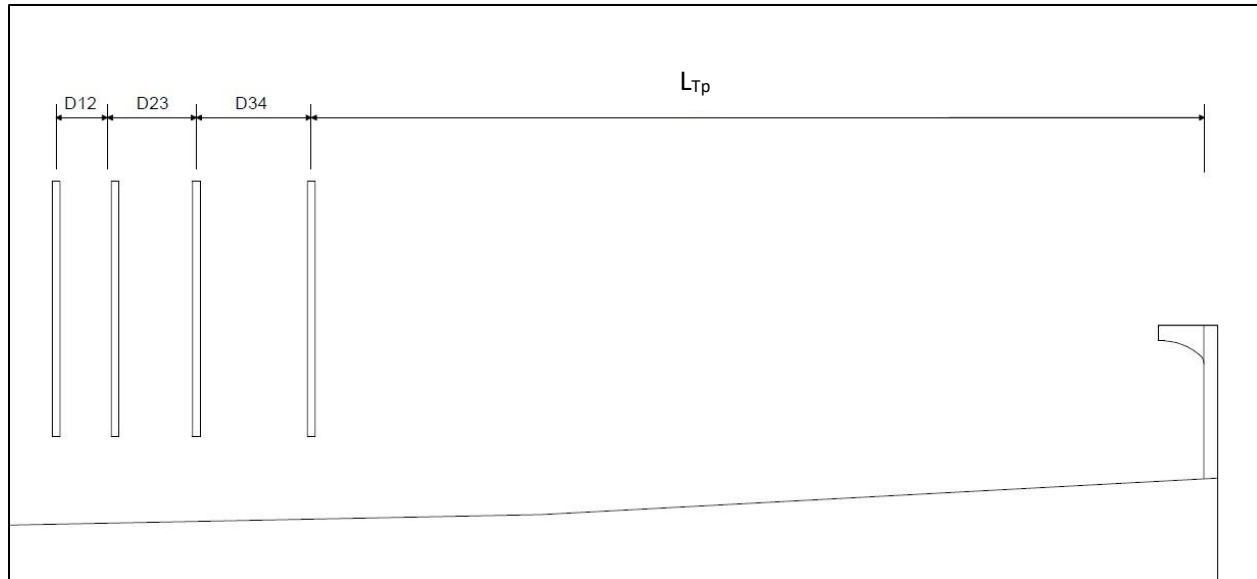


Figure 3-6: Probe spacing for overtopping tests

Above the overtopping bin, a funnel structure was built from four PVC boards to ensure that all the overtopping water was guided into the bin. The boards were sealed against the back of the seawall and the side of the flume to prevent any leakage. A large wooden frame, with two large plastic screens on either side of the flume, extending from the recurve seawall towards the wavemaker was also constructed to minimise water loss during violent overtopping events. The boards that guide the water into the overtopping bin, as well as the splash screens, can be seen in Figure 3-7.

Small overtopping volumes were measured by pumping the water from the overtopping bin into a small bucket with the help of a small rotary pump. The bucket was then weighed to determine the mass of the overtopped water, from which the overtopping volume could be calculated. For large overtopping events, a submersible pump was placed inside the overtopping container. When the overtopping bin became too full, the pump was used to pump the overtopped water into a bin, which was placed on a scale, behind the wavemaker. The scale measured the weight of the overtopped water, from which the volume was determined. During all overtopping tests, when 5 litres of water overtopped, 5 litres of water was transferred back into the wave flume behind the wavemaker, to ensure limited disturbance to the water surface in the wave flume.



Figure 3-7: Overtopping bin, funnel boards and splash screens

3.6. Post-processing

The HR DAQ (data acquisition) software, which was connected to the wave probes, recorded the wave surface profile readings for every wave sequence. A spectral analysis was then done for every wave sequence, also by the HR DAQ software. The spectral analysis produced a significant wave height (H_{m0}) for each probe. As a set of probes consisted of 4 probes in total, the average significant wave height between the four probes had to be calculated. The average significant wave height represented the wave height at that specific location of the nearshore profile.

However, because the recorded wave data included both incident (H_i) and reflected (H_r) wave readings, the significant wave height could not be used to represent the incoming wave height. Therefore, because wave overtopping is extremely sensitive to a change in wave height, the reflected waves had to be separated from the recorded wave data. To separate the incident and reflected waves, the least-squares method, developed by Mansard and Funke (1980), was further developed into a formula that could be used to calculate the incident wave height as a function of the bulk reflection coefficient (K_r) and significant wave height (H_{m0}).

The HR DAQ software has a reflection analysis tool, which was used to calculate the bulk reflection coefficient, given the probe spacing and the water depth in which the probes were placed. When initially

calculating the probe spacing, HR DAQ had to be used to determine the range of allowable reflection frequencies. Figure 3-8 and Figure 3-9 provide examples of the reflection analysis interface.

Having calculated both the bulk reflection coefficient and the significant wave height, the method developed by Mansard and Funke (1980) was then used to calculate the incident wave height, with Equation 3.1.

$$H_i = \frac{H_{m0}}{\sqrt{1 + K_r^2}} \quad (3.1)$$

The derivation of Equation 3.1 comes from the least-squares method, developed by Mansard and Funke (1980) and shown below.

$$H_{m0}^2 = H_i^2 + H_r^2 \quad (3.2)$$

$$H_{m0} = \sqrt{H_i^2 + H_r^2} \quad (3.3)$$

$$H_r = K_r H_i \quad (3.4)$$

substituting (3.4) in (3.3):

$$H_{m0} = \sqrt{H_i^2 + K_r^2 H_i^2} \quad (3.5)$$

$$H_{m0} = H_i \sqrt{1 + K_r^2} \quad (3.6)$$

$$H_i = \frac{H_{m0}}{\sqrt{1 + K_r^2}} \quad (3.7)$$

Where:

H_{m0} = spectral significant wave height (measured by the probes).

H_i = incident wave height.

H_r = reflected wave height.

K_r = bulk reflection coefficient.

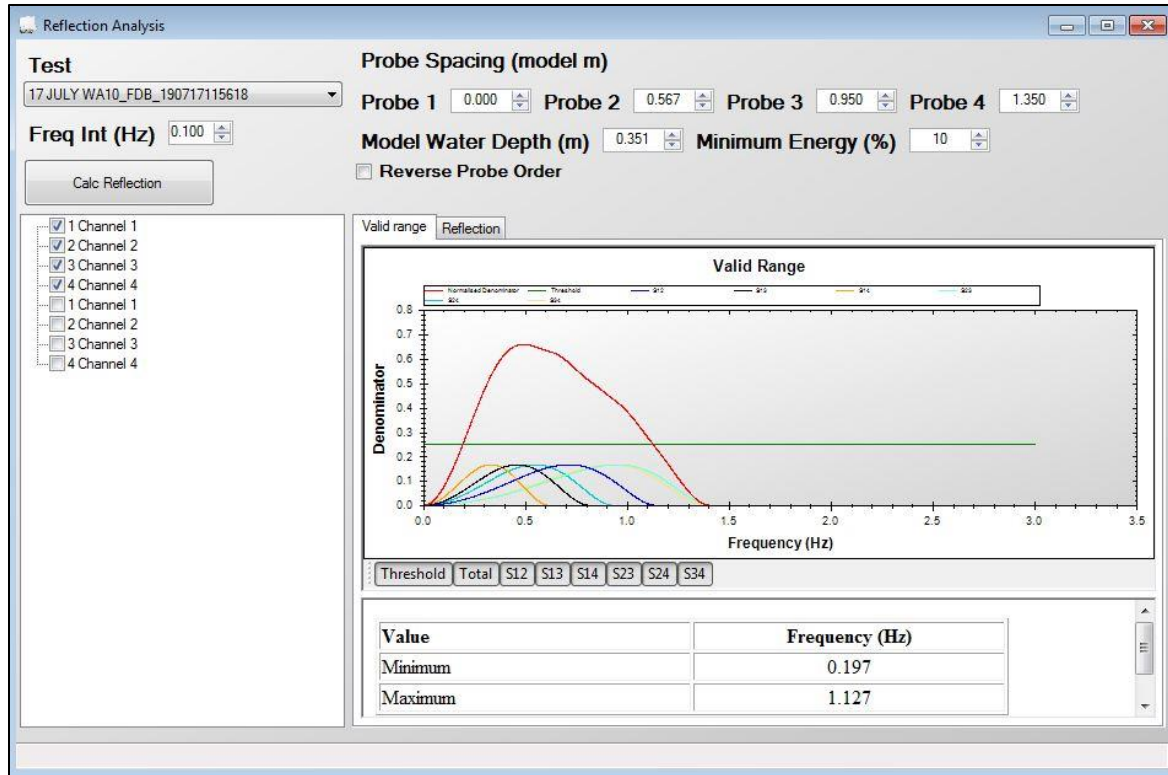


Figure 3-8: Reflection Analysis valid frequency range

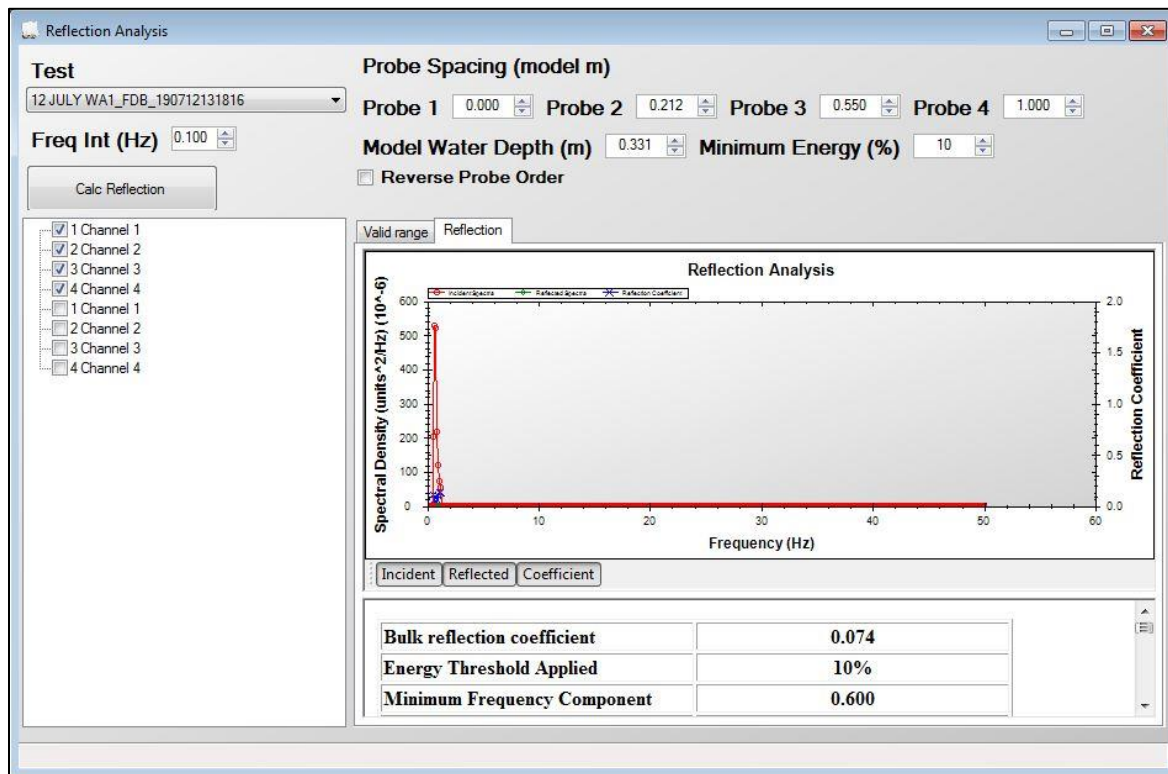


Figure 3-9: Reflection Analysis bulk reflection coefficient calculator

3.7. Test conditions and summary

Test conditions were selected to represent typical nearshore wave conditions along the Southern African coast, complementing the Southern African nearshore profiles that were going to be modelled.

HR Wavemaker, a wave generation software package developed by HR Wallingford, was used to create the wave generation signal files for each test. The signal file consists of a wave train signal which specifies the desired wave spectrum, wave height and wave period to be created by the wavemaker for a certain water level. For every test, the wavemaker also required an absorption gain value to be specified. The absorption gain parameter calibrates the wavemaker to correctly absorb reflected waves and produce accurate wave heights, thereby also reducing some of the unwanted 2D effects in the wave flume. The absorption gain values were obtained from a chart set up for the specific wavemaker and flume by HR Wallingford (2010).

The type of waves to be modelled was chosen to follow the JONSWAP irregular wave spectrum, as the JONSWAP spectrum closely resembles the actual wave spectrum along the South-African coast (Rossouw, 1989). Rossouw (1989) found that the value of the peak enhancement factor along the South African coast varies from 1 to 6, with an average value of $\gamma = 2.2$ and a standard deviation of 1.0. However, as $\gamma = 3.3$ is the value most often used in wave overtopping studies worldwide, a peak enhancement factor of $\gamma = 3.3$ was chosen as peak enhancement factor to enable the results to be compared to other overtopping studies worldwide.

In order to ensure that sufficient wave data is collected and to ensure that the significant wave heights obtained from the test are representative of the specific wave set, Reis *et al.* (2008) specified that the test duration should be at least 1000 times the peak wave period. Therefore, the test durations were set to be $1000T_p$.

3.8. Repeatability and accuracy

To determine the measure of repeatability and model uncertainty, a number of tests had to be repeated. When tests were repeated, the average of the measured overtopping discharges was calculated and used as a more reliable overtopping discharge.

Additionally, to ensure that the test set-up was correct, experiments were repeated on the same profile used by Schoonees (2014), Swart (2016), Kretschmer (2017) and Walker (2018), thereby creating the

opportunity to compare test results to previous results obtained from exactly the same test conditions. Results from the repeated tests showed that the overtopping measurements could vary slightly with no apparent change in the test conditions. The difference in results is attributed to various factors, such as the slight inaccuracy of the overtopping measurements, especially for small overtopping volumes, and the over- or underestimation of the input wave heights due to limitations of the wavemaker and measuring equipment. Ineffective absorption of the reflected waves can also lead to re-reflection of waves in the flume, which can influence the accuracy of wave height measurements.

During testing, some difficulties were also experienced due to changing water salinity. Every time the flume was filled with water, after the construction of a new profile, the cement in the screed layer started releasing salts into the water. The constant rise in salinity led to a rise in the water conductivity. Therefore, while a wave sequence was running, the water conductivity would rise gradually, causing the data analysis software to conclude that the water level was rising.

To get rid of the salts, the flume had to be flushed by running a wave sequence for an entire day to stir up the salts. Then, after running the wave sequence for a day, the flume was drained. Flushing had to be done for at least four consecutive days to reach manageable levels of salinity. Only after completing the flushing procedure, testing could begin. However, probes still had to be calibrated for every test, especially in the morning, when water was not yet mixed well. After a few hours of testing, the salinity levels stabilised. By regularly calibrating the probes, maximum accuracy and reliability were ensured. After the shallow water wave measurement tests were completed, the flume was drained to install the overtopping equipment. After filling the flume to commence with the overtopping tests, usually no more problems were experienced with changing water salinity.

Also, because of the size of the overtopping container, small overtopping volumes from less than 2 litres could not be measured accurately. Therefore, it is advised to interpret overtopping discharges smaller than 0.08 L/s/m cautiously.

4. Results

4.1. Overview

This study comprised 215 physical model tests to gain a better understanding of how the nearshore profile affects the overtopping of recurve seawalls. Initially, 120 tests were specified, as for each of the four nearshore profiles, three water levels had to be tested, each with the five different wave periods. Of the 215 tests, 95 tests were repeated tests, as the active wave absorption input parameters had to be adjusted to obtain the correct incident wave height. In order to verify the repeatability of the physical model tests, 5 critical overtopping tests and 3 wave height tests were repeated with exactly the same input parameters.

Section 4.2 summarises and provides a complete overview of the acquired test results, showing the effect that the nearshore profile has on wave transformation, as well as on the overtopping of the recurve seawall. The detailed analyses and interpretation of the test results are included in Chapter 5. The results from the physical model studies are summarised in Appendix C, showing both the results from the shallow water wave height- and overtopping tests. The tables include both prototype and model values for all the test input parameters and results. Furthermore, the spectral significant wave height (H_{m0}), incident wave height (H_i), overtopping volumes and overtopping rates are presented in the results.

4.2. Physical model test results

The general performance of the recurve seawall, shown in Section 3.2.4, in reducing wave overtopping on the average- and three typical Southern African nearshore profiles is discussed in Sections 4.2.1 to 4.2.5.

4.2.1. Nearshore profile A

Nearshore profile A, the average Southern African nearshore slope calculated by Schoonees (2014), was chosen as the first nearshore profile to be tested. Using nearshore profile A as one of the nearshore profiles during physical modelling enabled the comparison of results obtained from other nearshore profiles with previous studies by Schoonees (2014), Swart (2016), Kretschmer (2017) and Walker (2018). The performance of the recurve seawall on profile A was thus used as the basis against which to compare the performance of the recurve seawall on other nearshore profiles.

At the 1.6 m toe water level, the recurve seawall effectively reflected incoming waves, allowing little to zero wave overtopping. The overtopping which did occur at the 1.6 m water level, was too small to be measured, as overtopping occurred mostly as water spray. Due to the relatively low water level and high freeboard, most of the incident waves collided with the vertical part of the wall, from which the wave would be transferred upwards into the recurve section, which projected it back seawards as a water jet. However, during the 14 s wave period, some individual white-water overtopping started to occur due to the impulsive wave conditions brought on by large waves breaking onto the recurve seawall. An effective reflection of a wave during a test at the 1.6 m toe water level and a wave period of 10 s is shown in Figure 4-1.

A clear increase in overtopping started to occur between the 1.6 m and 2.0 m toe water level. During the longer wave periods, from 10 s onwards, impulsive wave conditions led to small white-water overtopping. The overtopping was brought on by large waves that started breaking onto the vertical face, recurve section and overhang edge simultaneously, which caused water to be projected straight up into the air instead of back seaward. The momentum of the incoming wave then simply carried the vertical water column onto or over the crest. An example of a white-water overtopping event is shown in Figure 4-2, where a wave with a 14 s wave period collides with the recurve seawall at the 2 m toe water level.

The highest overtopping volumes occurred at the 2.4 m toe water level, with the critical wave overtopping experienced during the 14 s wave period. Due to the high water level at the toe of the structure, waves with long wavelengths completely submerged the recurve wall, making the wall ineffective at reflecting the wave energy effectively. Submerged conditions allowed large volumes of water to overtop the seawall, as both white- and green water overtopping. Wave overtopping during a “submerged” condition can be seen in Figure 4-3 for a 14 s wave period at a 2.4 m toe water level.

4.2.2. Nearshore profile B

Nearshore profile B was chosen to represent a steep Southern African nearshore profile. As mentioned in Section 0, the nearshore profile was measured in 1999 by Schoonees *et al.* (1999), when the possibility of the Walvis Bay sand spit being breached was studied. Figure 2-31 shows the steepness of the Walvis Bay nearshore profile in comparison with other typical Southern African nearshore profiles.



Figure 4-1: Wave reflection at nearshore profile A ($WL_{toe} = 1.6$ m, $T_p = 10$ s)



Figure 4-2: Wave overtopping at nearshore profile A ($WL_{toe} = 2.0$ m, $T_p = 14$ s)



Figure 4-3: Wave overtopping at nearshore profile A ($WL_{toe} = 2.4$ m, $T_p = 14$ s)



Figure 4-4: Wave reflection at nearshore profile B ($WL_{toe} = 1.6$ m, $T_p = 14$ s)

When comparing the overtopping of the recurve seawall over nearshore profile B with all the other profiles, results showed that the recurve seawall on profile B experienced the least amount of overtopping. For nearshore profile B, the recurve seawall performed extremely well in reflecting any waves at the 1.6 m toe water level, with no overtopping occurring at any of the wave periods. Due to the pulsating wave conditions, the majority of the waves were reflected off the vertical part of the wall, without even breaking. Occasionally a large wave would start to break and then get reflected back seaward by the recurve section.

The pulsating wave behaviour is attributed to the steepness of the nearshore profile, which allowed little shoaling, with the result that waves only started steepening at the last moment before colliding with the seawall. The waves at nearshore profile B, therefore, reached the recurve seawall, with a wavelength close to its deep water wavelength, and without the steepened wave face. Due to the flat wave face, the recurve seawall easily absorbed the incoming wave, and if the recurve section had enough capacity to hold the wave's volume, the wall effectively reflected the wave back seaward. An example of the pulsating behaviour is shown in Figure 4-4 for a water depth of 1.6 m and a wave period of 8 s.

The same pulsating wave conditions were experienced at the 2 m toe water level. The case of a 12 s wave period, where some of the larger waves started steepening and then breaking onto the vertical face of the wall, which transferred the water mass upwards into the recurve section to be reflected back seaward is shown in Figure 4-5. Occasionally, during the 14 s wave period, some of the larger waves in the sequence submerged the recurve seawall, projecting water straight over the seawall crest, instead of reflecting the wave back seaward.

For the longer wavelengths, the recurve seawall occasionally became "submerged". Submerged conditions typically occurred at high water levels, when the recurve seawall did not have the capacity to absorb the entire wave volume, resulting in the wall becoming submerged. Submerged conditions made the recurve seawall ineffective at reflecting wave energy, which led to large volumes of water spilling over the crest of the structure in a coherent water mass, termed green water overtopping. A submerged wall condition, experienced at the 2.4 m toe water level and 14 s wave period is shown in Figure 4-6. As with nearshore profile A, the 14 s wave period also led to the critical overtopping volume for the recurve seawall on nearshore profile B. The overtopping was, however, significantly less than that experienced over nearshore profile A.



Figure 4-5: Wave reflection at nearshore profile B ($WL_{toe} = 2.0$ m, $T_p = 12$ s)



Figure 4-6: Wave overtopping at nearshore profile B ($WL_{toe} = 2.4$ m, $T_p = 14$ s)

4.2.3. Nearshore profile C

Profile C was chosen to represent a mild nearshore profile, with an offshore berm, a typical nearshore profile found along the Kwazulu-Natal coast of South Africa. The Richards Bay nearshore profile, which was chosen as the representative profile, is an averaged nearshore profile compiled by Theron (2016).

The results show that the recurve seawall performed well at reflecting waves of all periods at the 1.6 m toe water level. However, because of the low water level and mild nearshore profile, waves started shoaling and steepening, which led to waves breaking impulsively onto the vertical face of the wall. During some of the tests with long wave periods, small reflected waves occasionally got caught between the wall and a large incoming wave, providing a source for local wave set-up, which caused the incoming wave to break against and over the crest of the seawall.

At the 2.0 m toe water level, the recurve seawall proved to be less effective than on the steeper nearshore profiles A and B. Significant overtopping started to occur at the 8 s wave period when, just as with the 1.6 m toe water level, reflected waves started to get caught up between the wall and an incoming wave. The result was that the waves superimposed directly before the wall, leading to large individual overtopping events. One of the large overtopping events which occurred for an 8 s wave period, at the 2 m toe water level is shown in Figure 4-7. However, for the 10 s wave period, none of the wave collisions were experienced. Then, for the wave periods of 12 and 14 s, the reflected waves started colliding with the incident waves again, leading to more overtopping.

As on nearshore profiles A and B, the critical overtopping event occurred at the 2.4 m toe water level, for the 14 s wave period. From the 10 s wave period, waves started submerging the recurve seawall, making the wall ineffective at reflecting wave energy. Submerged conditions led to large volumes of water overtopping the recurve seawall as both white and green water overtopping. For the 12 and 14 s wave periods, small waves collided with the vertical face of the wall, from where the water was transferred as a water mass upwards into the recurve section, which projected the jet of water back seawards. The water mass would then plunge onto the toe of a larger incoming wave, superimposing the incoming wave. An example of such a large overtopping event that overtopped the recurve seawall because of wave superposition is shown in Figure 4-8.



Figure 4-7: Wave overtopping at nearshore profile C ($WL_{toe} = 2.0$ m, $T_p = 8$ s)



Figure 4-8: Wave overtopping at nearshore profile C ($WL_{toe} = 2.4$ m, $T_p = 14$ s)

4.2.4. Nearshore profile D

Nearshore profile D was chosen to represent a typical flat Southern African nearshore profile. The profile was obtained from a bathymetric survey done in False Bay by the CSIR in 1983 (Swart *et al.*, 1983).

As shown in Figure 4-10, most of the larger waves at a water depth of 1.6 m started breaking as spilling breakers before reaching the seawall. The shallow water wave tests, discussed in Section 5.2.5, confirmed the finding by showing the wave height decreasing from deeper to shallower water. The reason waves started to break on nearshore profile D, was because the gentle nearshore profile caused significant shoaling and steepening of the incident waves, which led to waves becoming unstable, causing it to break.

With the lower incident wave height, the recurve seawall could reflect the incoming waves more effectively, resulting in very little overtopping at the 1.6 m water level. Occasionally, a small reflected wave would be caught up between an incoming wave and the recurve seawall, acting as a source for local wave set-up. The local wave set-up allowed the incoming wave to break onto the overhanging recurve edge, projecting the water straight into the air and then over the seawall crest.

Overtopping that occurred at the 2.0 m water depth generally occurred as white-water overtopping during impulsive wave conditions. Due to the flat nearshore profile, which led to an increase in the shoaling distance, waves typically broke onto the seawall's vertical face, recurve section and overhang edge simultaneously, causing water to be projected straight into the air and over the crest of the seawall. Additional to the white-water overtopping, waves with wave periods of 12 and 14 s started submerging the recurve section, because of the large volume of water carried by the wave. The submerged conditions prevented the seawall from reflecting wave energy effectively, which caused large volumes of water to spill over the crest of the seawall as green water overtopping.

As shown in Figure 4-9, the recurve seawall was found to be the most ineffective at the 2.4 m toe water level, especially for wave periods of 10 s and larger. At the high toe water levels, overtopping occurred as both white and green water overtopping, similar to the overtopping experienced at the 2 m water depth, but in much larger volumes. As determined for nearshore profiles A, B and C, the critical overtopping event for nearshore profile D also occurred at a water depth of 2.4 m, with a wave period of 14 s. The critical overtopping rate for nearshore profile D was also found to be very close to the overtopping rate experienced at nearshore profile C for the same conditions.



Figure 4-10: Wave overtopping at nearshore profile D ($WL_{toe} = 1.6$ m, $T_p = 14$ s)



Figure 4-9: Wave overtopping at nearshore profile D ($WL_{toe} = 2.4$ m, $T_p = 14$ s)

4.2.5. Summary of test results

The physical model test results together with the prototype values are included in tabular form in Appendix C. Tests are arranged by water depth, with the wave period increasing from 6 to 14 s.

All the relevant test results obtained from the physical model tests are presented in Figure 4-11 as a graph plotting the dimensionless discharge ($q/(gH_{m0}^3)^{0.5}$) versus relative crest freeboard (R_c/H_{m0}). Test repetitions are included in the plot; however, overtopping results obtained by using the incorrect input wave height are excluded. It should also be noted that zero overtopping results are not included in the plot, as nil parameters cannot be plotted on a semi-log graph. Also note that the discharge parameter, q , is in $m^3/s/m$.

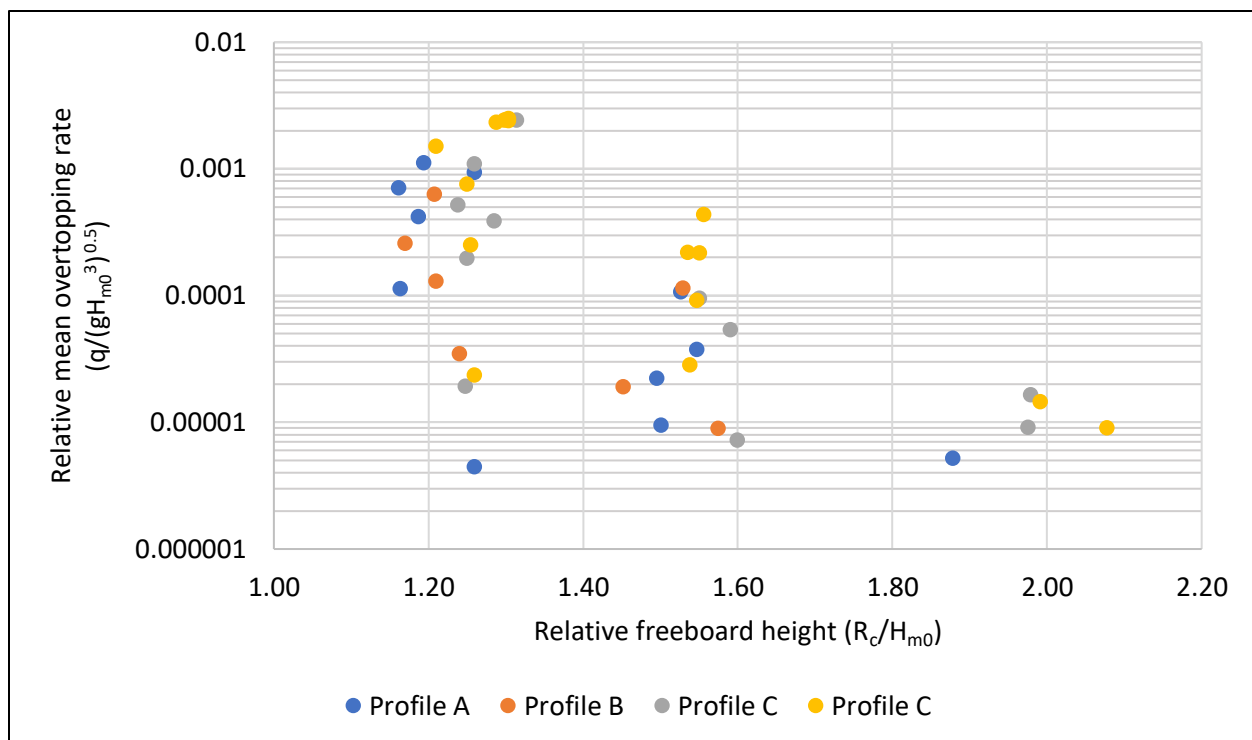


Figure 4-11: Complete overtopping data set

5. Analysis and discussion

5.1. Overview

Section 5.2 presents an in-depth analysis and discussion of the results from Chapter 4. The performance of the recurve seawall on each nearshore profile was compared for several significant hydraulic parameters. For the purpose of validating the results obtained from this study, the results were compared with the results from previous studies. A safety evaluation was done for each recurve seawall and nearshore profile pairing by comparing the acquired results to the allowable overtopping rates from the EurOtop Manual (2018). Furthermore, the procedure followed to ensure the repeatability and accuracy of tests was also completed.

5.2. Physical model tests

5.2.1. Comparison of overall test results

In terms of overtopping rates, the performance of the recurve seawall on each of the nearshore profiles is presented in Figure 5-1.

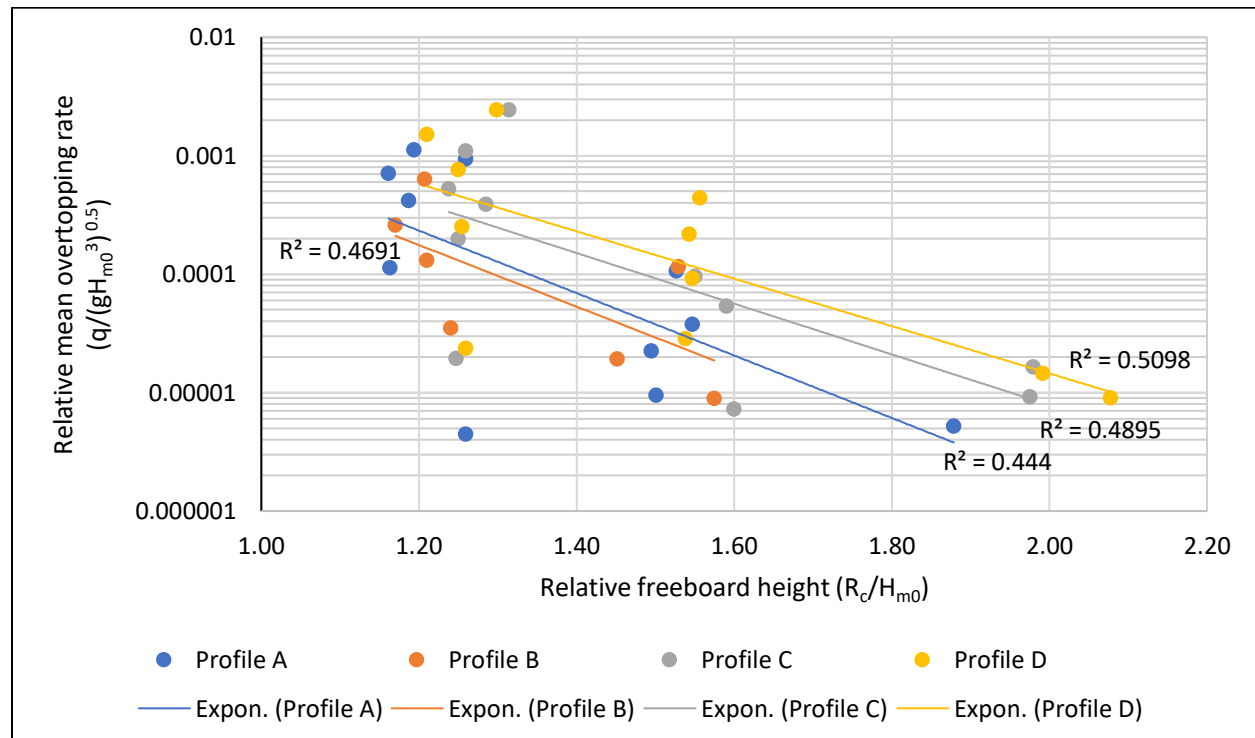


Figure 5-1: Comparison of test results obtained from all nearshore profiles

As discussed in Section 4, certain tests were repeated with the same input parameters to investigate the repeatability of tests. Therefore, in Figure 5-1, the averages are taken for results obtained from repeated tests. Taking the averages ensures that the trendline is not skewed because of duplicate tests being plotted. For Figure 5-1, the logarithmic vertical axis represents the dimensionless relative overtopping rate, whereas the linear horizontal axis represents the dimensionless relative freeboard parameter, as in EurOtop (2018).

For every nearshore profile, a reduction in the relative freeboard led to a decrease in the effectiveness of the recurve seawall in reducing wave overtopping. A recurve seawall's effectiveness, therefore, decreases with an increase in water level or wave height ($R_c/H_{m0} \leq 1.4$). As mentioned in Chapter 4, the recurve sections often became submerged during the high water levels, preventing them from reflecting wave energy effectively. The submerging of the recurve sections allowed large volumes of water to flow over the crest of the structure as green water overtopping. This observation supports the findings of Kortenhaus *et al.* (2003), which states that lower freeboards and higher waves causes recurve seawalls to not effectively reflect wave energy, making them ineffective for high water levels and wave heights.

Furthermore, Figure 5-1, illustrates that a significant reduction in overtopping was experienced for high relative freeboard conditions ($R_c/H_{m0} > 1.4$), over all four of the nearshore profiles. For the lower water levels ($R_c/H_{m0} > 1.8$), waves tended to break onto the vertical face of the seawall, but the recurve seawall effectively deflected uprushing waves back seaward as a water jet.

The spacing of the trend lines in Figure 5-1, shows that the steepness of the nearshore profile had a definite influence on the recurve seawall's ability to reduce overtopping. The plot also clearly shows an increase in overtopping rate as the nearshore profile becomes gentler. The lowest overtopping rates were found to occur on the steepest nearshore profile, profile B. On the contrary, the highest overtopping rates were found to occur on the flatter nearshore profile, profile D. However, for the test case on profile C, with a water level of 2 m and a wave period of 8 s, an exception to the norm occurred, which is further discussed in Section 5.2.2.

5.2.2. Influence of wave period

As discussed in Section 3.3, the wave period ranged from 6 to 14 s, in 2 s intervals, the same range used by Kretschmer (2017) and Walker (2018) in previous studies on wave overtopping of recurve seawalls. Although a short wave period of 6 s does not typically fall inside the swell spectrum along the South African coast, it was still included in this study to investigate the effect that wind waves have on overtopping of recurve seawalls for different nearshore profiles. The 14 s wave period was added to investigate the effect that storm sea conditions have on the overtopping of recurve seawalls for different nearshore profiles.

The sensitivity of overtopping to wave period for all the nearshore profiles, at a toe water level of 2.4 m, is shown in Figure 5-2. Appendix D includes the plots for the 2.4 m, 2.0 m and 1.6 m water levels, illustrating the sensitivity of overtopping to wave period for all four the nearshore profiles.

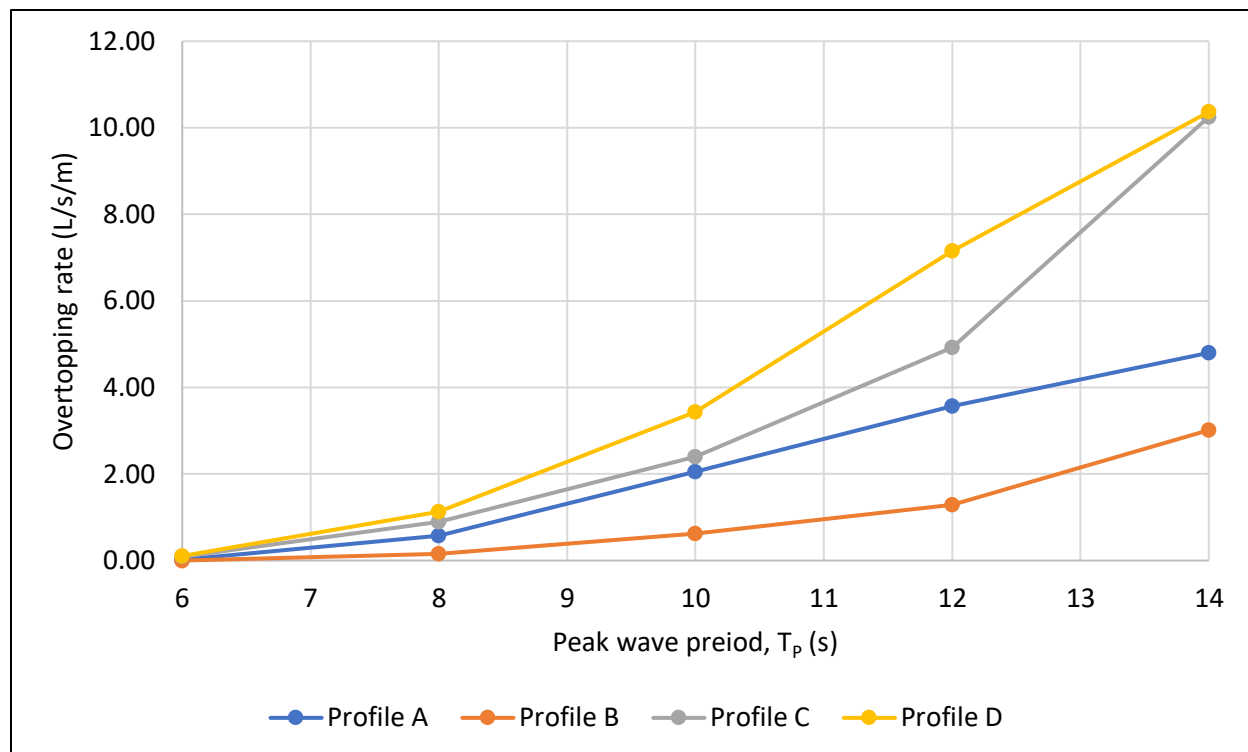


Figure 5-2: Overtopping rate as a function of wave period for a 2.4 m water depth

It can be deduced from Figure 5-2 and Appendix D that for all four nearshore profiles, the overtopping rate increases with an increase in the wave period. The finding corresponds with that of Kretschmer (2017) but contradicts Roux (2013), who found that overtopping increases with an increase in wave period, but only up to a wave period of 12 s, after which wavelengths become too big, causing waves

to reach their depth-induced breaking limit. The variance in Roux's results could be because Roux (2013) performed overtopping tests on a much gentler beach profile than Kretschmer (2017), causing the waves with large wavelengths to break before reaching the seawall.

The only outlier occurred on nearshore profile C, at a water depth of 2.0 m, where the overtopping rate decreased with 0.19 L/s/m from the 8 to the 10 s peak wave period (Appendix D.2). The increased overtopping which occurred at the 8 s wave period were caused by the collision of reflected and incident waves, which caused the waves to superimpose right in front of the seawall, causing the momentum of the incoming wave to carry the water column onto and over the crest of the recurve seawall.

Figure 5-2 shows that a wave period of 6 s results in negligibly small overtopping rates. However, because wind waves are typically formed by onshore wind, overtopping volumes can increase dramatically in practice in the form of spray overtopping, which is caused primarily by the collision of reflected and incident waves. The increase in the overtopping experienced over all four nearshore profiles, between the 6 and 8 s wave periods, generally proved to be the smallest in terms of overtopping rate; however, in terms of percentage, it was the largest, as the overtopping rate generally increased from almost zero to more significant overtopping rates.

Figure 5-2 shows that between the 8 and 10 s wave periods, the most significant increase in overtopping occurred over nearshore profile D, with an increase of 2.3 L/s/m, from 1.13 to 3.43 L/s/m. The smallest increase in overtopping between the 8 and 10 s wave periods was experienced over nearshore profile B, where the overtopping only increased by 0.46 L/s/m, from 0.16 to 0.62 L/s/m. The highest overtopping rate for the 10 s wave period, thus, occurred over nearshore profile D, where overtopping took place at a rate of 3.4 L/s/m.

Between the 10 and 12 s wave periods, the most significant increase in overtopping again occurred over nearshore profile D, where the overtopping rate increased with 3.73 L/s/m, from 3.43 to 7.16 L/s/m. The smallest increase in overtopping between the 10 and 12 s wave periods occurred over nearshore profile B, where the overtopping rate increased by 0.67 L/s/m, from 0.62 to 1.29 L/s/m. As shown in Figure 5-2, the highest overtopping rate of 7.16 L/s/m for the 12 s wave period occurred over nearshore profile D.

Although the highest overtopping rate of 10.4 L/s/m occurred during the 14 s wave period over nearshore profile D, the most significant increase in overtopping occurred between the 12 and 14 s wave periods over nearshore profile C. For nearshore profile C, the overtopping rate increased by 5.33 L/s/m, from 4.92

to 10.25 L/s/m. The smallest increase in overtopping between the 12 and 14 s wave periods was, however, experienced over nearshore profile A, where the overtopping rate increased with only 1.23 L/s/m, from 3.57 to 5.41 L/s/m. The significant increase in overtopping between the 12 and 14 s wave period over nearshore profile C is attributed to the occurrence where a small incoming wave would be reflected seawards as a jet of water, landing on the toe of a larger incoming wave (as explained in Section 4.2.3). The weight of the reflected jet falling on the toe of the incoming wave, along with the superposition of the reflected and incoming wave, resulted in a pendulum movement, which launched large volumes of water over the crest of the structure.

Figure 5-2 shows that for all four the nearshore profiles, the highest overtopping rate occurred during the 14 s wave period when the volume of water contained within a wave became too large to be contained within the recurve section. An incoming wave would thus collide with the vertical part of the wall and fill the recurve, but because the volume of water contained within the wave was too large, the rest of the water would spill over the crest of the seawall in a coherent water mass, termed green water overtopping. Section 0 explains in detail why low overtopping rates were experienced at nearshore profile B.

The overtopping of the recurve seawall was therefore significantly influenced by the wave period, irrespective of the steepness of the nearshore profile. For all four nearshore profiles, an increase in wave period generally led to an increase in the overtopping rate. An explanation for the increase in overtopping due to an increase in wave period is that with an increased wave period, the wave celerity increases, which leads to more momentum being carried by the wave, resulting in both higher white- and green water overtopping. Another influencing factor is that longer wave periods lead to longer wavelengths, which means that a larger volume of water is carried by a wave. During testing, waves with longer periods tended to fill the recurve area first, making the recurve seawall ineffective at reflecting the wave energy. Consequently, large volumes of water were able to overtop the recurve seawall because the wall became submerged.

5.2.3. Influence of water depth

The toe water levels of 1.6 m, 2.0 m and 2.4 m are the three highest water levels that were tested by Schoonees (2014), Swart (2016), Kretschmer (2017) and Walker (2018). As the recurve seawall had a design height of 4 m, the corresponding freeboard heights were, 2.4 m, 2.0 m and 1.6 m.

The plots showing the overtopping rate as a function of the water level for the 6, 8, 10, 12 and 14 s wave periods, over all four nearshore profiles are included in Appendix E. As mentioned in Section 5.2.4., the highest overtopping rate for each of the nearshore profiles occurred at the 14 s wave period. The overtopping rate as a function of the toe water level for a wave period of 14 s is shown in Figure 5-3.

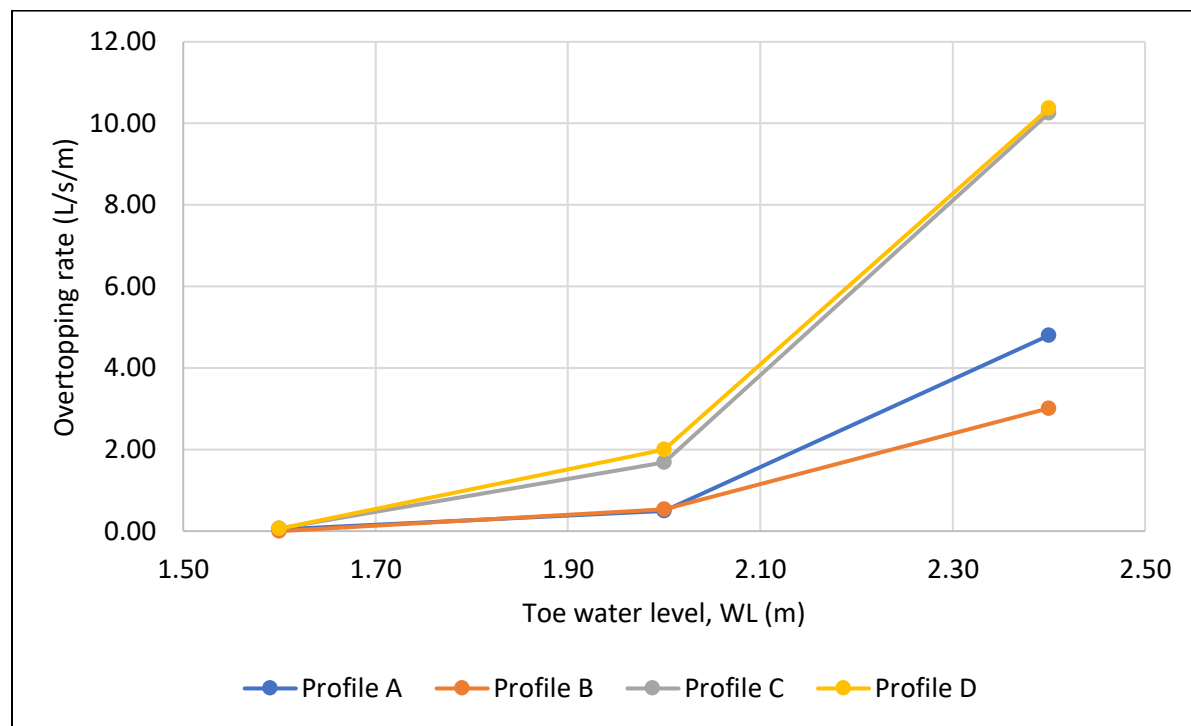


Figure 5-3: Overtopping rate as a function of water level for a 14 s wave period

Figure 5-3 shows that between the 1.6 and 2.0 m toe water level, the most significant increase in overtopping occurred over nearshore profile D, where the overtopping rate increased by 1.94 L/s/m, from 0.06 to 2 L/s/m. The highest increase in overtopping for the 14 s wave period, however, occurred between the toe water levels of 2.0 and 2.4 m, where the overtopping rate increased by 8.6 L/s/m, from 1.7 to 10.3 L/s/m.

Appendix E shows that for each of the nearshore profiles, and all 5 wave periods, the most significant increase in overtopping occurred between the 2.0 and 2.4 m water levels. Section 5.2.2 explains in detail how the significant increase in overtopping between the 2.0 and 2.4 m toe water levels can be attributed to the low freeboard height, which allows the recurve seawall to become submerged more regularly, making the seawall a lot less effective in reflecting wave energy. Due to the consequent ineffectiveness of the recurve seawall in reflecting the wave energy, large volumes of green water overtopping start to occur, especially for the longer wave periods of 12 and 14 s.

It can, therefore, be concluded that overtopping increases with an increasing water level, or decreasing freeboard height, irrespective of the wave period and nearshore profile. The magnitude of the increase in overtopping between different water levels emphasises that care should be taken when designing the crest level of recurve seawalls, especially if the recurve could become submerged at times.

5.2.4. Influence of the nearshore profile

The nearshore profiles were chosen to represent typical Southern African nearshore profiles. As mentioned in Section 3.2.3, the first nearshore profile tested was an average Southern African beach slope calculated by Schoonees (2014), and then also used by Swart (2016), Kretschmer (2017) and Walker (2018).

Overtopping tests showed a definitive increase in overtopping as the nearshore profile became gentler and the shoaling distance increased. As discussed further in Section 5.2.5, shoaling causes an increase in the wave height and a steepening of the wave face as the wave moves from deeper to shallower water. Therefore, if the shoaling distance increases, more significant shoaling of the waves takes place, leading to an increase in both the wave height and wave steepness. On the other hand, for the steep nearshore profiles, the wave height still increased without the wave face becoming steeper. The increase in overtopping can, therefore, be attributed mostly to the increase in wave steepness, which made it difficult for the recurve seawall to reflect large waves, which broke onto the vertical wall face and overhang crest simultaneously.

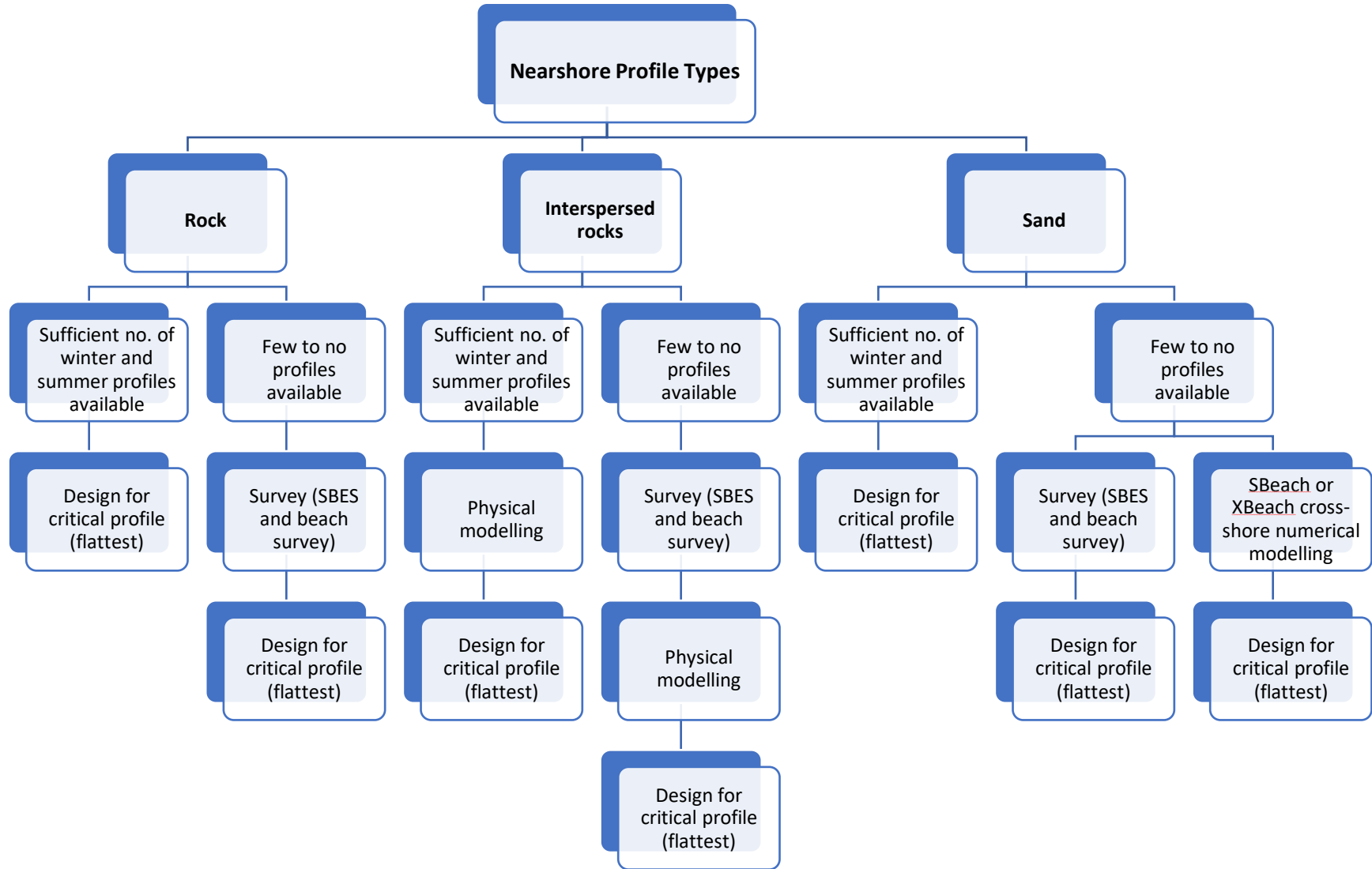


Figure 5-4: Decision chart to aid recurve seawall design

The graphs in Appendix D and E confirm the findings that wave overtopping increases with a decrease in the slope of the nearshore profile, irrespective of the water depth or wave period. The lowest overtopping rates were found to occur on the steepest nearshore profile, profile B, which has the shortest shoaling distance, whereas the highest overtopping rates were experienced on the flattest nearshore profile, profile D, which had the longest shoaling distance. The results support the findings by Roux (2013), who found that a decrease in the beach slope led to an increase in the shoaling distance, which, in turn resulted in an increase in overtopping at the recurve seawall.

The only significant exception occurred at the 1.6 m water level, where nearshore profile C led to higher overtopping rates than the gentler nearshore profile D. As will be further discussed in Section 5.2.5, the gentler nearshore profile D caused significant shoaling of the waves at the 1.6 m water level, causing waves to start breaking before reaching the recurve seawall. The breaking of waves led to a decrease in the wave heights colliding with the seawall, which, in turn, led to a decrease in the volume of overtopping.

Overtopping volume typically increases with a decrease in the steepness of the nearshore profile and vice versa. The change in overtopping volume experienced over the different nearshore profiles was attributed to their different shoaling distances. A gentler nearshore profile, which had a longer shoaling distance, caused waves to undergo more shoaling, making them steeper. Steeper waves were found to cause more significant overtopping, due to the impulsive wave conditions that typically accompanies the steep waves.

A decision chart to aid in the design of a recurve seawall is provided in Figure 5-4. The decision chart summarises the design process to follow when designing recurve seawalls on solid rock- and sand nearshore profiles, as well as the design process to follow if a nearshore profile with interspersed rock is present.

The design of recurve seawalls on coastal areas consisting entirely out of solid rock entails designing the recurve seawall for the critical nearshore profile, which is the flattest nearshore profile in the area. However, when too few nearshore profiles are available, Single Beam Echo Sounding (SBES) and beach surveys should be done to obtain the critical nearshore profile.

The design of recurve seawalls on coastal areas with nearshore profiles consisting primarily of sand with interspersed rocks should include physical modelling, irrespective of the number of surveyed profiles available. However, when few to no measured profiles are available, SBES and beach surveys should be done. Probing should also be done to find the depth of bedrock. After SBES and probing, physical

modelling should be carried out to determine the critical nearshore profile, from which the design of the recurve seawall should be completed.

Possible future changes to the nearshore zone, due to interruption of the natural sediment movement, should be considered during all project stages on sandy nearshore profiles. Nonetheless, given a sufficient number of summer and winter profiles are available, the recurve seawall can be designed for the critical, flattest profile. Should only a few measured profiles be available, cross-shore numerical modelling could be carried out to determine the critical profile. Should no profiles be available, SBES and beach surveys should be done to determine the critical nearshore profile. As the depth of the bedrock is critically important, probing should always be done, unless information from geophysical or geotechnical studies are available. Again, the recurve seawall can be designed for the critical nearshore profile.

5.2.5. Influence of wave height

According to recommendations by Mansard and Funke (1980), when measuring the wave heights in front of a reflective structure, the probes have to be located at a distance of at least one peak wavelength away from the structure in order for the reflected wave spectrum to be effectively removed by the outlined method. Therefore, the exact wave height at the toe of the reflected structure couldn't be measured with the recurve seawall in place.

As already mentioned, the solution was to construct the nearshore profile and extend the slope to the 2.0 m wave run-up height. The exact same wave input files used for the overtopping tests were run on the nearshore profiles, with the wave heights measured at the toe of the seawall, as well as at one peak wavelength in front of the planned structure. The measurement of the wave heights at the two different locations gave an indication of the change in wave height that would be experienced from one peak wavelength away from the seawall to the toe of the seawall during the overtopping tests.

Table 5-1 shows the wave height factors that were calculated by dividing the wave height at the toe of the seawall (H_t) by the incident wave height (H_i). Appendix G included the plots of the wave height factors against wave period, for each water level.

The graphs in Appendix G shows how the wave height generally increased from a peak wavelength seaward up to the face of the seawall. However, no connection could be established between the steepness of the nearshore profile and by exactly how much the wave height increased. The wave did, however, steepen more on gentler nearshore profiles, as shown in Figure 5-5, where the wave steepness

at nearshore profiles B and C are compared for the same input water level of 2.0 m and wave period of 10 s. Figure 5-7 and Appendix G show that two exceptions occurred at nearshore profile D, where waves at the 1.6 m water level started breaking before reaching the seawall, decreasing the wave height experienced in front of the structure. The second exception was where some of the larger waves on nearshore profile D also started to break at the 2.0 m water level, for wave periods between 8 and 14 s. The waves broke due to the significant shoaling and steepening experienced on the flat nearshore profile, which resulted in waves becoming unstable, causing them to break.



Figure 5-5: Wave steepness on nearshore profiles B (left) and D (right) (WL_{toe} = 2.4 m, T_p = 14 s)



Figure 5-6: Wave steepness on nearshore profiles B (left) and C (right) (WL_{toe} = 2.0 m, T_p = 10 s)

Outliers were found at nearshore profile B, at a water level of 1.6 m, between the wave heights of 8 and 14 s, where the wave height factor varies between 1.16 and 1.25. The variations were found to have occurred because the incident wave heights for tests WB2 to WB5 were slightly larger than the design wave height of 1.0 m. Table 5-1 also shows that wave tests WB7, WB8, WC11 and WC12 produced slightly higher wave height factors than some of the other tests which were done on the same nearshore profiles and water levels. The cause for the higher wave factors could be a calibration error or a mistake made setting up the absorption gain. As the errors were only realised during the analysis stage, when the slopes

had already been broken out and due to the fact that the exact same slope would be impossible to construct again, a decision was made not to redo the tests. Another factor which contributed to the decision to not redo the faulty tests was that the corresponding overtopping tests experienced nil to very little overtopping, making them non-critical tests. It is, therefore, advised that the abovementioned wave height factors should not be used for analysis and design, but that physical model tests should rather be performed for each specific construction project.

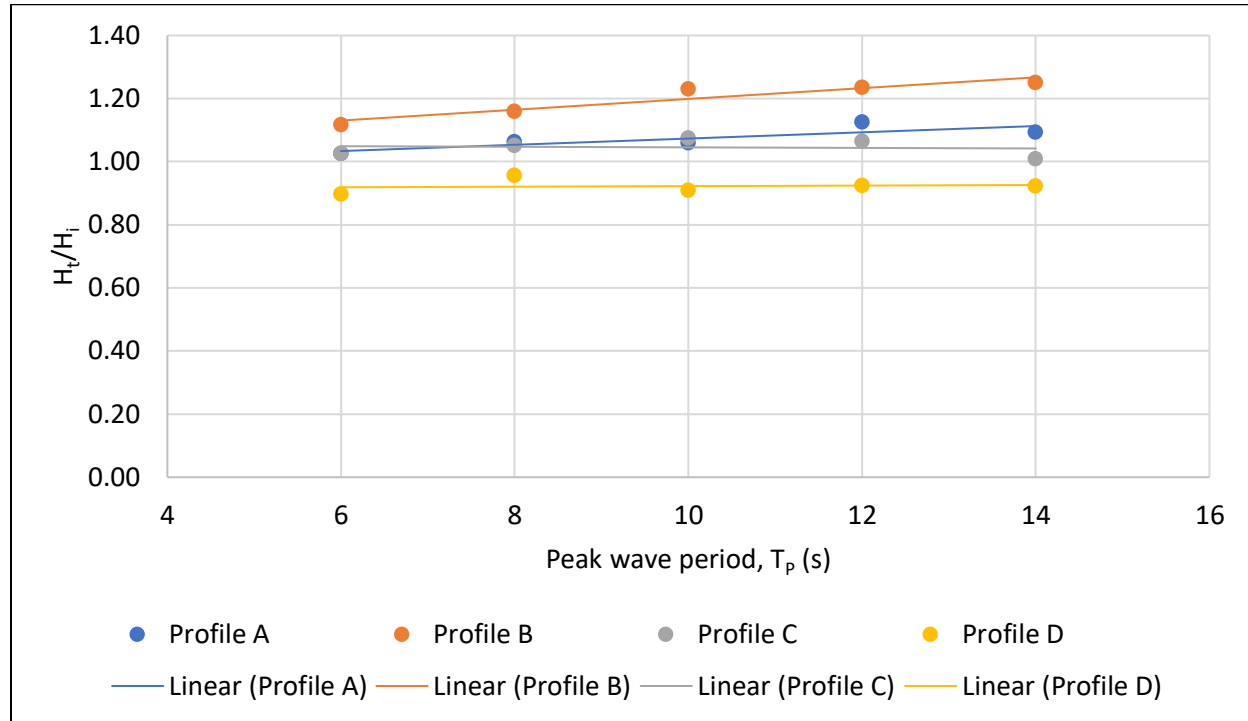


Figure 5-7: Influence of the wave period on wave height factors for 1.6 m toe water level

Table 5-1: Wave height factors (H_t/H_i)

WL _{toe} (m)		1.6					2.0					2.4				
		6	8	10	12	14	6	8	10	12	14	6	8	10	12	14
Nearshore profile	A	1.03	1.06	1.06	1.13	1.09	1.01	1.04	1.06	1.09	1.08	1.09	1.14	1.13	1.10	1.08
	B	1.12	1.16	1.23	1.24	1.25	1.10	1.21	1.22	1.08	1.05	1.14	1.19	1.18	1.17	1.19
	C	1.03	1.05	1.08	1.06	1.01	1.13	1.11	1.14	1.11	1.16	1.31	1.38	1.16	1.17	1.18
	D	0.90	0.96	0.91	0.92	0.92	1.11	1.01	0.95	1.00	1.00	1.04	1.09	1.08	1.07	1.06

5.3. Comparison with previous studies

5.3.1. Walker (2018) and Kretschmer (2017)

According to Kretschmer (2017), a recurve seawall with a rounded overhang edge had a significantly higher overtopping rate when compared to a recurve seawall with a square overhang edge. Kretschmer (2017) ascribed the increase in overtopping to the combination of strong adhesion forces between the water and rounded overhang edge, which allowed water staying adhered to the recurve surface during overtopping to traverse around and over the overhang crest. Therefore, based on the results, it would be preferable to install a recurve seawall with a square overhang edge as opposed to a recurve seawall with a bullnose overhang. However, to prevent the edges of the structure from chipping, the edges are often chamfered.

Walker (2018), therefore set out to determine the effect that chamfered edges have on the overtopping of the recurve seawall with squared overhang edges, as designed by Kretschmer (2017). The same recurve seawall design, with the chamfered edges, that was used by Walker (2018) was also used as the preferred recurve seawall design for the current study.

A comparison of the critical overtopping rates obtained by Kretschmer (2017) for both the square edged overhang and the bullnose overhang, as well as the results obtained by Walker (2018) for the recurve seawall with chamfered edges is presented in Table 5-2. The results were compared to the overtopping results obtained from tests done on nearshore profile A.

Table 5-2 shows that Walker (2018) measured much higher overtopping rates for the chamfered overhang, than what Kretschmer (2017) measured for the bullnose shaped overhang. As the chamfering produces less curvature around the overhang edge than the bullnose, the chamfered overhang is actually expected to produce better reduction in overtopping than the bullnose overhang.

The reason why Walker (2018) obtained such high overtopping rates was found to be due to the post-processing procedure used. Instead of doing a spectral analysis to obtain the spectral significant wave heights (H_{m0}), Walker (2018) did a statistical analysis of the data by doing the zero up-crossing method. After comparing the significant wave heights (H_s) obtained from the zero up-crossing and spectral analysis methods, findings showed that the zero up-crossing method gave slightly lower significant wave heights. Therefore, a larger wave height had to be used as input to obtain a 1 m incident wave height, which, because of overtopping's sensitivity to wave height, led to the larger overtopping rates.

The overtopping rates obtained over nearshore profile A, firstly confirm that chamfering reduces the effectiveness of a recurve seawall. Secondly, the overtopping measured in the current study, for the chamfered recurve seawall, proved to be 1.5% lower than the overtopping measured at the bullnose overhang by Kretschmer (2017), but 46% higher than what was measured at the square edged overhang. The chamfered overhang is, however, expected to provide better reduction in overtopping compared to the bullnose overhang, but because of the recurve seawall's sensitivity to wave height and the fact that the chamfered overhang had to reflect slightly larger incoming waves, the exact difference in reduction between the two overhangs can differ slightly.

Table 5-2: Comparison of overtopping from previous studies with overtopping experienced over nearshore profile A

Square edged overhang tested by Kretschmer (2017)				
Test		B-35	B-45-2	B-55-2
WL_{toe}	m	1.60	2.00	2.40
R_c	m	2.40	2.00	1.60
T_p	s	14.00	14.00	14.00
H_i	m	0.95	0.96	0.97
Overtopped volume	L	2222.00	51112.00	919096.00
Overtopping rate	L/s/m	0.01	0.18	3.28
Bullnose shaped overhang tested by Kretschmer (2017)				
Test		D-35	D-45	D-55-2
WL_{toe}	m	1.60	2.00	2.40
R_c	m	2.40	2.00	1.60
T_p	s	14.00	14.00	14.00
H_i	m	0.96	1.00	0.99
Overtopped volume	L	28889.00	151120.00	1364160.00
Overtopping rate	L/s/m	0.10	0.54	4.87

Chamfered overhang tested by (Walker, 2018)				
Test		B-15-3	B-20-2	B-25-1
WL_{toe}	m	1.60	2.00	2.40
R_c	m	2.40	2.00	1.60
T_p	s	14.00	14.00	14.00
H_i	m	0.99	1.01	0.98
Overtopped volume	L	64756.00	518044.00	3735111.00
Overtopping rate	L/s/m	0.23	1.85	13.34
Nearshore profile A				
Test		A5	A10	A15_avg
WL_{toe}	m	1.60	2.00	2.40
R_c	m	2.40	2.00	1.60
T_p	s	14.00	14.00	14.00
H_i	m	1.06	1.04	1.00
Overtopped volume	L	12000.00	140000.00	1344000.00
Overtopping rate	L/s/m	0.04	0.50	4.80

5.4. Repeatability and accuracy of tests performed

The accuracy of the results was improved by repeating tests with the same input parameters, and then evaluating the variability of the test results by determining a coefficient of variation (CoV) for the tests.

Combined with identical test conditions that were carried out to ensure the accuracy and reliability of results, the results of the recurve seawall tested were compared with those obtained by Walker (2018), who studied the effect that chamfering has on the overtopping of a recurve seawall. In addition, the results were also compared to the results obtained by Kretschmer (2017), who studied the overtopping of the same recurve seawall tested by Walker (2018), but without chamfering.

The coefficient of variation of the repeated tests were calculated with Equation 5.1 (EurOtop, 2018).

$$CoV(\%) = \frac{\sigma}{\mu} \times 100 \quad (5.1)$$

Where:

- σ = Standard deviation of the overtopping rates
- = Standard deviation of shallow water wave heights.

- μ = Average of the overtopping rates.
 = Average of the shallow water wave heights.

The coefficient of variation was calculated for tests WD15 and D15, which are both tests done on nearshore profile D, for water depth of 2.4 m and a wave period of 14 s. Test WD15, which was done three times, measured the wave height above the seawall toe before the installation. Test D15, which experienced the highest overtopping rate, were chosen to be repeated five times to analyse the accuracy of the acquired results.

From Table 5-3, it can be seen that the coefficient of variation for tests D15 to D15_5 were found to be 1.73%. It can be seen in Table 5-4 that the coefficient of variation for tests WD15 to WD15_3 is 0.4%. According to De Rouck *et al.* (2005), for the CLASH project, the overtopping rates for repeated tests differed by up to 12%. The EurOtop Manual (2007) also found that test repetitions done for the CLASH project produced coefficient of variation values of 10% and 13% for the two wave flumes used during testing. Therefore, considering the number of test repetitions carried out, it can be concluded that the coefficients of variation obtained are good and the test technique thus acceptable.

Table 5-3: Accuracy of tests D15 evaluated by CoV (WLtoe = 2.4 m; Tp = 14 s)

		Accuracy of tests evaluated by CoV (WLtoe = 2.4 m; Tp = 14 s)					
Test			D15	D15_2	D15_3	D15_4	D15_5
Model	T _p	s	3.130	3.130	3.130	3.130	3.130
	WL _{toe}	m	0.12	0.12	0.12	0.12	0.12
	R _c	m	0.08	0.08	0.08	0.08	0.08
	Test duration (1000 waves)	s	3130	3130	3130	3130	3130
	H _{m0}	mm	62	62	62	61	61
	H _i	mm	48	47	47	47	47
	Overtopping volume	L	361	362	366	357	368
Prototype	T _p	s	14	14	14	14	14
	WL _{toe}	m	2.40	2.40	2.40	2.40	2.40
	R _c	m	1.60	1.60	1.60	1.60	1.60
	H _{m0}	m	1.24	1.23	1.23	1.23	1.23
	H _i	m	0.96	0.95	0.95	0.95	0.95
	Overtopping volume	L	2846000	2910800	2936400	2856800	2962800
	Overtopping rate	L/s/m	10.16	10.40	10.49	10.20	10.58
	CoV	%	1.73				

Table 5-4: Accuracy of tests WD15 evaluated by CoV (WLtoe = 2.4 m; Tp = 14 s)

		Accuracy of tests evaluated by CoV (WLtoe = 2.4 m; Tp = 14 s)			
Test		WD15	WD15_2	WD15_3	
Model	T_p	s	3.130	3.130	3.130
	WL_{toe}	m	0.12	0.12	0.12
	R_c	m	0.08	0.08	0.08
	WL_{paddle}	m	0.536	0.536	0.536
	Test duration (1000 waves)	s	3130	3130	3130
	H_{m0} (shallow)	mm	56	56	56
	H_t (shallow)	mm	55	55	55
Prototype	T_p	s	14	14	14
	WL_{toe}	m	2.40	2.40	2.40
	Freeboard, R_c	m	1.60	1.60	1.60
	H_{m0} (shallow)	m	1.12	1.12	1.11
	H_t (shallow)	m	1.10	1.10	1.09
	CoV	%	0.40		

5.5. Additional aspects to consider

5.5.1. Safety limitations related to allowable overtopping rates

In order to provide a safety evaluation of the recurve seawall, the critical overtopping rates experienced for each nearshore profile and water level is summarised in Table 5-5. In Table 5-5, the critical overtopping rates are compared to the allowable mean overtopping discharges, which were provided in Table 2-2.

The critical overtopping rates for the recurve seawall, for all of the nearshore profiles and an incident wave height of 1 m was compared with the allowable mean overtopping discharges from the EurOtop Manual (2018) in Table 2-2. The comparison shows that the recurve seawall's overtopping reduction is acceptable in ensuring the safety of unprotected properties or equipment behind the seawall, as well as people standing close to the seawall. Railways and roads located close to the recurve seawall are also deemed safe at the maximum overtopping volumes experienced at the recurve seawall.

Table 5-5: Summary of critical overtopping rates for each nearshore profile

Nearshore profile A				
Test		A5	A10	A15_avg
WL _{toe}	m	1.60	2.00	2.40
R _c	m	2.40	2.00	1.60
T _p	s	14.00	14.00	14.00
H _i	m	1.06	1.04	1.00
Overtopped volume	L	12000.00	140000.00	1344000.00
Overtopping rate	L/s/m	0.04	0.50	4.80
Nearshore profile B				
Test		B5_2	B10_2	B15_2
WL _{toe}	m	1.60	2.00	2.40
R _c	m	2.40	2.00	1.60
T _p	s	14.00	14.00	14.00
H _i	m	1.02	1.00	1.00
Overtopped volume	L	0.00	150400.00	843600.00
Overtopping rate	L/s/m	0.00	0.54	3.01
Nearshore profile C				
Test		C5	C10_3	C15_2
WL _{toe}	m	1.60	2.00	2.40
R _c	m	2.40	2.00	1.60
T _p	s	14.00	14.00	14.00
H _i	m	1.01	0.99	0.95
Overtopped volume	L	19200.00	471600.00	2870000.00
Overtopping rate	L/s/m	0.07	1.68	10.25
Nearshore profile D				
Test		D5	D10	D15_avg
WL _{toe}	m	1.60	2.00	2.40
R _c	m	2.40	2.00	1.60
T _p	s	14.00	14.00	14.00
H _i	m	1.01	1.00	0.95
Overtopped volume	L	16842.11	559052.63	2902560.00
Overtopping rate	L/s/m	0.06	2.00	10.37

6. Conclusions and recommendations

6.1. General

Due to climate change and the consequent rise in sea level, the flooding risk of coastal properties is increasing. Reduction of overtopping at coastal defensive structures is therefore crucial in terms of the design, management and adaptation of coastal structures, especially when existing coastal defensive structures are evaluated for suitability in future conditions.

The crest level of existing structures can be raised in order to counter the increased wave attack caused by rising sea levels; however, raising the crest level may obstruct the sea view. Vertical seawall structures are often converted to recurve seawalls by constructing a recurve shaped overhang, on top of a new or existing vertical seawall. By adding a recurve section to seawall, the increase in the crest height of the structure can be minimised.

6.2. Findings from physical model tests

6.2.1. Effect of the nearshore profile

Physical model tests were performed on four different nearshore profiles: Nearshore profile A, which is an average Southern African nearshore profile calculated by Schoonees (2014), nearshore profile B, which is a steep Southern African nearshore profile, nearshore profile C, which is a mild Southern African nearshore profile with an offshore berm and nearshore profile D, which is a very gentle Southern African nearshore profile.

Figure 5-1 shows that the nearshore profile had a significant influence on the wave overtopping of the recurve seawall. Plots showing the overtopping against the water level and wave period also proved that wave overtopping increases with a decrease in the steepness of the nearshore profile. The lowest overtopping rates occurred on the steepest nearshore profile, profile B. On the contrary, the highest overtopping rates were found to occur on the gentler nearshore profile D. The overtopping at nearshore profiles B and D were found to differ by 244 percent for the most critical overtopping event.

The change in overtopping between different nearshore profiles was attributed to their different shoaling distances. A gentler nearshore profile, which had a longer shoaling distance, caused waves to undergo

more shoaling, making them steeper. Steeper waves were found to cause more significant overtopping, due to the impulsive wave conditions they were typically accompanied by.

Recommendations on how to integrate the effect of the nearshore profile into the design of new recurve seawalls were provided in Section 0. Furthermore, a decision chart showing the design process to follow when designing recurve seawalls on solid rock and sand nearshore profiles, as well as for nearshore profiles with interspersed rock is summarised in Figure 5-4.

6.2.2. Effect of water level

Several previous studies have found that the freeboard height and water depth at the toe of a seawall are amongst the most influential parameters for wave overtopping. Test results obtained confirm the finding, as results show that an increase in the water depth leads to an increase in the volume of overtopping, irrespective of the wave period or nearshore profile. The magnitude of the increase in overtopping between different water levels emphasises that care should be taken when designing the crest level of recurve seawalls, especially if the recurve could become submerged.

6.2.3. Effect of wave period

The general trend displayed by all the tests performed was that an increase in wave period led to an increase in wave overtopping, irrespective of the nearshore profile. Therefore, findings corresponded to the results of Kretschmer (2017), but contradict Roux (2013), who found that overtopping increased up to a wave period of 12 s, after which overtopping decreases due to wave breaking.

6.2.4. Effect of wave height

Wave height was not a variable parameter, as the incident wave height was specified to be 1 m. However, due to the irregular wave spectrum generated by the wave generator, small variations in the wave height occurred. The small variations in the incident wave height were found to have a large impact on the wave height measured at the toe of the seawall, after shoaling. The wave height at the toe of the seawall, in turn, significantly affected the overtopping rate measured at the recurve seawall.

The wave height generally increased from a peak wavelength seaward up to the face of the seawall. However, no connection could be established between the steepness of the nearshore profile and by exactly how much the wave height increased. Due to the large impact that a change in wave height can have on wave overtopping, it was crucial to ensure that the incident wave heights were accurate.

Therefore, in order to ensure accurate results were obtained, several tests had to be repeated to achieve the correct input wave height.

6.3. Comparison with previous research

The overtopping rates obtained over nearshore profile A firstly confirm that chamfering reduces the effectiveness of a recurve seawall. Secondly, the overtopping measured for the chamfered overhang was found to be 1.5% lower than the overtopping measured at the bullnose overhang, but 46% higher than what was measured at the square edged overhang, designed by Kretschmer (2017). The results make sense, since the chamfering produces less curvature around the overhang edge than the bullnose, making it more difficult for water to track around the overhang edge due to the adhesion forces between the water molecules and the structure.

6.4. Recommendations for further research

The variations in wave height caused by the wave generator were found to have a significant influence on the overtopping volumes measured for the recurve seawall. Therefore, it is recommended that further studies be conducted on the effect of wave height on wave overtopping of a recurve seawall.

It is also recommended that further model tests should be conducted on the effect that beach erosion or accretion has on the overtopping of recurve seawalls. Observation of physical model tests during the study showed that waves which shoaled to finally break onto the seawall had a much higher impact on the structure. Therefore, further studies into the forces exerted by different wave conditions could be studied and combined with research on the structural integrity of a recurve seawall.

References

- Allsop, N.W.H., Pullen, T.A., Van der Meer, J.W., Bruce, T., Schüttrumpf, H. and Kortenhaus, A., 2008. Improvements in wave overtopping analysis: the EurOtop overtopping manual and calculation tool. *Proc. COPEDEC VII, Dubai, UAE*.
- Allsop, W., Alderson, J. and Chapman, A., 2007. Defending buildings and people against wave overtopping. In *Coastal Structures 2007*: (pp. 1253-1262).
- Allsop, W., Bruce, T., Pearson, J. and Besley, P., 2005. Wave overtopping at vertical and steep seawalls. In *Proceedings of the Institution of Civil Engineers-Maritime Engineering* (Vol. 158, No. 3, pp. 103-114). Thomas Telford Ltd.
- Banyard, L. and Herbert, D.M., 1995. The effect of wave angle on the overtopping of seawalls. *HR Wallingford, Report SR396*.
- Berkeley-Thorn, R. and Roberts, A.C., 1981. Sea defense and coast protection works. London: *Thomas Telford Ltd*.
- Bradbury, A.P. and Allsop, N.W.H., and Stephens, R.V., 1988. Hydraulic Performance of Breakwater Crown Walls. In *Design of breakwaters* (pp. 1-108). Thomas Telford Publishing.
- Bruce, T., Van Der Meer, J., Pullen, T. and Allsop, W., 2009. Wave overtopping at vertical and steep structures. In *Handbook of coastal and ocean engineering* (pp. 411-439).
- Castellino, M., Lara, J.L., Romano, A., Losada, I.J. and De Girolamo, P., 2018. Wave Loading for Recurved Parapet Walls in Non-Breaking Wave Conditions: Analysis of the Induced Impulsive Forces. *Coastal Engineering Proceedings*, 1(36).
- Chadwick, A. J., Morfett, J. C. and Borthwick, M., 2013. *Hydraulics in Civil and Environmental Engineering*. 5th edn. Boca Raton: CRC Press.
- EurOtop Manual, 2007. Wave Overtopping of Sea Defences and Related Structures–Assessment Manual. UK: NWH Allsop, T. Pullen, T. Bruce. NL: JW van der Meer. DE: H. Schüttrumpf, A. Kortenhaus. www.overtopping-manual.com.

EurOtop, 2018. Manual on wave overtopping of sea defences and related structures. An overtopping manual largely based on European research, but for worldwide application. Van der Meer, J.W., Allsop, N.W.H., Bruce, T., De Rouck, J., Kortenhaus, A., Pullen, T., Schüttrumpf, H., Troch, P. and Zanuttigh, B., www.overtopping-manual.com.

Franco, L., De Gerloni, M. and Van der Meer, J.W., 1994. Wave overtopping on vertical and composite breakwaters. In *Coastal Engineering 1994* (pp. 1030-1045).

HR Wallingford, 2010. *Large Flume wave absorption System: User and Technical Manual Supplied to University of Stellenbosch*.

Hughes, S.A., 1993. *Physical models and laboratory techniques in coastal engineering* (Vol. 7). World Scientific.

Kamikubo, Y., Murakami, K., Irie, I., Kataoka, Y. and Takehana, N., 2003, January. Reduction of wave overtopping and water spray with using flaring shaped seawall. In *the Thirteenth International Offshore and Polar Engineering Conference*. International Society of Offshore and Polar Engineers.

Kortenhaus, A., Pearson, J., Bruce, T., Allsop, N.W.H. and Van der Meer, J.W., 2003. Influence of parapets and recures on wave overtopping and wave loading of complex vertical walls. In *Coastal Structures 2003* (pp. 369-381).

Kretschmer, M.M., 2017. *Effect of the form of the overhang of a recurve seawall to reduce wave overtopping* (Master's thesis, Stellenbosch: Stellenbosch University).

Mansard, E.P. and Funke, E.R., 1980. The measurement of incident and reflected spectra using a least squares method. In *Coastal Engineering 1980* (pp. 154-172).

Murakami, K., Irie, I. and Kamikubo, Y., 1996. Experiments on a non-wave overtopping type seawall. In *Coastal Engineering 1996* (pp. 1840-1851).

Murakami, K., Kamikubo, Y. and Takehana, N., 2004. 'Hydraulic efficiencies of non-wave overtopping type seawall installed on a mound', in Cheng, L. and Yeow, K. (eds) *Hydrodynamics VI: Theory and Applications: Proceedings of the 6th International Conference of Hydrodynamics*. London: Taylor & Francis Group, pp. 255–260.

Murakami, K., Kamikubo, Y. and Kataoka, Y., 2008, January. Hydraulic performances of non-wave overtopping type seawall against sea level rise due to global warming. In *the Eighteenth International Offshore and Polar Engineering Conference*. International Society of Offshore and Polar Engineers (pp. 706–712).

Murakami, K., Maki, D. and Takehana, N., 2011. Wave overtopping on flaring shaped seawall under oblique incident waves. In *Asian And Pacific Coasts 2011* (pp. 1865-1872).

Owen, M.W., 1980. Design of seawalls allowing for overtopping. *HR Wallingford, Report EX924*.

Owen, M. W. and Steele, A. A. J., 1993. *Effectiveness of recurved wave return walls. Report SR 261: HR Wallingford*.

Pearson, J., Bruce, T., Allsop, W., Kortenhaus, A. and Van der Meer, J.W., 2004. Effectiveness of recurve walls in reducing wave overtopping on seawalls and breakwaters. In *Coastal Engineering 2004: (In 4 Volumes)* (pp. 4404-4416).

Pearson, J., Bruce, T., Allsop, W. and Gironella, X., 2002. Violent wave overtopping—measurements at large and small scale. In *Coastal Engineering 2002: Solving Coastal Conundrums* (pp. 2203-2215).

PRDW, Entech and CSIR, 1997. Algoa Bay Industrial Port: Feasibility Study. Tech. Rep., Prestedge Retief Dresner Wijnberg, Cape Town, South Africa.

Reis, M.T., Neves, M.G. and Hedges, T., 2008. Investigating the lengths of scale model tests to determine mean wave overtopping discharges. *Coastal engineering journal*, 50(4), pp.441-462.

Rossouw, J., 1989. *Design waves for the South African coastline* (Doctoral dissertation, Stellenbosch: University of Stellenbosch).

Roux, G.B., 2013. *Reduction of seawall overtopping at the Strand* (Doctoral dissertation, Stellenbosch: Stellenbosch University).

Rutherford, K., 2015. *Shoreline changes and longshore transport at the Port of Ngqura* (Master's thesis, Stellenbosch: Stellenbosch University).

SA Navy, 2018. *South African Tide Tables*. Tokai.

Schoonees, J. S., Weitz, N., Schonegevel, L., Theron, A. K., Davids, G. and Hughes, S., 2005. Sedimentation of the small-craft harbour at Swakopmund. CSIR report ENV-S-C 2005-004. Stellenbosch.

Schoonees, J.S., Lynn, B.C., Le Roux, M. and Bouton, P., 2008. Development set-back line for southern beaches of Richards Bay. *Stellenbosch: WSP*.

Schoonees, J.S., Lenhoff, L. and Raw, A.J., 1999. Preventing natural breaching of the major sand spit protecting the port of Walvis Bay. In *Coastal Engineering 1998* (pp. 1475-1488).

Schoonees, T., 2014. *Impermeable recurve seawalls to reduce wave overtopping* (Master's thesis, Stellenbosch: Stellenbosch University).

Soltau, C., 2009. *The cross-shore distribution of grain size in the longshore transport zone* (Master's thesis, Stellenbosch: University of Stellenbosch).

Swart, D. H., Schoonees, J. S., Scholtz, D. J. P., Van Tonder, A., Moller, J. P. and Lenhoff, L., 1983. Valsbaai: Velddataverslag, Volume II: Figure. WNNR-VERSLAG C/SEA 8219/2. Stellenbosch.

Swart, E., 2016. *Effect of the overhang length of a recurve seawall in reducing wave overtopping* (Master's thesis, Stellenbosch: Stellenbosch University).

Swarzenski, P., 2014. *Assessing the Vulnerability of Pacific Atolls to Climate Change*. Available at: <https://soundwaves.usgs.gov/2014/04/> (Accessed: 14 March 2019).

Theron, A.K., 2016. *Methods for determination of coastal development setback lines in South Africa* (Doctoral dissertation, Stellenbosch: Stellenbosch University).

Theron, A. K., De Wet, P. D., Watt, L. J., and Von St Ange, U., 2010. Durban Beach Monitoring Progress Report: July 2007 to June 2008, Volume I: Main Report. CSIR report CSIR/NRE/ CO/ER/2009/0105/C Vol1. Stellenbosch, South Africa

USACE, 1984. *Shore Protection Manual (Vol. 4)*. US Government Printing Office, Washington DC.

USACE, 1991. *Reduction of wave overtopping by parapets*. Mississippi.

Van Doorslaer, K. and De Rouck, J., 2011. Reduction on wave overtopping on a smooth dike by means of a parapet. *Coastal Engineering Proceedings*, 1(32), p.6.

Veale, W., Suzuki, T., Verwaest, T., Trouw, K. and Mertens, T., 2012. Integrated design of coastal protection works for Wenduine, Belgium. *Coastal Engineering Proceedings*, 1(33), p.70.

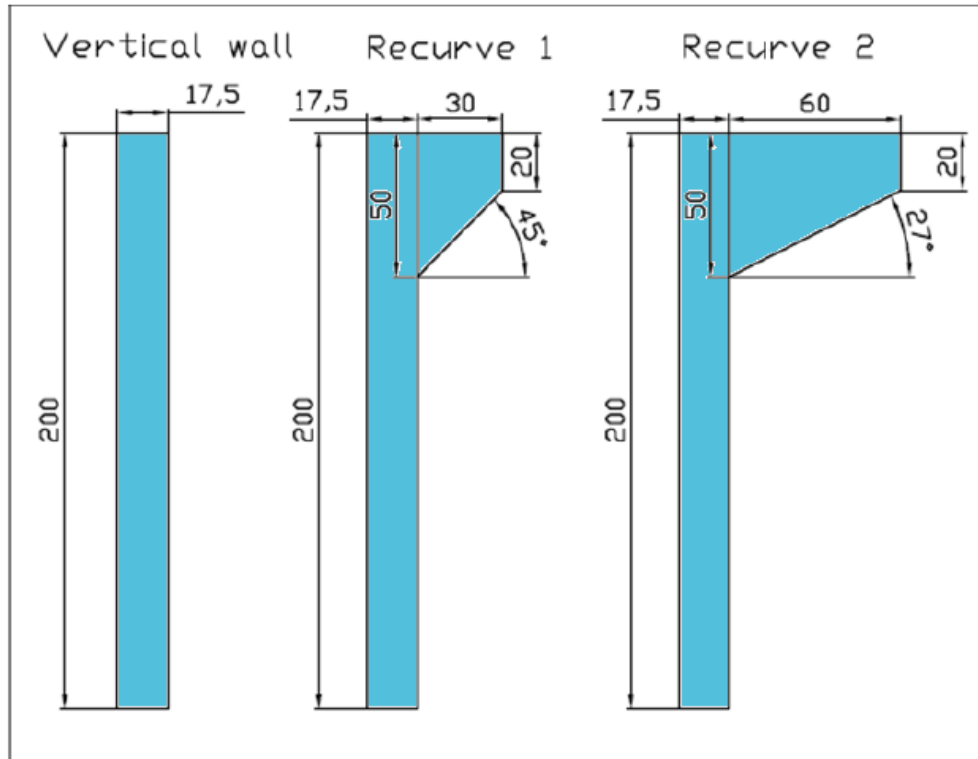
Walker, S. R., 2018. *The effect on wave overtopping of the addition of a kerb to a parapet seawall* (Master's project, Stellenbosch: Stellenbosch University).

List of Appendices

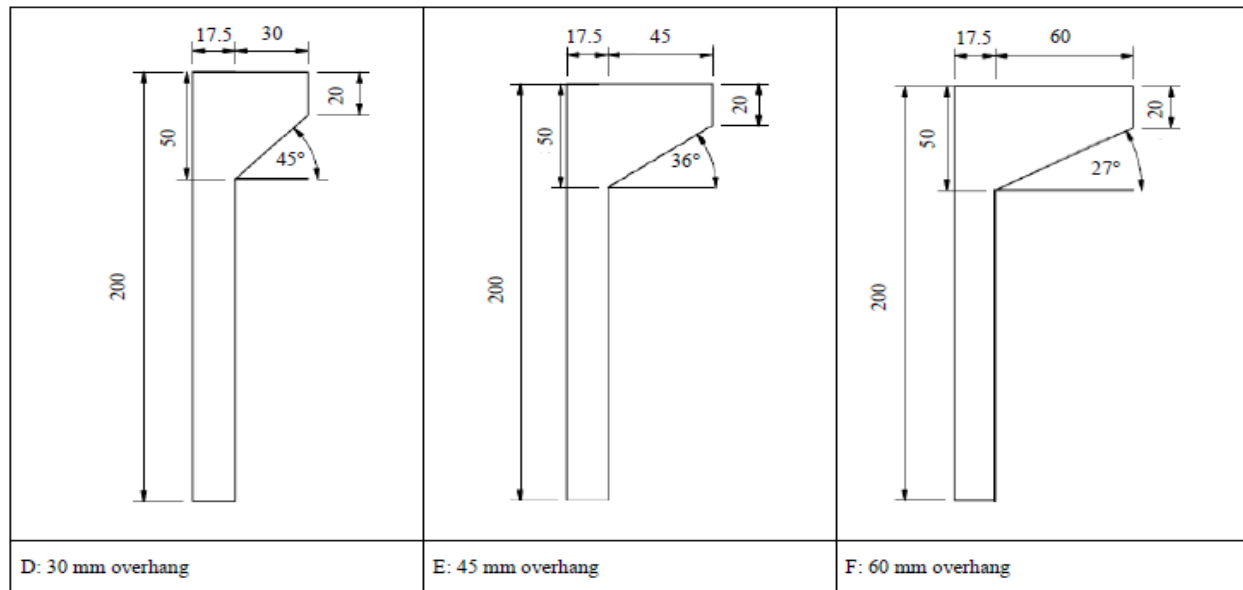
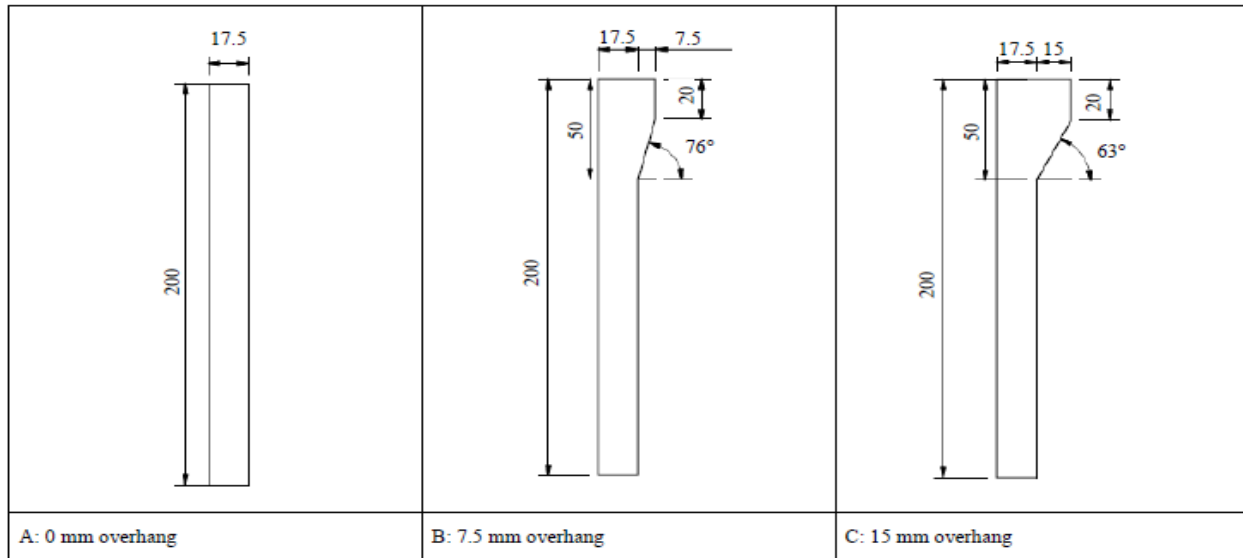
- Appendix A: Recurve seawall designs from previous studies
- Appendix B: Long-sections of the wave flume, built-in profiles
- Appendix C: Physical model results
- Appendix D: Influence of wave period on overtopping
- Appendix E: Influence of water depth on overtopping
- Appendix F: Influence of the nearshore slope on overtopping
- Appendix G: Influence of nearshore slope on wave height
- Appendix H: Probe spacings

Appendix A: Recurve seawall designs from previous studies

A.1. Schoonees (2014) model recurve seawall designs

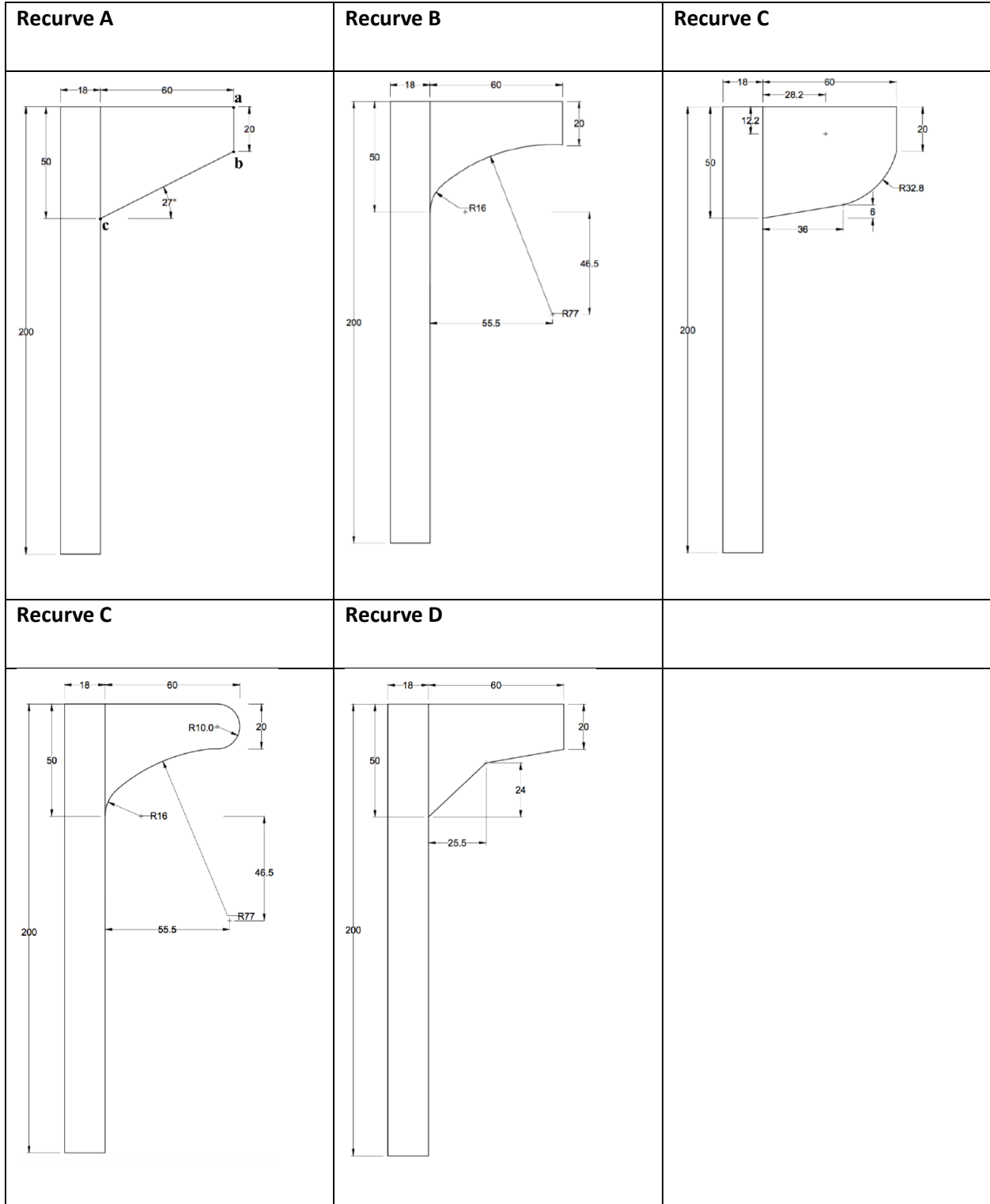


A.2. Swart (2016) model recurve seawall designs



<p>Technical drawing of a T-section with a 75 mm overhang. The stem height is 200 mm, the flange thickness is 20 mm, and the flange width is 75 mm. The fillet radius is 17.5 mm. The fillet angle is 22 degrees.</p>	<p>Technical drawing of a T-section with a 90 mm overhang. The stem height is 200 mm, the flange thickness is 20 mm, and the flange width is 90 mm. The fillet radius is 17.5 mm. The fillet angle is 18 degrees.</p>	<p>Technical drawing of a T-section with a 105 mm overhang. The stem height is 200 mm, the flange thickness is 20 mm, and the flange width is 105 mm. The fillet radius is 17.5 mm. The fillet angle is 16 degrees.</p>
<p>G: 75 mm overhang</p>	<p>H: 90 mm overhang</p>	<p>I: 105 mm overhang</p>

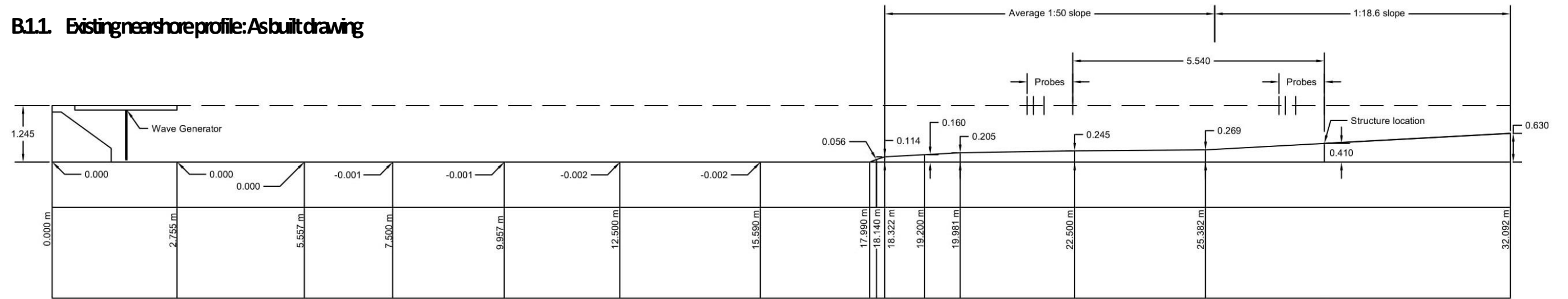
A.3. Kretschmer (2017) model recurve seawall designs



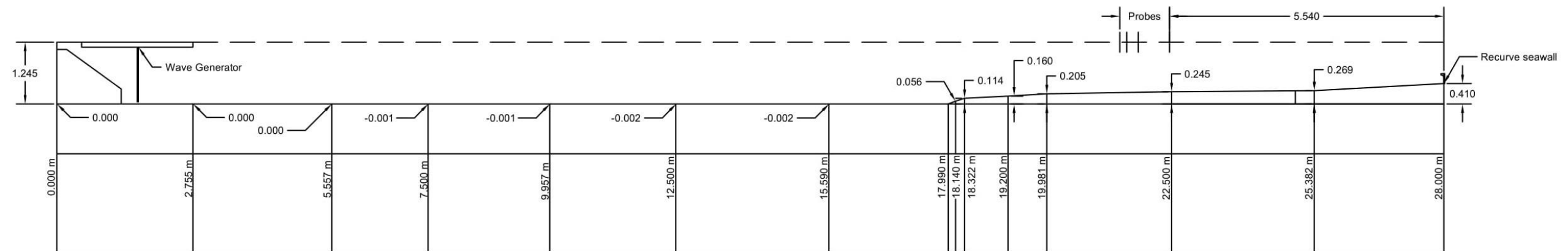
Appendix B: Long-sections of the wave flume, built-in profiles

B.1. Wave flume long section: Existing nearshore profile

B.1.1. Existing nearshore profile: As built drawing

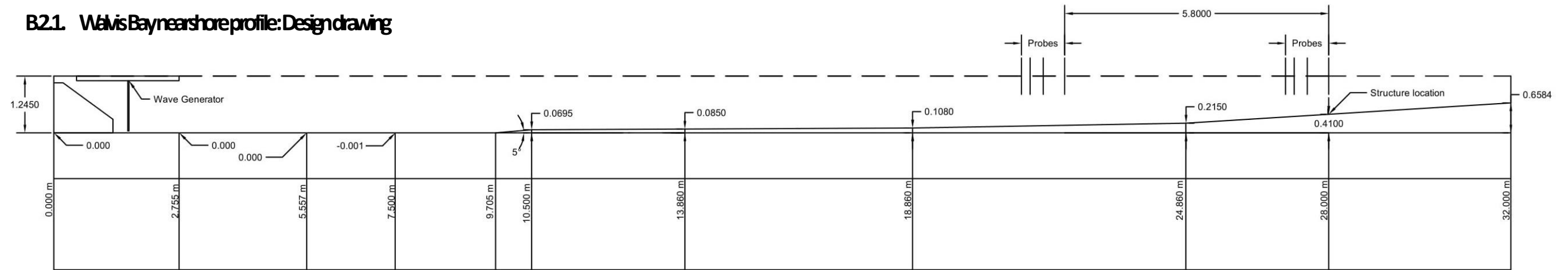


B.1.2. Existing nearshore profile: As built drawing

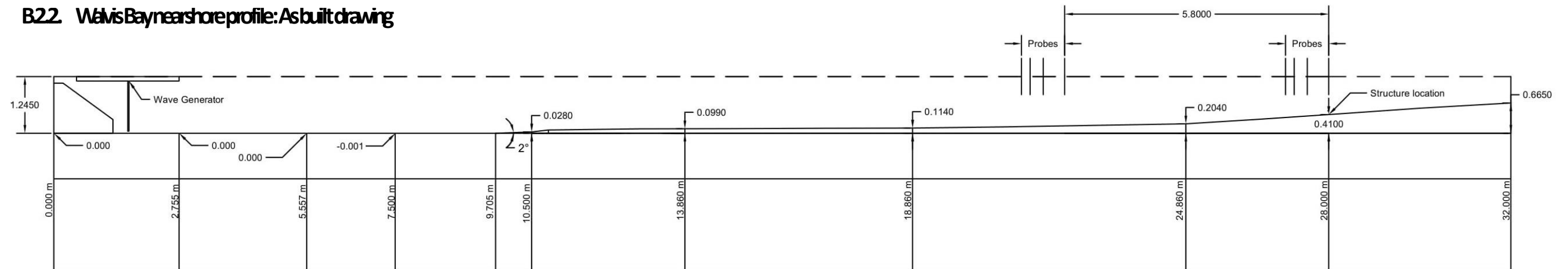


B.2. Wave flume long section: Walvis Bay nearshore profile

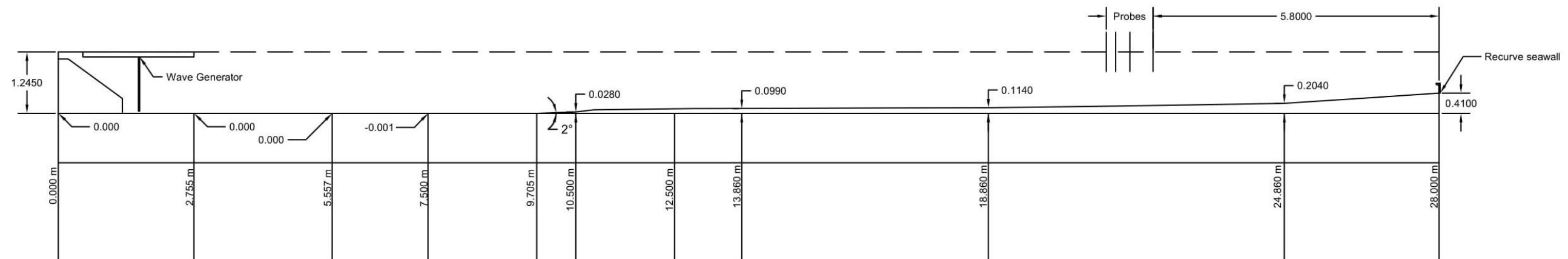
B2.1. Walvis Bay nearshore profile: Design drawing



B2.2. Walvis Bay nearshore profile: As built drawing

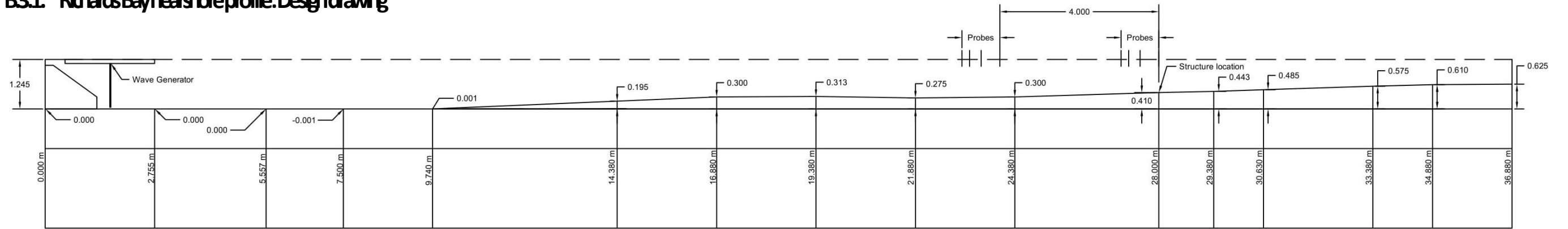


B2.3. Walvis Bay nearshore profile: As built drawing

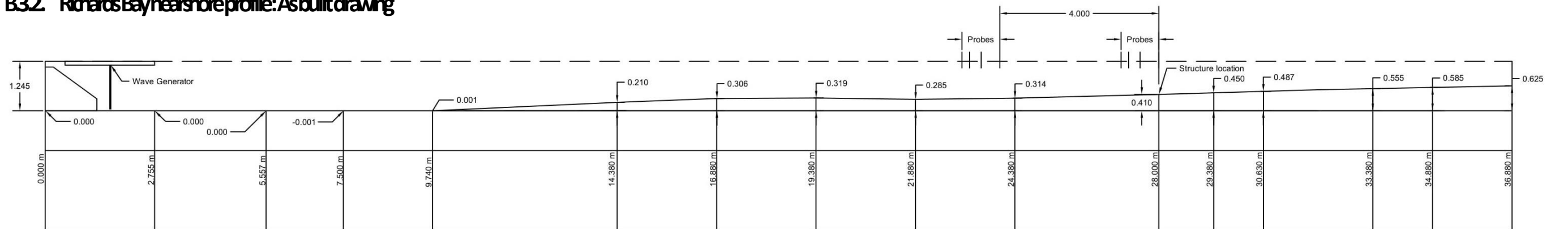


B.3. Wave flume long section: Richards Bay nearshore profile

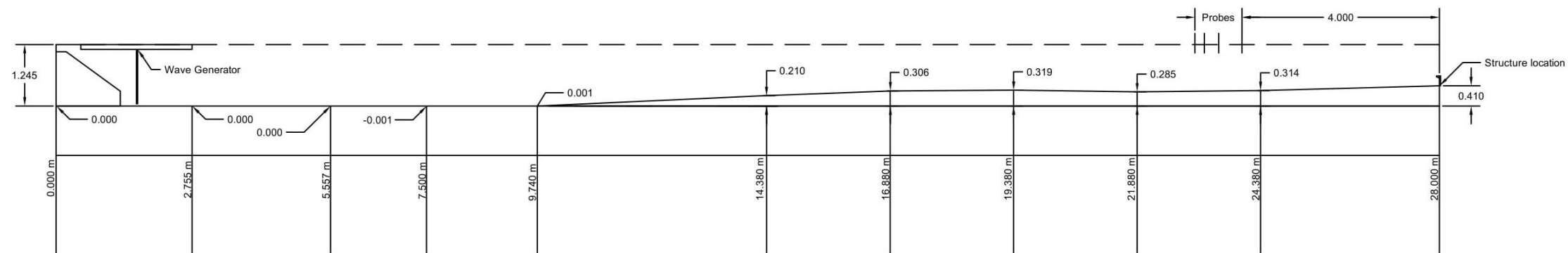
B3.1. Richards Bay nearshore profile: Design drawing



B3.2. Richards Bay nearshore profile: As built drawing

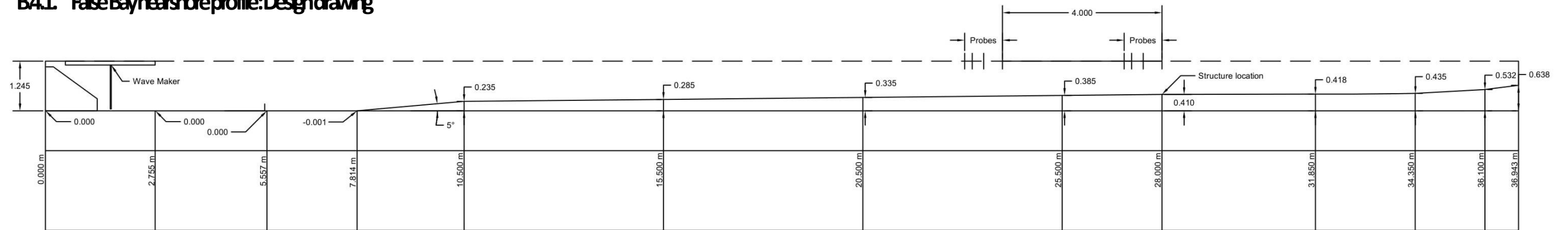


B3.3. Richards Bay nearshore profile: As built drawing

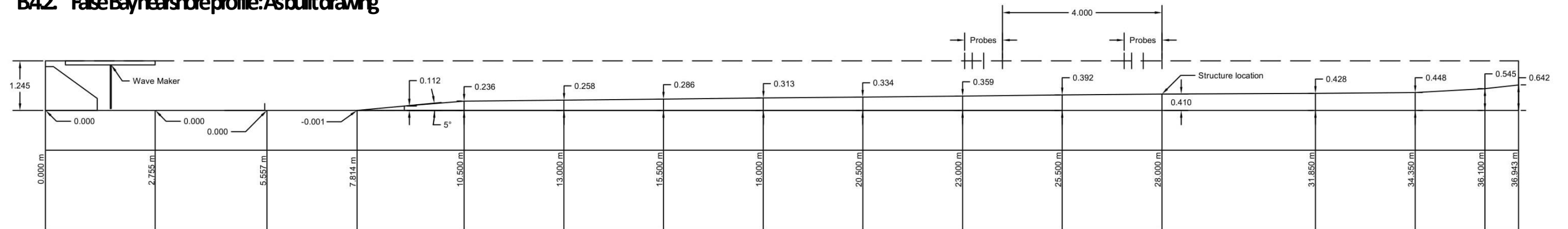


B.4. Wave flume long section: False Bay nearshore profile

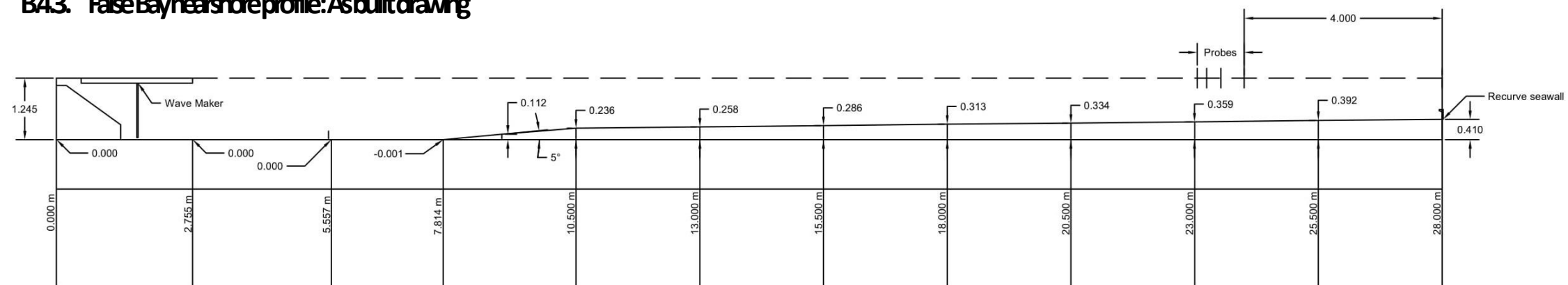
B4.1. False Bay nearshore profile: Design drawing



B4.2. False Bay nearshore profile: As built drawing



B4.3. False Bay nearshore profile: As built drawing



Appendix C: Physical model results

C.1. Profile A: Existing nearshore profile

C.1.1 Overtopping test results

Profile A: Existing nearshore slope			A1	A1_2	A2	A3	A4	A5
Model	T _p	s	1.342	1.342	1.789	2.236	2.683	3.130
	WL _{toe}	m	0.08	0.08	0.08	0.08	0.08	0.08
	R _c	m	0.12	0.12	0.12	0.12	0.12	0.12
	WL _{paddle}	m	0.496	0.496	0.496	0.496	0.496	0.496
	Test duration (1000 waves)	s	1342	1342	1789	2236	2683	3130
	H _{m0}	mm	67	64	65	62	64	64
	H _i	mm	54	51	52	50	52	53
	Overtopping volume	L	0.00	0.00	0.00	0.00	0.70	1.50
Prototype								
Prototype	T _p	s	6	6	8	10	12	14
	WL _{toe}	m	1.60	1.60	1.60	1.60	1.60	1.60
	R _c	m	2.40	2.40	2.40	2.40	2.40	2.40
	H _{m0}	m	1.34	1.27	1.30	1.25	1.28	1.28
	H _i	m	1.08	1.02	1.04	0.99	1.03	1.06
	Overtopping volume	L	0	0	0	0	5600	12000
	Overtopping rate	L/s/m	0.00	0.00	0.00	0.00	0.02	0.04

Profile A: Existing nearshore slope			A6	A6_2	A7	A7_2	A7_3	A8	A8_2	A9	A10
Model	T _p	s	1.342	1.342	1.789	1.789	1.789	2.236	2.236	2.683	3.130
	WL _{toe}	m	0.10	0.10	0.10	0.10	0.10	0.10	0.10	0.10	0.10
	R _c	m	0.10	0.10	0.10	0.10	0.10	0.10	0.10	0.10	0.10
	WL _{paddle}	m	0.516	0.516	0.516	0.516	0.516	0.516	0.516	0.516	0.516
	Test duration (1000 waves)	s	1342	1342	1789	1789	1789	2236	2236	2683	3130
	H _{m0}	mm	60	67	71	66	66	69	67	65	66
	H _i	mm	46	52	55	51	51	53	52	50	52
	Overtopping volume	L	0.00	0.00	0.00	0.00	0.00	3.10	2.70	5.20	17.50
Prototype	T _p	s	6	6	8	8	8	10	10	12	14
	WL _{toe}	m	2.00	2.00	2.00	2.00	2.00	2.00	2.00	2.00	2.00
	R _c	m	2.00	2.00	2.00	2.00	2.00	2.00	2.00	2.00	2.00
	H _{m0}	m	1.21	1.33	1.41	1.32	1.32	1.39	1.34	1.29	1.31
	H _i	m	0.92	1.04	1.11	1.02	1.02	1.07	1.04	1.00	1.04
	Overtopping volume	L	0	0	0	0	0	24800	21600	41600	140000
	Overtopping rate	L/s/m	0.00	0.00	0.00	0.00	0.00	0.12	0.11	0.17	0.50

Profile A: Existing nearshore slope			A11	A12	A12_2	A13	A14	A15	A15_2
Model	T _p	s	1.342	1.789	1.789	2.236	2.683	3.130	3.130
	WL _{toe}	m	0.12	0.12	0.12	0.12	0.12	0.12	0.12
	R _c	m	0.08	0.08	0.08	0.08	0.08	0.08	0.08
	WL _{paddle}	m	0.536	0.536	0.536	0.536	0.536	0.536	0.536
	Test duration (1000 waves)	s	1342	1789	1789	2236	2683	3130	3130
	H _{m0}	mm	64	69	69	67	69	64	67
	H _i	mm	48	52	53	51	53	49	52
	Overtopping volume	L	0.30	11.45	12.35	51.30	107.15	146.65	189.35
Prototype	T _p	s	6	8	8	10	12	14	14
	WL _{toe}	m	2.40	2.40	2.40	2.40	2.40	2.40	2.40
	R _c	m	1.60	1.60	1.60	1.60	1.60	1.60	1.60
	H _{m0}	m	1.27	1.38	1.38	1.35	1.38	1.27	1.34
	H _i	m	0.96	1.04	1.05	1.02	1.05	0.97	1.03
	Overtopping volume	L	2400	91600	98800	410400	857200	1173200	1514800
	Overtopping rate	L/s/m	0.02	0.57	0.62	2.05	3.57	4.19	5.41

C.1.2 Shallow water wave test results

Profile A: Existing nearshore slope			WA1	WA1_2	WA2	WA2_2	WA3	WA3_2	W_A3_3	WA4	WA4_2	W_A5	WA5_2
Model	T _p	s	1.342	1.342	1.789	1.789	2.236	2.236	2.236	2.683	2.683	3.130	3.130
	WL _{toe}	m	0.08	0.08	0.08	0.08	0.08	0.08	0.08	0.08	0.08	0.08	0.08
	Freeboard, R _c	m	0.12	0.12	0.12	0.12	0.12	0.12	0.12	0.12	0.12	0.12	0.12
	WL _{paddle}	m	0.496	0.496	0.496	0.496	0.496	0.496	0.496	0.496	0.496	0.496	0.496
	Test duration (1000 waves)	s	1342	1342	1789	1789	2236	2236	2236	2683	2683	3130	3130
	H _{m0} (shallow)	mm	54	58	55	61	61	64	56	62	64	59	57
	H _t (shallow)	mm	54	58	55	60	61	64	56	61	63	56	57
	H _{m0} (deep)	mm	53	57	52	57	57	60	53	55	58	54	49
	H _i (deep)	mm	53	57	52	57	57	60	52	54	58	51	49
Prototype	T _p	s	6	6	8	8	10	10	10	12	12	14	14
	WL _{toe}	m	1.60	1.60	1.60	1.60	1.60	1.60	1.60	1.60	1.60	1.60	1.60
	Freeboard, R _c	m	2.40	2.40	2.40	2.40	2.40	2.40	2.40	2.40	2.40	2.40	2.40
	H _{m0} (shallow)	m	1.09	1.17	1.11	1.21	1.22	1.28	1.12	1.23	1.27	1.17	1.14
	H _t (shallow)	m	1.08	1.16	1.10	1.21	1.22	1.27	1.11	1.22	1.27	1.12	1.13
	H _{m0} (deep)	m	1.06	1.15	1.04	1.14	1.14	1.20	1.06	1.09	1.16	1.07	0.98
	H _i (deep)	m	1.06	1.14	1.04	1.14	1.14	1.20	1.05	1.09	1.15	1.03	0.97
	H _t / H _i	-	1.03	1.02	1.06	1.06	1.07	1.06	1.06	1.13	1.10	1.09	1.17

Profile A: Existing nearshore slope		WA6	WA6_2	WA6_3	WA7	WA7_2	WA8	W_A8_2	WA8_3	W_A9	W_A10	
Model	T _p	s	1.342	1.342	1.342	1.789	1.789	2.236	2.236	2.236	2.683	3.130
	WL _{toe}	m	0.10	0.10	0.10	0.10	0.10	0.10	0.10	0.10	0.10	0.10
	Freeboard, R _c	m	0.10	0.10	0.10	0.10	0.10	0.10	0.10	0.10	0.10	0.10
	WL _{paddle}	m	0.516	0.516	0.516	0.516	0.516	0.516	0.516	0.516	0.516	0.516
	Test duration (1000 waves)	s	1342	1342	1342	1789	1789	2236	2236	2236	2683	3130
	H _{m0} (shallow)	mm	58	60	53	49	62	58	57	54	55	55
	H _t (shallow)	mm	58	60	53	49	62	57	57	54	55	54
	H _{m0} (deep)	mm	58	57	53	48	58	52	53	51	51	50
	H _i (deep)	mm	58	57	52	47	57	52	52	51	51	50
Prototype	T _p	s	6	6	6	8	8	10	10	10	12	14
	WL _{toe}	m	2.00	2.00	2.00	2.00	2.00	2.00	2.00	2.00	2.00	2.00
	Freeboard, R _c	m	2.00	2.00	2.00	2.00	2.00	2.00	2.00	2.00	2.00	2.00
	H _{m0} (shallow)	m	1.16	1.20	1.06	0.99	1.24	1.15	1.14	1.09	1.11	1.09
	H _t (shallow)	m	1.15	1.19	1.06	0.98	1.23	1.15	1.14	1.08	1.10	1.08
	H _{m0} (deep)	m	1.16	1.14	1.05	0.95	1.15	1.05	1.05	1.02	1.02	1.01
	H _i (deep)	m	1.16	1.14	1.05	0.95	1.15	1.04	1.05	1.02	1.02	1.00
	H _t / H _i	-	1.00	1.05	1.01	1.04	1.07	1.10	1.08	1.06	1.09	1.08

Profile A: Existing nearshore slope			WA11	WA11_2	WA12	WA12_2	WA13	WA13_2	W_A14	WA14_2	WA14_3	WA15_2	WA15_3	WA15_4
Model	T _p	s	1.342	1.342	1.789	1.789	2.236	2.236	2.683	2.683	2.683	3.130	3.130	3.130
	WL _{toe}	m	0.12	0.12	0.12	0.12	0.12	0.12	0.12	0.12	0.12	0.12	0.12	0.12
	Freeboard, R _c	m	0.08	0.08	0.08	0.08	0.08	0.08	0.08	0.08	0.08	0.08	0.08	0.08
	WL _{paddle}	m	0.536	0.536	0.536	0.536	0.536	0.536	0.536	0.536	0.536	0.536	0.536	0.536
	Test duration (1000 waves)	s	1342	1342	1789	1789	2236	2236	2683	2683	2683	3130	3130	3130
	H _{m0} (shallow)	mm	55	60	57	60	54	58	51	54	59	61	53	59
	H _t (shallow)	mm	55	60	56	60	54	57	51	54	59	60	53	58
	H _{m0} (deep)	mm	50	57	50	55	48	51	46	49	55	55	49	54
	H _i (deep)	mm	50	57	49	54	47	51	46	49	55	54	49	54
Prototype	T _p	s	6	6	8	8	10	10	12	12	12	14	14	14
	WL _{toe}	m	2.40	2.40	2.40	2.40	2.40	2.40	2.40	2.40	2.40	2.40	2.40	2.40
	Freeboard, R _c	m	1.60	1.60	1.60	1.60	1.60	1.60	1.60	1.60	1.60	1.60	1.60	1.60
	H _{m0} (shallow)	m	1.10	1.21	1.13	1.20	1.08	1.15	1.02	1.09	1.19	1.21	1.06	1.18
	H _t (shallow)	m	1.09	1.21	1.13	1.20	1.08	1.14	1.02	1.08	1.18	1.20	1.05	1.17
	H _{m0} (deep)	m	1.00	1.14	0.99	1.09	0.95	1.02	0.92	0.98	1.11	1.09	0.98	1.09
	H _i (deep)	m	1.00	1.14	0.99	1.09	0.95	1.01	0.92	0.98	1.10	1.08	0.97	1.08
	H _t / H _i	-	1.09	1.06	1.14	1.10	1.14	1.13	1.11	1.10	1.07	1.11	1.08	1.08

C.2. Profile B: Walvis Bay nearshore profile

C.2.1 Overtopping test results

Profile B: Walvis Bay nearshore profile			B1	B1_2	B1_3	B2	B3	B4	B5	B5_2
Model	T _p	s	1.342	1.342	1.342	1.789	2.236	2.683	3.130	3.130
	WL _{toe}	m	0.08	0.08	0.08	0.08	0.08	0.08	0.08	0.08
	R _c	m	0.12	0.12	0.12	0.12	0.12	0.12	0.12	0.12
	WL _{paddle}	m	0.496	0.496	0.496	0.496	0.496	0.496	0.496	0.496
	Test duration (1000 waves)	s	1342	1342	1342	1789	2236	2683	3130	3130
	H _{m0}	mm	78	68	62	61	64	67	58	64
	H _i	mm	65	54	49	48	50	51	45	51
	Overtopping volume	L	1	0	0	0	0	0	0	0
Prototype	T _p	s	6	6	6	8	10	12	14	14
	WL _{toe}	m	1.60	1.60	1.60	1.60	1.60	1.60	1.60	1.60
	R _c	m	2.40	2.40	2.40	2.40	2.40	2.40	2.40	2.40
	H _{m0}	m	1.56	1.35	1.23	1.23	1.29	1.33	1.15	1.29
	H _i	m	1.30	1.09	0.97	0.96	1.01	1.02	0.90	1.02
	Overtopping volume	L	4000	0	0	0	0	0	0	0
	Overtopping rate	L/s/m	0.03	0.00	0.00	0.00	0.00	0.00	0.00	0.00

Profile B: Walvis Bay nearshore profile			B6	B6_2	B7	B7_2	B8	B9	B10	B10_2
Model	T _p	s	1.342	1.342	1.789	1.789	2.236	2.683	3.130	3.130
	WL _{toe}	m	0.10	0.10	0.10	0.10	0.10	0.10	0.10	0.10
	R _c	m	0.10	0.10	0.10	0.10	0.10	0.10	0.10	0.10
	WL _{paddle}	m	0.516	0.516	0.516	0.516	0.516	0.516	0.516	0.516
	Test duration (1000 waves)	s	1342	1342	1789	1789	2236	2683	3130	3130
	H _{m0}	mm	70	67	61	65	64	69	57	65
	H _i	mm	54	51	46	49	48	53	43	50
	Overtopping volume	L	0	0	0	0	1	3	7	19
Prototype	T _p	s	6	6	8	8	10	12	14	14
	WL _{toe}	m	2.00	2.00	2.00	2.00	2.00	2.00	2.00	2.00
	R _c	m	2.00	2.00	2.00	2.00	2.00	2.00	2.00	2.00
	H _{m0}	m	1.40	1.34	1.23	1.30	1.27	1.38	1.15	1.31
	H _i	m	1.09	1.02	0.92	0.98	0.96	1.05	0.87	1.00
	Overtopping volume	L	0	0	0	0	8000	23200	58800	150400
	Overtopping rate	L/s/m	0.00	0.00	0.00	0.00	0.04	0.10	0.21	0.54

Profile B: Walvis Bay nearshore profile			B11	B11_2	B12	B13	B14	B14_2	B15	B15_2
Model	T _p	s	1.342	1.342	1.789	2.236	2.683	2.683	3.130	3.130
	WL _{toe}	m	0.12	0.12	0.12	0.12	0.12	0.12	0.12	0.12
	R _c	m	0.08	0.08	0.08	0.08	0.08	0.08	0.08	0.08
	WL _{paddle}	m	0.536	0.536	0.536	0.536	0.536	0.536	0.536	0.536
	Test duration (1000 waves)	s	1342	1342	1789	2236	2683	2683	3130	3130
	H _{m0}	mm	62	66	65	66	71	68	61	66
	H _i	mm	47	50	49	50	54	52	45	50
	Overtopping volume	L	0	0	3	16	50	39	80	105
Prototype	T _p	s	6	6	8	10	12	12	14	14
	WL _{toe}	m	2.40	2.40	2.40	2.40	2.40	2.40	2.40	2.40
	R _c	m	1.60	1.60	1.60	1.60	1.60	1.60	1.60	1.60
	H _{m0}	m	1.24	1.32	1.29	1.32	1.42	1.37	1.21	1.33
	H _i	m	0.95	1.00	0.97	0.99	1.08	1.03	0.91	1.00
	Overtopping volume	L	0	0	25600	124000	401600	310400	638400	843600
	Overtopping rate	L/s/m	0.00	0.00	0.16	0.62	1.67	1.29	2.28	3.01

C.2.2 Shallow water wave test results

Profile B: Walvis Bay nearshore profile			WB1	WB1_2	WB2_2	WB3	WB4	WB4_2	WB4_3	WB5_2	WB5_3	WB5_4	WB5_5
Model	T_p	s	1.342	1.342	1.789	2.236	2.683	2.683	2.683	3.130	3.130	3.130	3.130
	WL_{toe}	m	0.08	0.08	0.08	0.08	0.08	0.08	0.08	0.08	0.08	0.08	0.08
	Freeboard, R_c	m	0.12	0.12	0.12	0.12	0.12	0.12	0.12	0.12	0.12	0.12	0.12
	WL_{paddle}	m	0.496	0.496	0.496	0.496	0.496	0.496	0.496	0.496	0.496	0.496	0.496
	Test duration (1000 waves)	s	1342	1342	1789	2236	2683	2683	2683	3130	3130	3130	3130
	H_{m0} (shallow)	mm	68	57	63	65	71	71	68	67	48	57	67
	H_t (shallow)	mm	67	56	62	64	70	70	67	66	47	56	66
	H_{m0} (deep)	mm	56	51	54	53	56	58	55	57	40	46	53
	H_i (deep)	mm	56	50	54	52	56	57	55	56	39	45	53
<hr/>													
Prototype	T_p	s	6	6	8	10	12	12	12	14	14	14	14
	WL_{toe}	m	1.60	1.60	1.60	1.60	1.60	1.60	1.60	1.60	1.60	1.60	1.60
	Freeboard, R_c	m	2.40	2.40	2.40	2.40	2.40	2.40	2.40	2.40	2.40	2.40	2.40
	H_{m0} (shallow)	m	1.35	1.14	1.26	1.30	1.41	1.42	1.36	1.34	0.96	1.14	1.34
	H_t (shallow)	m	1.34	1.12	1.25	1.28	1.39	1.41	1.35	1.32	0.95	1.12	1.32
	H_{m0} (deep)	m	1.13	1.02	1.08	1.05	1.13	1.15	1.10	1.14	0.80	0.92	1.07
	H_i (deep)	m	1.11	1.01	1.07	1.04	1.11	1.14	1.09	1.13	0.79	0.90	1.06
	H_t/H_i	-	1.20	1.12	1.16	1.23	1.25	1.23	1.24	1.17	1.21	1.24	1.25

Profile B: Walvis Bay nearshore profile			WB6	WB7	WB8	WB9	WB9_2	WB9_3	WB10
Model	T_p	s	1.342	1.789	2.236	2.683	2.683	2.683	3.130
	WL_{toe}	m	0.10	0.10	0.10	0.10	0.10	0.10	0.10
	Freeboard, R_c	m	0.10	0.10	0.10	0.10	0.10	0.10	0.10
	WL_{paddle}	m	0.516	0.516	0.516	0.516	0.516	0.516	0.516
	Test duration (1000 waves)	s	1342	1789	2236	2683	2683	2683	3130
	H_{m0} (shallow)	mm	58	61	63	71	63	55	54
	H_t (shallow)	mm	57	61	63	70	63	55	53
	H_{m0} (deep)	mm	53	51	52	58	57	51	51
H_i (deep)	mm	52	50	51	57	57	51	51	
Prototype	T_p	s	6	8	10	12	12	12	14
	WL_{toe}	m	2.00	2.00	2.00	2.00	2.00	2.00	2.00
	Freeboard, R_c	m	2.00	2.00	2.00	2.00	2.00	2.00	2.00
	H_{m0} (shallow)	m	1.16	1.23	1.26	1.42	1.27	1.11	1.08
	H_t (shallow)	m	1.15	1.22	1.25	1.40	1.26	1.10	1.07
	H_{m0} (deep)	m	1.05	1.02	1.03	1.16	1.14	1.03	1.03
	H_i (deep)	m	1.04	1.01	1.02	1.15	1.14	1.02	1.02
	H_t/H_i	-	1.10	1.21	1.22	1.22	1.11	1.08	1.05

Profile B: Walvis Bay nearshore profile			WB11	WB11_2	WB12	WB13	WB13_2	WB14	WB15	WB15_2	WB15_3
Model	T _p	s	1.342	1.342	1.789	2.236	2.236	2.683	3.130	3.130	3.130
	WL _{toe}	m	0.12	0.12	0.12	0.12	0.12	0.12	0.12	0.12	0.12
	Freeboard, R _c	m	0.08	0.08	0.08	0.08	0.08	0.08	0.08	0.08	0.08
	WL _{paddle}	m	0.536	0.536	0.536	0.536	0.536	0.536	0.536	0.536	0.536
	Test duration (1000 waves)	s	1342	1342	1789	2236	2236	2683	3130	3130	3130
	H _{m0} (shallow)	mm	54	57	62	59	62	60	59	62	62
	H _t (shallow)	mm	54	57	62	58	62	59	58	62	62
	H _{m0} (deep)	mm	47	50	52	46	53	51	49	53	53
H _i (deep)	mm	47	50	52	46	52	51	49	52	52	
Prototype	T _p	s	6	6	8	10	10	12	14	14	14
	WL _{toe}	m	2.40	2.40	2.40	2.40	2.40	2.40	2.40	2.40	2.40
	Freeboard, R _c	m	1.60	1.60	1.60	1.60	1.60	1.60	1.60	1.60	1.60
	H _{m0} (shallow)	m	1.08	1.14	1.25	1.18	1.24	1.20	1.18	1.25	1.25
	H _t (shallow)	m	1.07	1.13	1.24	1.17	1.23	1.19	1.17	1.23	1.24
	H _{m0} (deep)	m	0.94	1.00	1.05	0.93	1.05	1.02	0.99	1.05	1.06
	H _i (deep)	m	0.94	0.99	1.04	0.92	1.04	1.01	0.98	1.04	1.05
	H _t / H _i	-	1.15	1.14	1.19	1.27	1.18	1.17	1.20	1.18	1.18

C.3. Profile C: Richards Bay nearshore profile

C.3.1 Overtopping test results

Profile C: Richards Bay nearshore profile			C1	C1_2	C2	C2_2	C3	C4	C4_2	C5
Model	T _p	s	1.342	1.342	1.789	1.789	2.236	2.683	2.683	3.130
	WL _{toe}	m	0.08	0.08	0.08	0.08	0.08	0.08	0.08	0.08
	R _c	m	0.12	0.12	0.12	0.12	0.12	0.12	0.12	0.12
	WL _{paddle}	m	0.496	0.496	0.496	0.496	0.496	0.496	0.496	0.496
	Test duration (1000 waves)	s	1342	1342	1789	1789	2236	2683	2683	3130
	H _{m0}	mm	68	64	67	61	61	56	61	61
	H _i	mm	57	53	56	50	49	45	49	51
	Overtopping volume	L	0.00	0.00	0.00	0.00	0.00	0.53	1.15	2.40
Prototype	T _p	s	6	6	8	8	10	12	12	14
	WL _{toe}	m	1.60	1.60	1.60	1.60	1.60	1.60	1.60	1.60
	R _c	m	2.40	2.40	2.40	2.40	2.40	2.40	2.40	2.40
	H _{m0}	m	1.35	1.28	1.35	1.22	1.22	1.12	1.22	1.21
	H _i	m	1.14	1.05	1.12	0.99	0.98	0.90	0.99	1.01
	Overtopping volume	L	0	0	0	0	0	4211	9200	19200
	Overtopping rate	L/s/m	0.00	0.00	0.00	0.00	0.00	0.02	0.04	0.07

Profile C: Richards Bay nearshore profile			C6	C6_2	C6_3	C7	C7_2	C7_3	C8	C8_2	C9	C9_2	C10_2	C10_3
Model	T _p	s	1.342	1.342	1.342	1.789	1.789	1.789	2.236	2.236	2.683	2.683	3.130	3.130
	WL _{toe}	m	0.10	0.10	0.10	0.10	0.10	0.10	0.10	0.10	0.10	0.10	0.10	0.12
	R _c	m	0.10	0.10	0.10	0.10	0.10	0.10	0.10	0.10	0.10	0.10	0.10	0.08
	WL _{paddle}	m	0.516	0.516	0.516	0.516	0.516	0.516	0.516	0.516	0.516	0.516	0.516	0.516
	Test duration (1000 waves)	s	1342	1342	1342	1789	1789	1789	2236	2236	2683	2683	3130	3130
	H _{m0}	mm	59	61	62	67	64	63	63	63	68	65	57	62
	H _i	mm	46	48	49	54	51	50	50	50	53	50	45	50
	Overtopping volume	L	0.00	0.00	0.00	5.79	4.21	4.74	0.74	0.79	23.68	13.16	15.79	58.95
Prototype	T _p	s	6	6	6	8	8	8	10	10	12	12	14	14
	WL _{toe}	m	2.00	2.00	2.00	2.00	2.00	2.00	2.00	2.00	2.00	2.00	2.00	2.40
	R _c	m	2.00	2.00	2.00	2.00	2.00	2.00	2.00	2.00	2.00	2.00	2.00	1.60
	H _{m0}	m	1.17	1.22	1.24	1.35	1.28	1.26	1.26	1.25	1.36	1.29	1.14	1.25
	H _i	m	0.91	0.97	0.98	1.08	1.01	1.00	0.99	0.99	1.07	1.00	0.89	0.99
	Overtopping volume	L	0	0	0	46320	33680	37920	5920	6320	189440	105280	126320	471600
	Overtopping rate	L/s/m	0.00	0.00	0.00	0.29	0.21	0.24	0.03	0.03	0.79	0.44	0.45	1.68

Profile C: Richards Bay nearshore profile			C11	C11_2	C12	C13	C14	C15	C15_2
Model	T _p	s	1.342	1.342	1.789	2.236	2.683	3.130	3.130
	WL _{toe}	m	0.12	0.12	0.12	0.12	0.12	0.12	0.12
	R _c	m	0.08	0.08	0.08	0.08	0.08	0.08	0.08
	WL _{paddle}	m	0.536	0.536	0.536	0.536	0.536	0.536	0.536
	Test duration (1000 waves)	s	1342	1342	1789	2236	2683	3130	3130
	H _{m0}	mm	57	64	64	65	64	60	61
	H _i	mm	44	51	50	50	48	46	47
	Overtopping volume	L	0.00	1.32	17.89	60.00	147.65	298.05	358.75
Prototype	T _p	s	6	6	8	10	12	14	14
	WL _{toe}	m	2.40	2.40	2.40	2.40	2.40	2.40	2.40
	R _c	m	1.60	1.60	1.60	1.60	1.60	1.60	1.60
	H _{m0}	m	1.14	1.28	1.28	1.29	1.27	1.21	1.22
	H _i	m	0.89	1.02	0.99	1.00	0.97	0.93	0.95
	Overtopping volume	L	0	10526	143158	480000	1181200	2384400	2870000
	Overtopping rate	L/s/m	0.00	0.09	0.89	2.40	4.92	8.52	10.25

C.3.2 Shallow water wave test results

Profile C: Richards Bay nearshore profile			WC1	WC1_2	WC1_3	WC2	WC2_2	WC2_3	WC3	WC4	WC5
Model	T_p	s	1.342	1.342	1.342	1.789	1.789	1.789	2.236	2.683	3.130
	WL_{toe}	m	0.08	0.08	0.08	0.08	0.08	0.08	0.08	0.08	0.08
	Freeboard, R_c	m	0.12	0.12	0.12	0.12	0.12	0.12	0.12	0.12	0.12
	WL_{paddle}	m	0.496	0.496	0.496	0.496	0.496	0.496	0.496	0.496	0.496
	Test duration (1000 waves)	s	1342	1342	1342	1789	1789	1789	2236	2683	3130
	H_{m0} (shallow)	mm	59	58	51	64	62	51	55	56	50
	H_t (shallow)	mm	59	58	51	64	62	51	55	55	48
	H_{m0} (deep)	mm	63	66	49	63	58	48	51	52	50
	H_i (deep)	mm	63	65	49	63	58	48	51	52	48
Prototype	T_p	s	6	6	6	8	8	8	10	12	14
	WL_{toe}	m	1.60	1.60	1.60	1.60	1.60	1.60	1.60	1.60	1.60
	Freeboard, R_c	m	2.40	2.40	2.40	2.40	2.40	2.40	2.40	2.40	2.40
	H_{m0} (shallow)	m	1.18	1.17	1.01	1.29	1.25	1.02	1.10	1.11	1.01
	H_t (shallow)	m	1.18	1.16	1.01	1.28	1.24	1.01	1.09	1.11	0.97
	H_{m0} (deep)	m	1.26	1.31	0.99	1.26	1.16	0.97	1.02	1.05	1.00
	H_i (deep)	m	1.25	1.31	0.99	1.26	1.16	0.96	1.02	1.04	0.96
	H_t/H_i	-	0.94	0.89	1.03	1.02	1.07	1.05	1.08	1.06	1.01

Profile C: Richards Bay nearshore profile			WC6	WC6_2	WC7	WC7_2	WC8	WC9	WC9_2	WC10
Model	T _p	s	1.342	1.342	1.789	1.789	2.236	2.683	2.683	3.130
	WL _{toe}	m	0.10	0.10	0.10	0.10	0.10	0.10	0.10	0.10
	Freeboard, R _c	m	0.10	0.10	0.10	0.10	0.10	0.10	0.10	0.10
	WL _{paddle}	m	0.516	0.516	0.516	0.516	0.516	0.516	0.516	0.516
	Test duration (1000 waves)	s	1342	1342	1789	1789	2236	2683	2683	3130
	H _{m0} (shallow)	mm	53	56	61	57	60	59	58	62
	H _t (shallow)	mm	53	55	60	56	60	59	58	62
	H _{m0} (deep)	mm	46	49	56	51	53	53	53	53
H _i (deep)	mm	45	49	55	51	52	53	52	53	
Prototype	T _p	s	6	6	8	8	10	12	12	14
	WL _{toe}	m	2.00	2.00	2.00	2.00	2.00	2.00	2.00	2.00
	Freeboard, R _c	m	2.00	2.00	2.00	2.00	2.00	2.00	2.00	2.00
	H _{m0} (shallow)	m	1.07	1.11	1.21	1.13	1.20	1.19	1.17	1.24
	H _t (shallow)	m	1.06	1.11	1.21	1.13	1.20	1.18	1.16	1.23
	H _{m0} (deep)	m	0.91	0.98	1.11	1.02	1.05	1.06	1.05	1.07
	H _i (deep)	m	0.90	0.98	1.11	1.02	1.05	1.06	1.05	1.06
	H _t / H _i	-	1.17	1.13	1.09	1.11	1.14	1.12	1.11	1.16

Profile C: Richards Bay nearshore profile			WC11	WC12	WC12_2	WC13	WC13_2	WC13_3	WC14	WC15	WC15_2
Model	T _p	s	1.342	1.789	1.789	2.236	2.236	2.236	2.683	3.130	3.130
	WL _{toe}	m	0.12	0.12	0.12	0.12	0.12	0.12	0.12	0.12	0.12
	Freeboard, R _c	m	0.08	0.08	0.08	0.08	0.08	0.08	0.08	0.08	0.08
	WL _{paddle}	m	0.536	0.536	0.536	0.536	0.536	0.536	0.536	0.536	0.536
	Test duration (1000 waves)	s	1342	1789	1789	2236	2236	2236	2683	3130	3130
	H _{m0} (shallow)	mm	64	69	58	50	52	55	57	59	61
	H _t (shallow)	mm	63	69	58	49	52	55	57	59	61
	H _{m0} (deep)	mm	49	50	48	45	46	48	49	50	50
H _i (deep)	mm	48	50	47	45	46	47	49	50	50	
Prototype	T _p	s	6	8	8	10	10	10	12	14	14
	WL _{toe}	m	2.40	2.40	2.40	2.40	2.40	2.40	2.40	2.40	2.40
	Freeboard, R _c	m	1.60	1.60	1.60	1.60	1.60	1.60	1.60	1.60	1.60
	H _{m0} (shallow)	m	1.27	1.38	1.16	0.99	1.04	1.11	1.14	1.19	1.23
	H _t (shallow)	m	1.27	1.38	1.16	0.99	1.04	1.10	1.14	1.18	1.22
	H _{m0} (deep)	m	0.97	1.00	0.95	0.90	0.92	0.95	0.98	1.01	1.01
	H _i (deep)	m	0.97	0.99	0.95	0.89	0.91	0.95	0.97	1.00	1.00
	H _t / H _i	-	1.31	1.38	1.22	1.11	1.13	1.16	1.17	1.18	1.22

C.4. Profile D: False Bay nearshore profile

C.4.1 Overtopping test results

Profile D: False Bay nearshore profile			D1	D1_2	D2	D3	D3_2	D3_3	D3_4	D3_5	D4	D5
Model	T _p	s	1.342	1.342	1.789	2.236	2.236	2.236	2.236	2.236	2.683	3.130
	WL _{toe}	m	0.08	0.08	0.08	0.08	0.08	0.08	0.08	0.08	0.08	0.08
	R _c	m	0.12	0.12	0.12	0.12	0.12	0.12	0.12	0.12	0.12	0.12
	WL _{paddle}	m	0.496	0.496	0.496	0.496	0.496	0.496	0.496	0.496	0.496	0.496
	Test duration (1000 waves)	s	1342	1342	1789	2236	2236	2236	2236	2236	2683	3130
	H _{m0}	mm	72	61	64	70	51	56	53	58	58	60
	H _i	mm	59	49	53	58	40	45	43	48	49	51
	Overtopping volume	L	0	0	0	0	0	0	0	0	0	1
Prototype	T _p	s	6	6	8	10	10	10	10	10	12	14
	WL _{toe}	m	1.60	1.60	1.60	1.60	1.60	1.60	1.60	1.60	1.60	1.60
	R _c	m	2.40	2.40	2.40	2.40	2.40	2.40	2.40	2.40	2.40	2.40
	H _{m0}	m	1.43	1.21	1.28	1.40	1.02	1.13	1.06	1.16	1.16	1.21
	H _i	m	1.19	0.97	1.05	1.16	0.81	0.91	0.86	0.96	0.97	1.01
	Overtopping volume	L	0	0	0	0	0	0	0	0	8421	16842
	Overtopping rate	L/s/m	0.00	0.00	0.00	0.00	0.00	0.00	0.00	0.00	0.04	0.06

Profile D: False Bay nearshore profile			D6	D6_2	D7	D7_2	D8	D9	D9_2	D10
Model	T _p	s	1.342	1.342	1.789	1.789	2.236	2.683	2.683	3.130
	WL _{toe}	m	0.10	0.10	0.10	0.10	0.10	0.10	0.10	0.10
	R _c	m	0.10	0.10	0.10	0.10	0.10	0.10	0.10	0.10
	WL _{paddle}	m	0.516	0.516	0.516	0.516	0.516	0.516	0.516	0.516
	Test duration (1000 waves)	s	1342	1342	1789	1789	2236	2683	2683	3130
	H _{m0}	mm	60	63	69	65	65	65	65	64
	H _i	mm	46	49	54	50	51	51	51	50
	Overtopping volume	L	0	0	4	3	11	31	30	70
Prototype	T _p	s	6	6	8	8	10	12	12	14
	WL _{toe}	m	2.00	2.00	2.00	2.00	2.00	2.00	2.00	2.00
	R _c	m	2.00	2.00	2.00	2.00	2.00	2.00	2.00	2.00
	H _{m0}	m	1.19	1.27	1.38	1.30	1.29	1.30	1.29	1.29
	H _i	m	0.91	0.98	1.08	1.00	1.01	1.02	1.01	1.00
	Overtopping volume	L	0	0	33684	21053	84211	244211	238400	559053
	Overtopping rate	L/s/m	0.00	0.00	0.21	0.13	0.42	1.02	0.99	2.00

Profile D: False Bay nearshore profile			D11	D11_2	D12	D12_3	D13	D14	D15	D15_2	D15_3	D15_4	D15_5
Model	T _p	s	1.342	1.342	1.789	1.789	2.236	2.683	3.130	3.130	3.130	3.130	3.130
	WL _{toe}	m	0.12	0.12	0.12	0.12	0.12	0.12	0.12	0.12	0.12	0.12	0.12
	R _c	m	0.08	0.08	0.08	0.08	0.08	0.08	0.08	0.08	0.08	0.08	0.08
	WL _{paddle}	m	0.536	0.536	0.536	0.536	0.536	0.536	0.536	0.536	0.536	0.536	0.536
	Test duration (1000 waves)	s	1342	1342	1789	1789	2236	2683	3130	3130	3130	3130	3130
	H _{m0}	mm	61	64	70	64	64	66	62	62	62	61	61
	H _i	mm	47	48	53	48	49	50	48	47	47	47	47
	Overtopping volume	L	1	2	50	23	86	215	356	364	367	357	370
Prototype	T _p	s	6	6	8	8	10	12	14	14	14	14	14
	WL _{toe}	m	2.40	2.40	2.40	2.40	2.40	2.40	2.40	2.40	2.40	2.40	2.40
	R _c	m	1.60	1.60	1.60	1.60	1.60	1.60	1.60	1.60	1.60	1.60	1.60
	H _{m0}	m	1.23	1.27	1.39	1.28	1.28	1.32	1.24	1.23	1.23	1.23	1.23
	H _i	m	0.94	0.97	1.06	0.96	0.97	1.01	0.96	0.95	0.95	0.95	0.95
	Overtopping volume	L	4211	12632	396611	180800	686484	1718274	2846000	2910800	2936400	2856800	2962800
	Overtopping rate	L/s/m	0.04	0.11	2.48	1.13	3.43	7.16	10.16	10.40	10.49	10.20	10.58

C.4.2 Shallow water wave test results

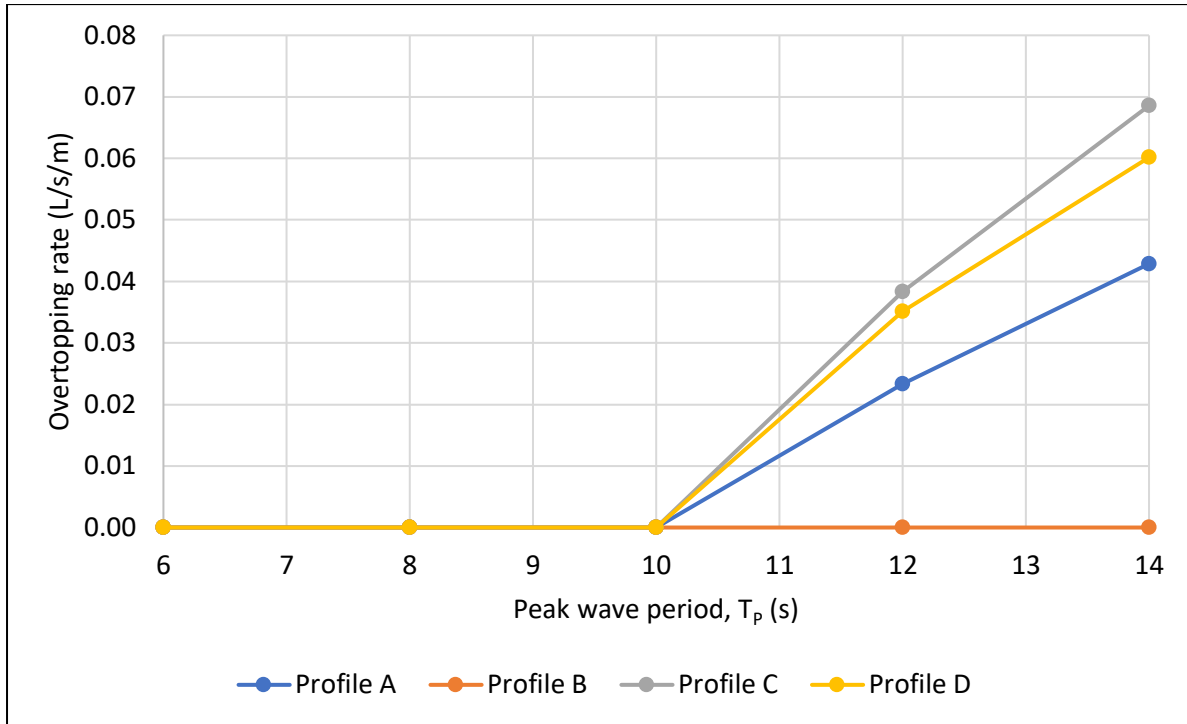
Profile D: False Bay nearshore profile			WD1	WD1_2	WD1_3	WD1_4	WD2	WD3	WD4	WD5
Model	T_p	s	1.342	1.342	1.342	1.342	1.789	2.236	2.683	3.130
	WL_{toe}	m	0.08	0.08	0.08	0.08	0.08	0.08	0.08	0.08
	Freeboard, R_c	m	0.12	0.12	0.12	0.12	0.12	0.12	0.12	0.12
	WL_{paddle}	m	0.496	0.496	0.496	0.496	0.496	0.496	0.496	0.496
	Test duration (1000 waves)	s	1342	1342	1342	1342	1789	2236	2683	3130
	H_{m0} (shallow)	mm	46	52	53	49	50	46	46	49
	H_t (shallow)	mm	45	51	52	48	50	45	45	47
	H_{m0} (deep)	mm	48	58	58	54	53	51	50	53
	H_i (deep)	mm	47	57	57	53	52	50	49	51
Prototype	T_p	s	6	6	6	6	8	10	12	14
	WL_{toe}	m	1.60	1.60	1.60	1.60	1.60	1.60	1.60	1.60
	Freeboard, R_c	m	2.40	2.40	2.40	2.40	2.40	2.40	2.40	2.40
	H_{m0} (shallow)	m	0.92	1.04	1.07	0.97	1.01	0.93	0.92	0.97
	H_t (shallow)	m	0.90	1.02	1.05	0.96	0.99	0.91	0.90	0.95
	H_{m0} (deep)	m	0.95	1.16	1.16	1.08	1.05	1.02	0.99	1.05
	H_i (deep)	m	0.93	1.14	1.14	1.06	1.04	1.00	0.97	1.03
	H_t/H_i	-	0.97	0.89	0.92	0.90	0.96	0.91	0.92	0.92

Profile D: False Bay nearshore profile			WD6	WD6_2	WD7	WD8	WD9	WD10
Model	T_p	s	1.342	1.342	1.789	2.236	2.683	3.130
	WL_{toe}	m	0.10	0.10	0.10	0.10	0.10	0.10
	Freeboard, R_c	m	0.10	0.10	0.10	0.10	0.10	0.10
	WL_{paddle}	m	0.516	0.516	0.516	0.516	0.516	0.516
	Test duration (1000 waves)	s	1342	1342	1789	2236	2683	3130
	H_{m0} (shallow)	mm	51	56	51	50	52	52
	H_t (shallow)	mm	51	56	50	49	51	51
	H_{m0} (deep)	mm	45	51	50	52	51	52
H_i (deep)	mm	45	50	50	51	50	51	
Prototype	T_p	s	6	6	8	10	12	14
	WL_{toe}	m	2.00	2.00	2.00	2.00	2.00	2.00
	Freeboard, R_c	m	2.00	2.00	2.00	2.00	2.00	2.00
	H_{m0} (shallow)	m	1.02	1.12	1.02	0.99	1.03	1.05
	H_t (shallow)	m	1.01	1.11	1.01	0.97	1.01	1.02
	H_{m0} (deep)	m	0.90	1.01	1.01	1.04	1.03	1.05
	H_i (deep)	m	0.89	1.00	0.99	1.02	1.01	1.02
	H_t/H_i	-	1.14	1.11	1.01	0.95	1.00	1.00

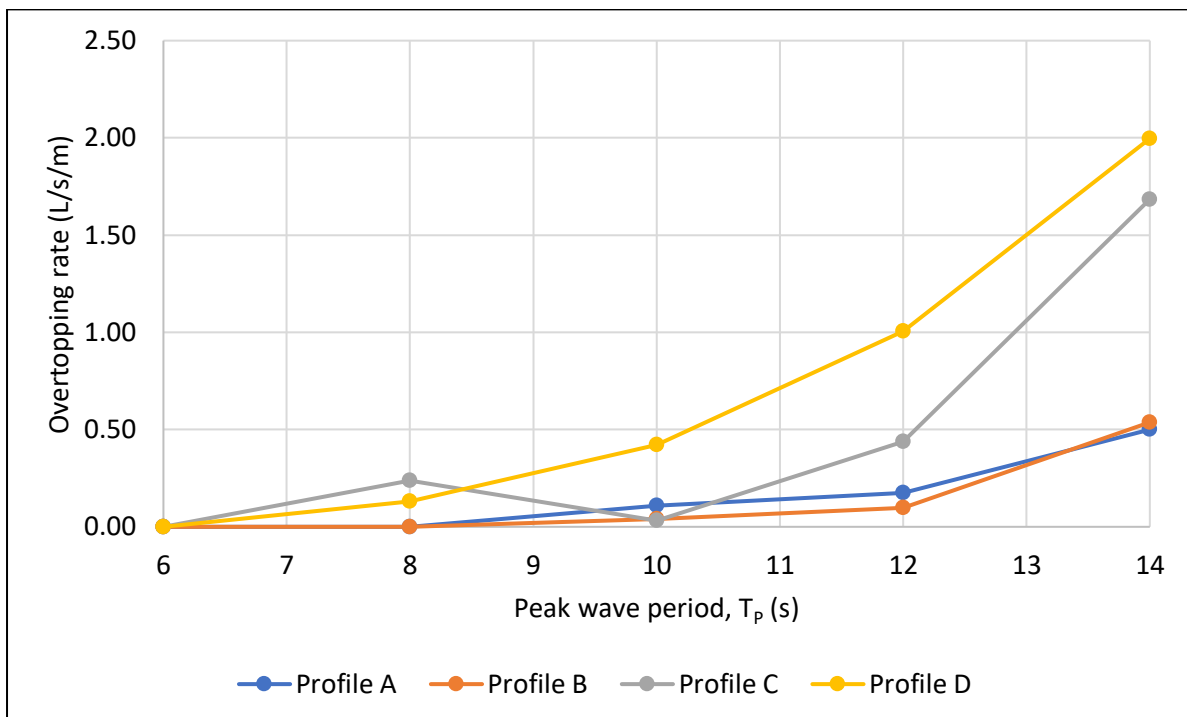
Profile D: False Bay nearshore profile			WD11	WD11_2	WD11_3	WD12	WD12_2	WD12_3	WD13	WD14	WD15	WD15_2	WD15_3
Model	T _p	s	1.342	1.342	1.342	1.789	1.789	1.789	2.236	2.683	3.130	3.130	3.130
	WL _{toe}	m	0.12	0.12	0.12	0.12	0.12	0.12	0.12	0.12	0.12	0.12	0.12
	Freeboard, R _c	m	0.08	0.08	0.08	0.08	0.08	0.08	0.08	0.08	0.08	0.08	0.08
	WL _{paddle}	m	0.536	0.536	0.536	0.536	0.536	0.536	0.536	0.536	0.536	0.536	0.536
	Test duration (1000 waves)	s	1342	1342	1342	1789	1789	1789	2236	2683	3130	3130	3130
	H _{m0} (shallow)	mm	53	60	53	59	51	53	56	57	56	56	56
	H _t (shallow)	mm	53	60	52	58	51	52	55	56	55	55	55
	H _{m0} (deep)	mm	42	45	51	58	47	49	52	53	53	53	52
H _i (deep)	mm	41	45	50	58	47	48	51	52	52	52	52	
Prototype	T _p	s	6	6	6	8	8	8	10	12	14	14	14
	WL _{toe}	m	2.40	2.40	2.40	2.40	2.40	2.40	2.40	2.40	2.40	2.40	2.40
	Freeboard, R _c	m	1.60	1.60	1.60	1.60	1.60	1.60	1.60	1.60	1.60	1.60	1.60
	H _{m0} (shallow)	m	1.07	1.21	1.05	1.17	1.03	1.06	1.12	1.14	1.12	1.12	1.11
	H _t (shallow)	m	1.06	1.20	1.05	1.16	1.02	1.05	1.10	1.12	1.10	1.10	1.09
	H _{m0} (deep)	m	0.83	0.91	1.01	1.16	0.95	0.97	1.03	1.06	1.06	1.06	1.05
	H _i (deep)	m	0.83	0.90	1.00	1.16	0.94	0.96	1.02	1.04	1.04	1.04	1.03
	H _t / H _i	-	1.28	1.33	1.04	1.01	1.08	1.09	1.08	1.07	1.06	1.06	1.06

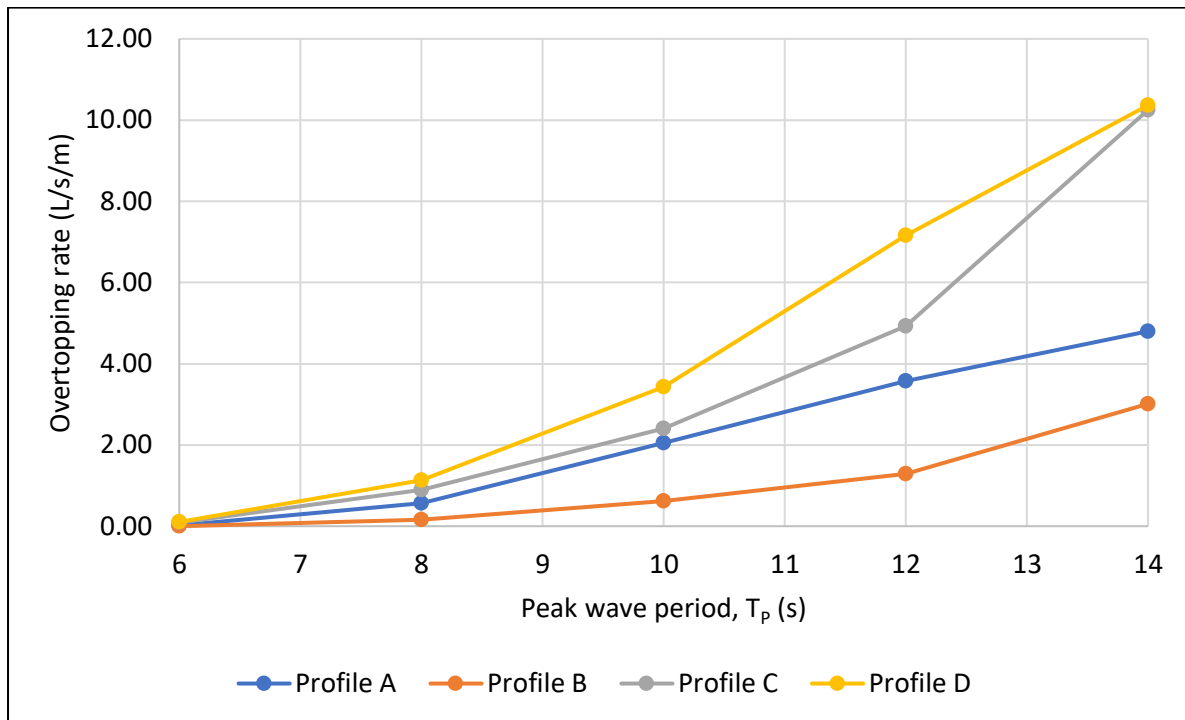
Appendix D: Influence of wave period on overtopping

D.1. Overtopping rate as a function of wave period for a 1.6 m water depth



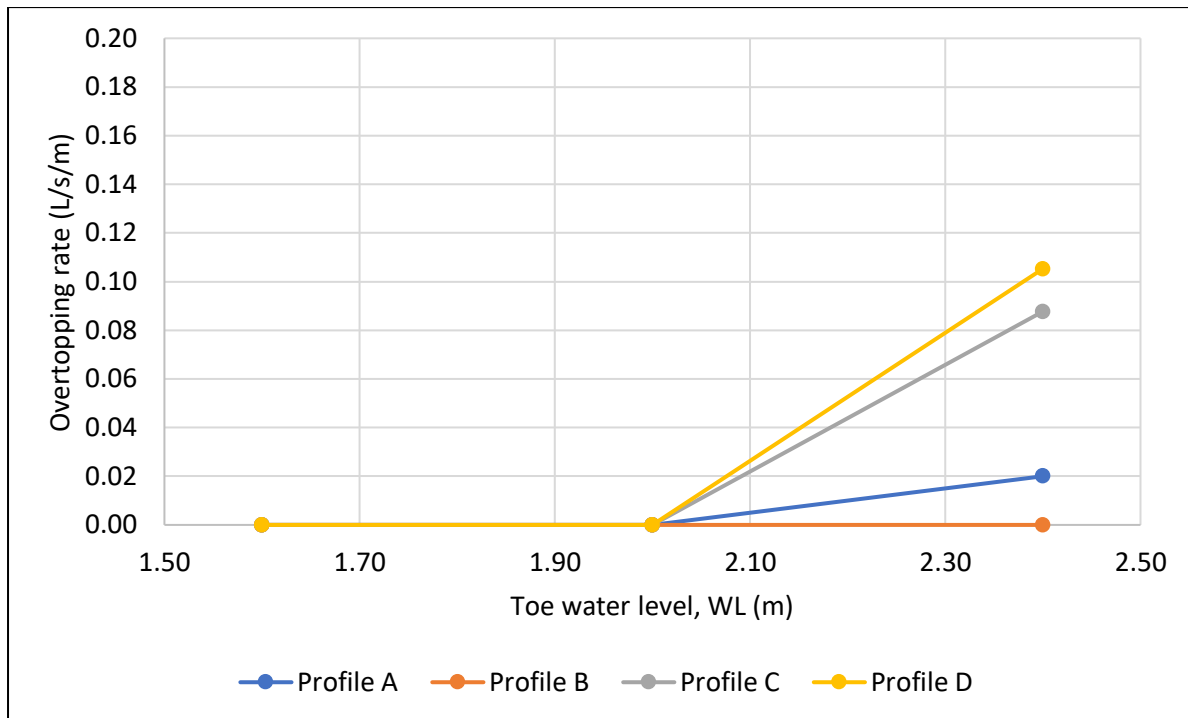
D.2. Overtopping rate as a function of wave period for a 2.0 m water depth



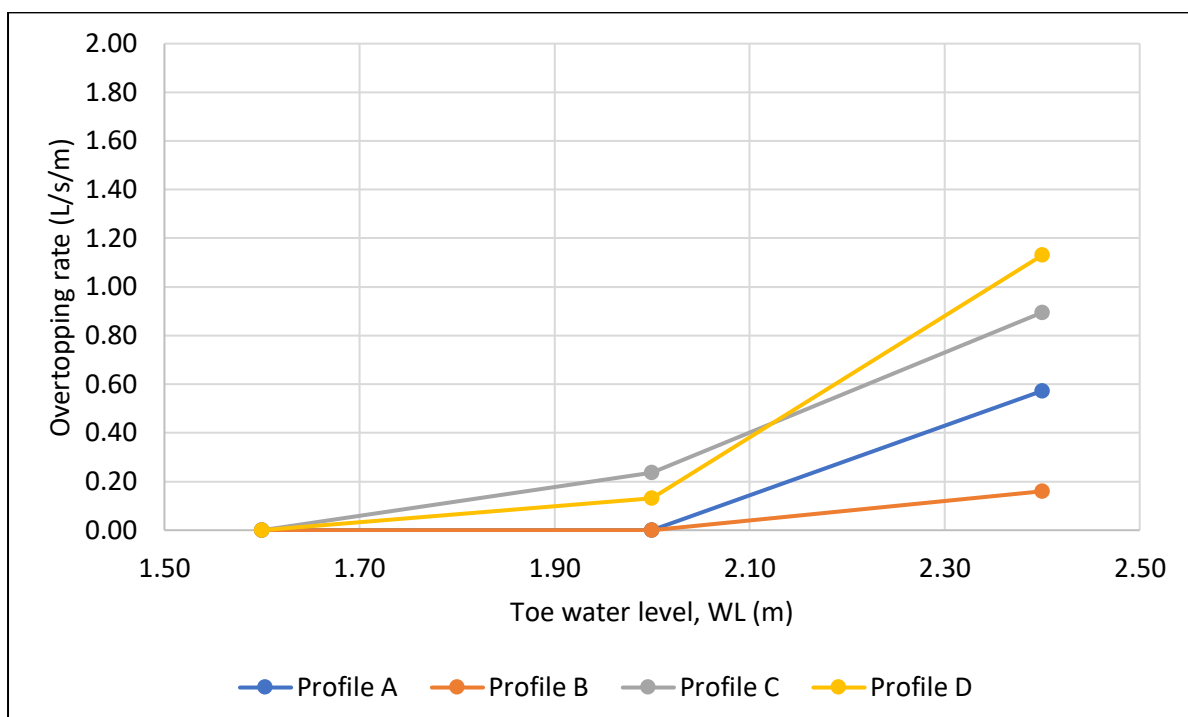
D.3. Overtopping rate as a function of wave period for a 2.4 m water depth

Appendix E: Influence of water level on overtopping

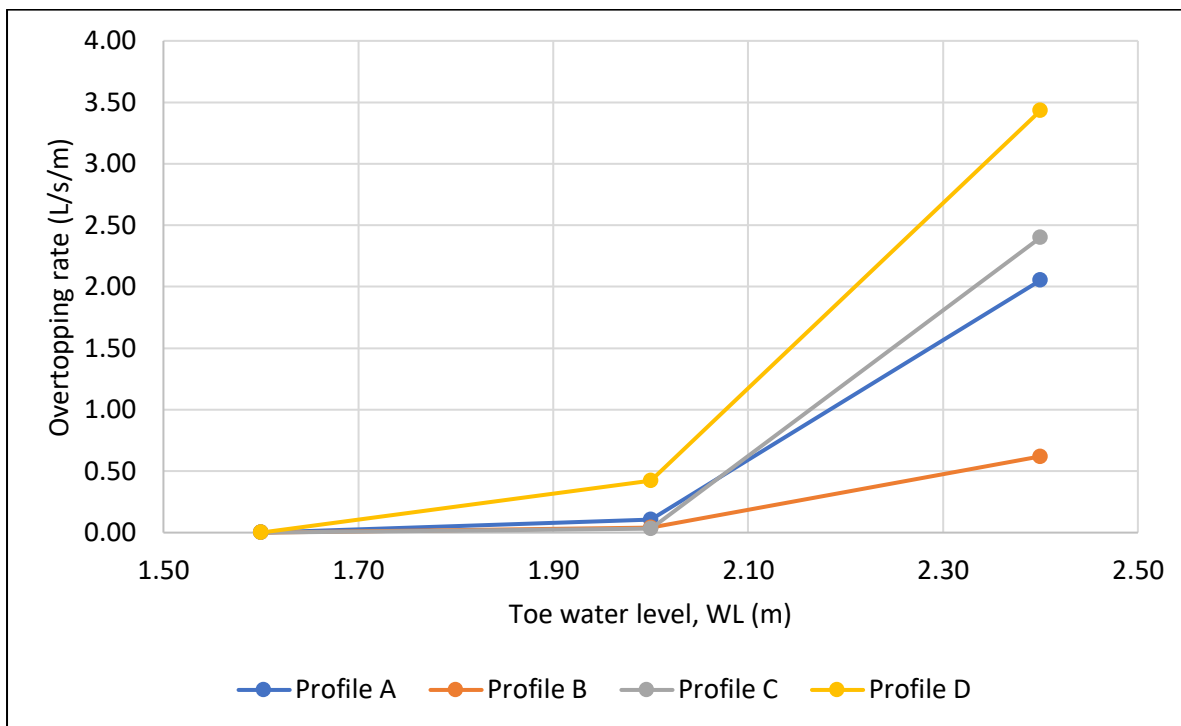
E.1. Overtopping rate as a function of water depth for a 6 s wave period



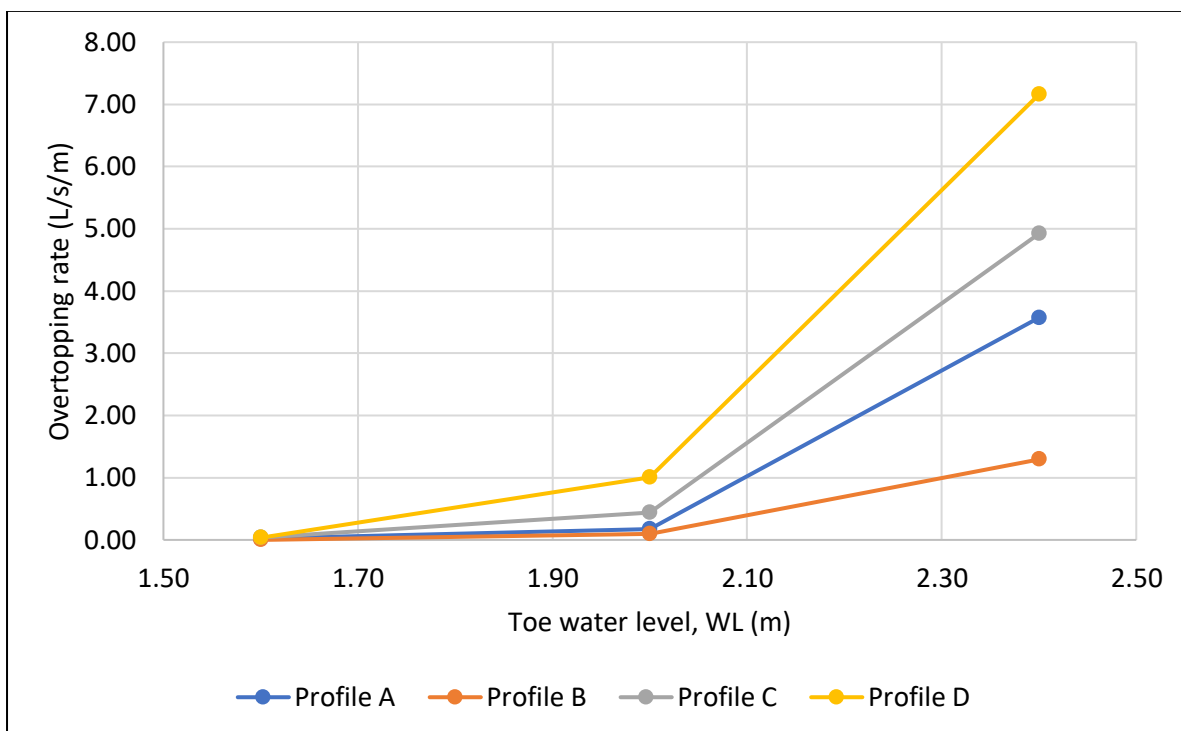
E.2. Overtopping rate as a function of water depth for an 8 s wave period

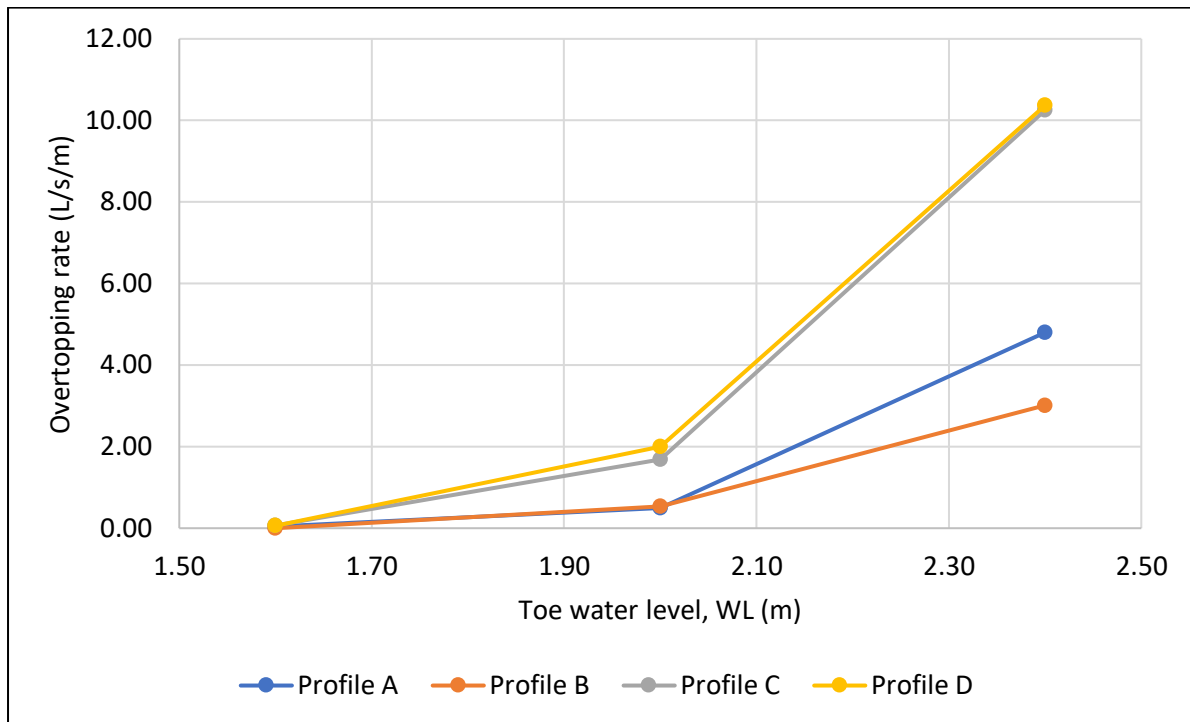


E.3. Overtopping rate as a function of water depth for a 10 s wave period



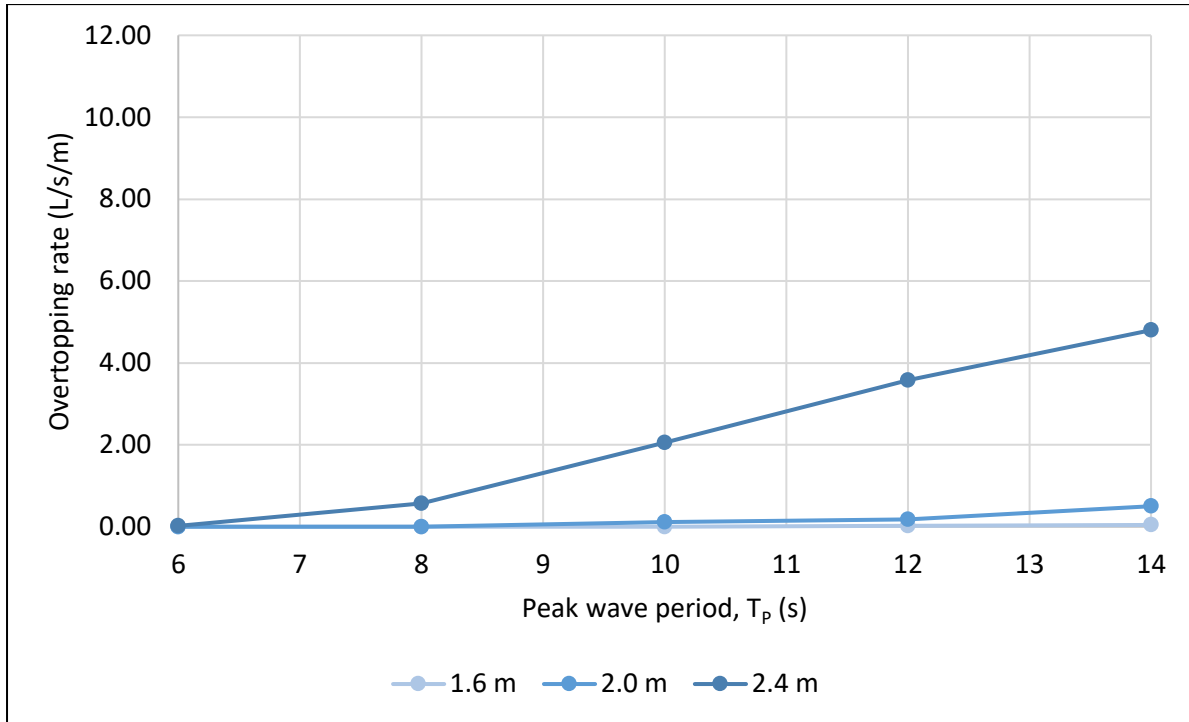
E.4. Overtopping rate as a function of water depth for a 12 s wave period



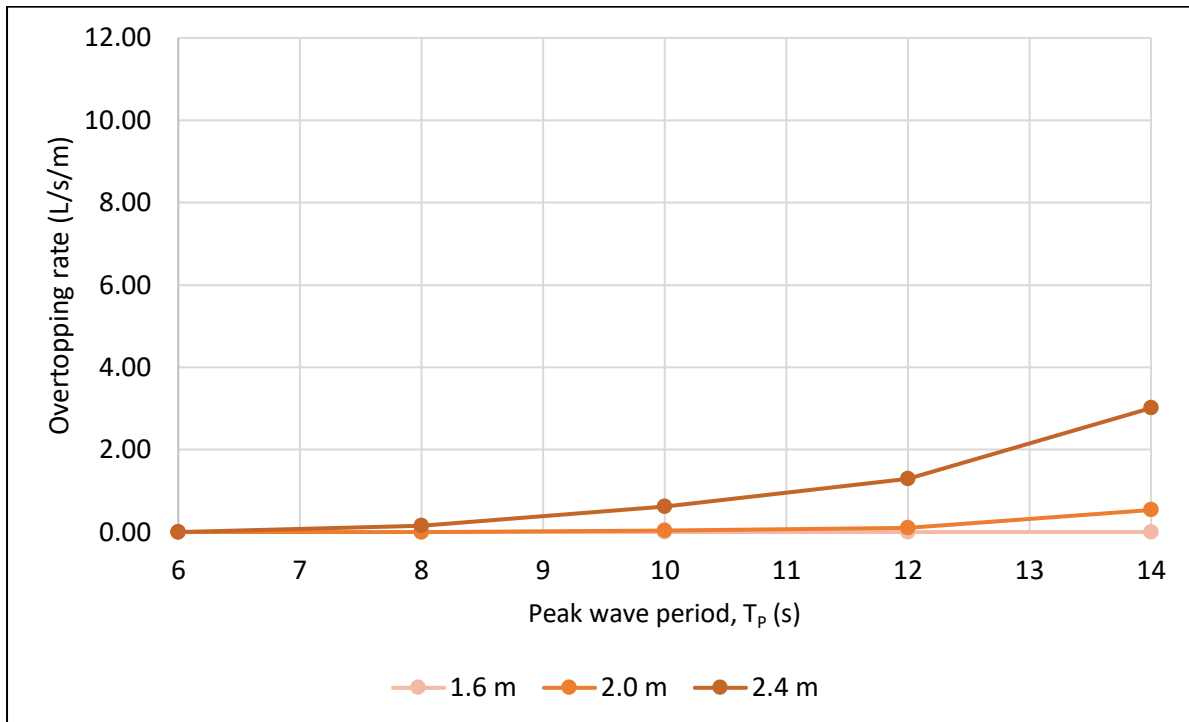
E.5. Overtopping rate as a function of water depth for a 14 s wave period

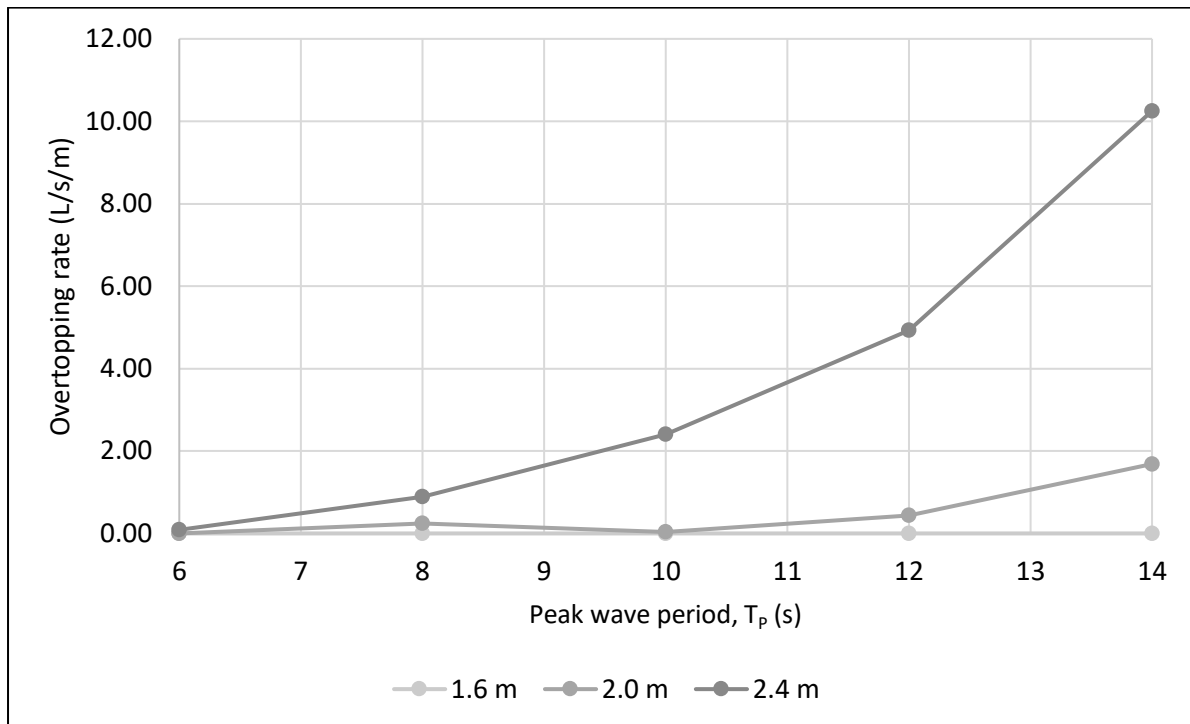
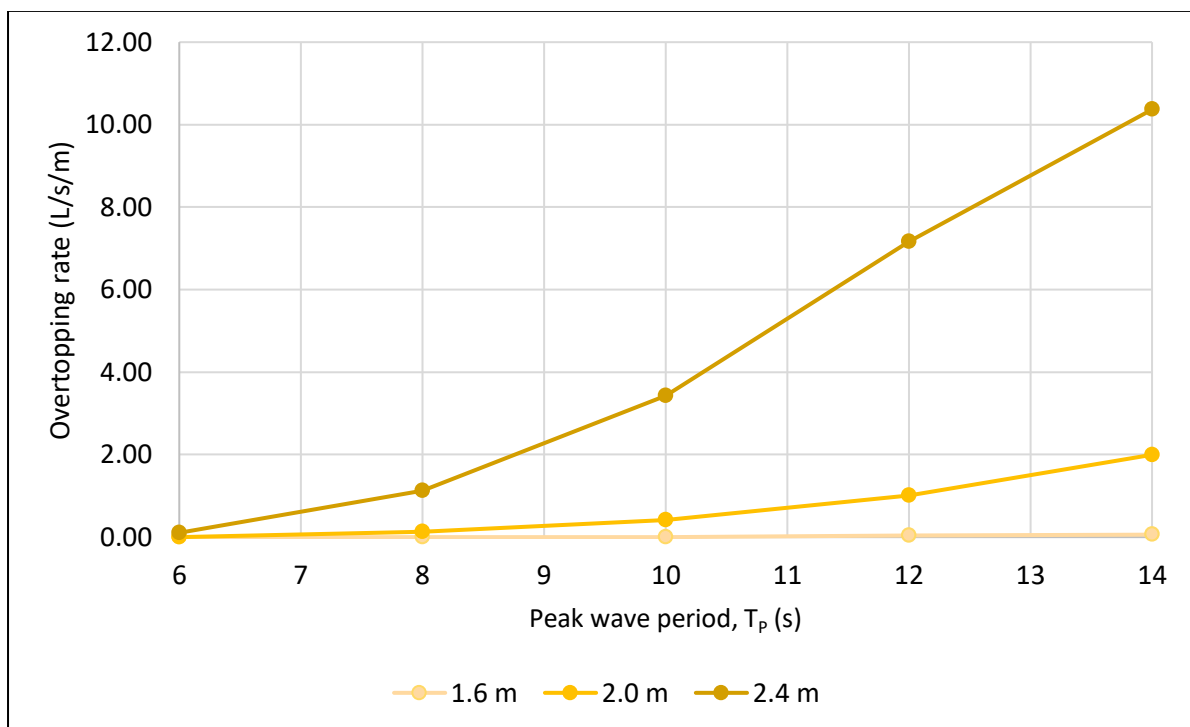
Appendix F: Influence of the nearshore slope on overtopping

F.1. Overtopping rate as a function of wave period for nearshore profile A



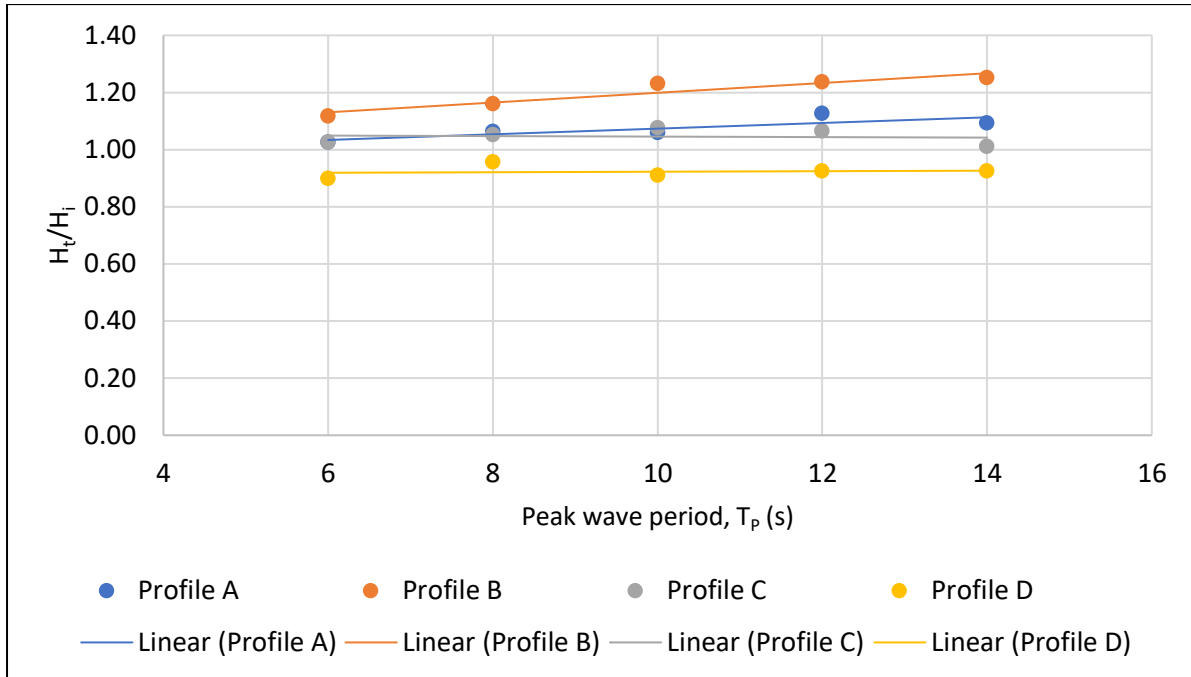
F.2. Overtopping rate as a function of wave period for nearshore profile B



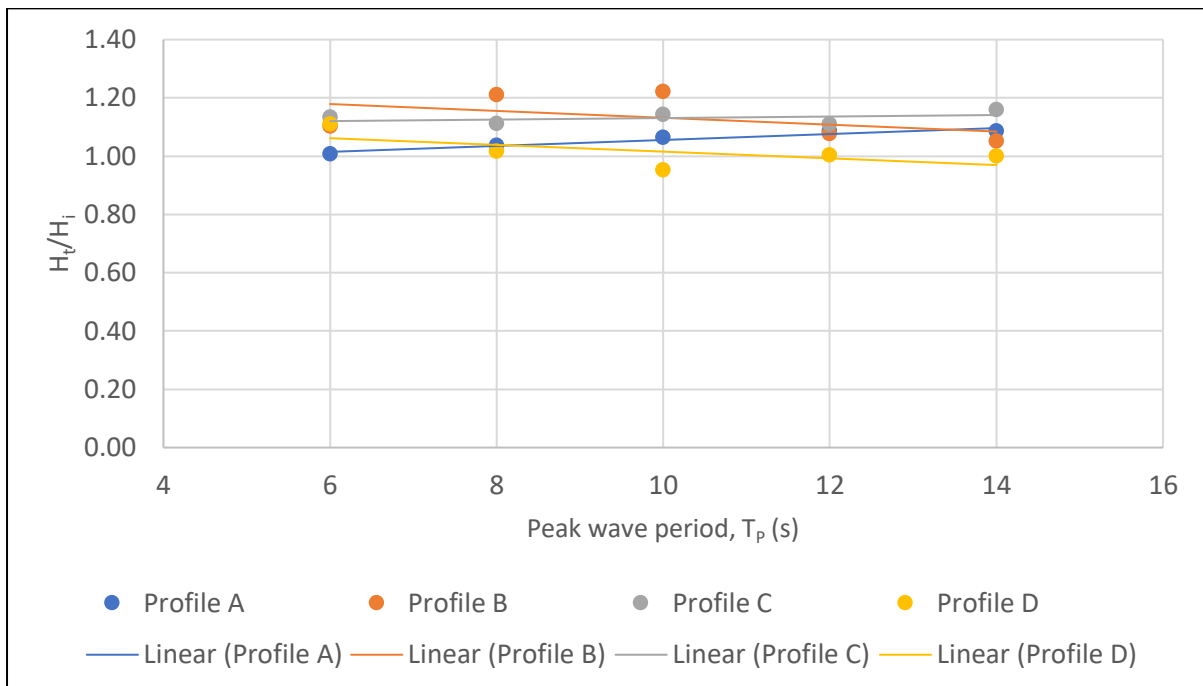
F.3. Overtopping rate as a function of wave period for nearshore profile C**F.4. Overtopping rate as a function of wave period for nearshore profile D**

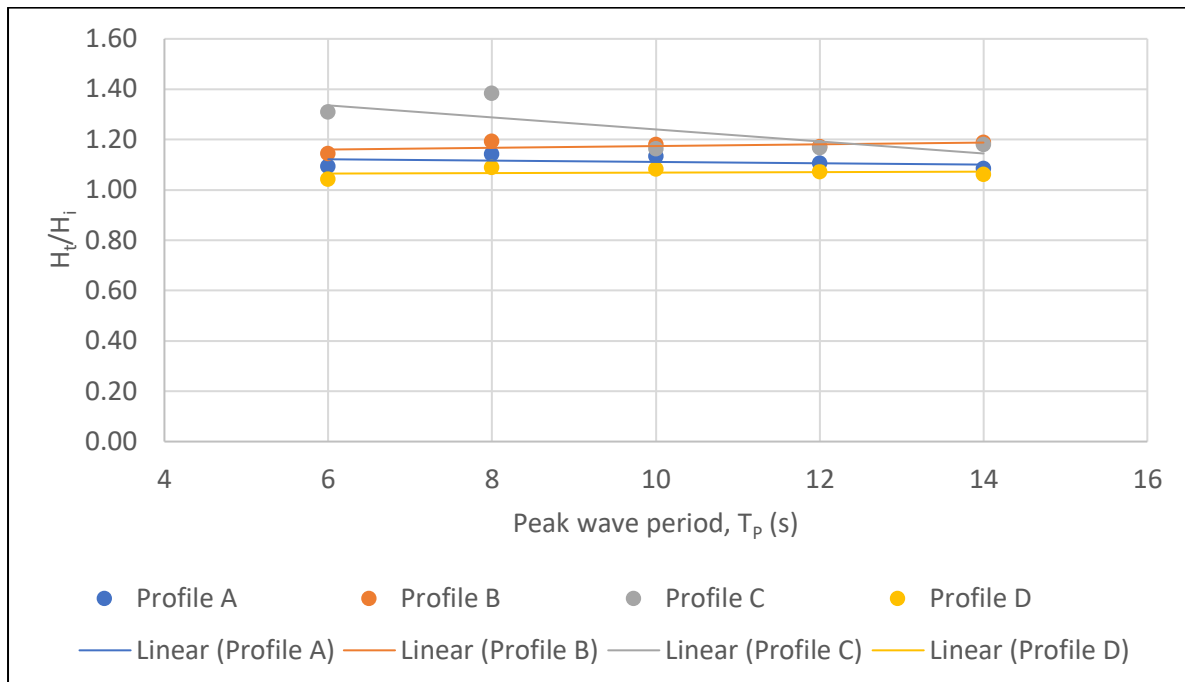
Appendix G: Influence of the nearshore slope on wave height

G.1. Change in wave height for the 1.6 m water level



G.2. Change in wave height for the 2.0 m water level



G.3. Change in wave height for the 2.4 m water level

Appendix H: Probe spacings

H.1. Nearshore profile A deep water probe spacings

H.1.1. 1.6 m toe water level

Case ID	X ₁₂ [mm]	X ₁₃ [mm]	X ₂₃ [mm]	X ₂₄ [mm]	X ₁₄ [mm]	X ₃₄ [mm]
Case-01	201	550	349	799	1000	450
Case-02	282	631	349	799	1081	450
Case-03	361	710	349	799	1160	450
Case-04	438	787	349	799	1237	450
Case-05	515	864	349	799	1314	450

H.1.2. 2.0 m toe water level

Case ID	X ₁₂ [mm]	X ₁₃ [mm]	X ₂₃ [mm]	X ₂₄ [mm]	X ₁₄ [mm]	X ₃₄ [mm]
Case-01	207	570	363	793	1000	430
Case-02	292	655	363	793	1085	430
Case-03	374	737	363	793	1167	430
Case-04	455	818	363	793	1248	430
Case-05	535	898	363	793	1328	430

H.1.3. 2.4 m toe water level

Case ID	X ₁₂ [mm]	X ₁₃ [mm]	X ₂₃ [mm]	X ₂₄ [mm]	X ₁₄ [mm]	X ₃₄ [mm]
Case-01	213	590	377	787	1000	410
Case-02	301	679	377	787	1089	410
Case-03	387	764	377	787	1174	410
Case-04	471	848	377	787	1258	410
Case-05	554	931	377	787	1341	410

H.2. Nearshore profile A shallow water probe spacings

H.2.1. 1.6 m toe water level

Case ID	X ₁₂ [mm]	X ₁₃ [mm]	X ₂₃ [mm]	X ₂₄ [mm]	X ₁₄ [mm]	X ₃₄ [mm]
Case-01	142	380	238	858	1000	620
Case-02	194	431	238	858	1051	620
Case-03	244	482	238	858	1102	620
Case-04	295	533	238	858	1153	620
Case-05	345	583	238	858	1203	620

H.2.2. 2.0 m toe water level

Case ID	X ₁₂ [mm]	X ₁₃ [mm]	X ₂₃ [mm]	X ₂₄ [mm]	X ₁₄ [mm]	X ₃₄ [mm]
Case-01	152	400	248	848	1000	600
Case-02	207	456	248	848	1056	600
Case-03	262	510	248	848	1110	600
Case-04	316	565	248	848	1165	600
Case-05	370	619	248	848	1219	600

H.2.3. 2.4 m toe water level

Case ID	X ₁₂ [mm]	X ₁₃ [mm]	X ₂₃ [mm]	X ₂₄ [mm]	X ₁₄ [mm]	X ₃₄ [mm]
Case-01	160	420	260	840	1000	580
Case-02	220	480	260	840	1060	580
Case-03	278	538	260	840	1118	580
Case-04	336	596	260	840	1176	580
Case-05	394	660	266	840	1234	574

H.3. Nearshore profile B deep water probe spacings

H.3.1. 1.6 m toe water level

Case ID	X ₁₂ [mm]	X ₁₃ [mm]	X ₂₃ [mm]	X ₂₄ [mm]	X ₁₄ [mm]	X ₃₄ [mm]
Case-01	212	550	338	788	1000	450
Case-02	300	638	338	788	1088	450
Case-03	385	723	338	788	1173	450
Case-04	468	807	338	788	1257	450
Case-05	551	920	369	788	1339	419

H.3.2. 2.0 m toe water level

Case ID	X ₁₂ [mm]	X ₁₃ [mm]	X ₂₃ [mm]	X ₂₄ [mm]	X ₁₄ [mm]	X ₃₄ [mm]
Case-01	216	570	354	784	1000	430
Case-02	307	661	354	784	1091	430
Case-03	395	749	354	784	1179	430
Case-04	481	835	354	784	1265	430
Case-05	567	950	383	784	1350	400

H.3.3. 2.4 m toe water level

Case ID	X ₁₂ [mm]	X ₁₃ [mm]	X ₂₃ [mm]	X ₂₄ [mm]	X ₁₄ [mm]	X ₃₄ [mm]
Case-01	220	590	370	780	1000	410
Case-02	314	684	370	780	1094	410
Case-03	405	775	370	780	1185	410
Case-04	494	863	370	780	1273	410
Case-05	600	970	370	780	1380	410

H.4. Nearshore profile B shallow water probe spacings

H.4.1. 1.6 m toe water level

Case ID	X ₁₂ [mm]	X ₁₃ [mm]	X ₂₃ [mm]	X ₂₄ [mm]	X ₁₄ [mm]	X ₃₄ [mm]
Case-01	147	380	233	853	1000	620
Case-02	200	433	233	853	1053	620
Case-03	253	486	233	853	1106	620
Case-04	305	538	233	853	1158	620
Case-05	357	600	243	853	1211	611

H.4.2. 2.0 m toe water level

Case ID	X ₁₂ [mm]	X ₁₃ [mm]	X ₂₃ [mm]	X ₂₄ [mm]	X ₁₄ [mm]	X ₃₄ [mm]
Case-01	156	400	244	844	1000	600
Case-02	213	457	244	844	1057	600
Case-03	270	514	244	844	1114	600
Case-04	326	570	244	844	1170	600
Case-05	382	640	258	844	1226	586

H.4.3. 2.4 m toe water level

Case ID	X ₁₂ [mm]	X ₁₃ [mm]	X ₂₃ [mm]	X ₂₄ [mm]	X ₁₄ [mm]	X ₃₄ [mm]
Case-01	164	430	266	836	1000	570
Case-02	225	491	266	836	1061	570
Case-03	285	551	266	836	1121	570
Case-04	345	611	266	836	1181	570
Case-05	410	676	266	836	1246	570

H.5. Nearshore profile C deep water probe spacings

H.5.1. 1.6 m toe water level

Case ID	X ₁₂ [mm]	X ₁₃ [mm]	X ₂₃ [mm]	X ₂₄ [mm]	X ₁₄ [mm]	X ₃₄ [mm]
Case-01	176	550	374	824	1000	450
Case-02	243	617	374	824	1067	450
Case-03	309	683	374	824	1133	450
Case-04	374	748	374	824	1198	450
Case-05	438	920	482	824	1263	343

H.5.2. 2.0 m toe water level

Case ID	X ₁₂ [mm]	X ₁₃ [mm]	X ₂₃ [mm]	X ₂₄ [mm]	X ₁₄ [mm]	X ₃₄ [mm]
Case-01	183	570	387	817	1000	430
Case-02	255	641	387	817	1071	430
Case-03	324	711	387	817	1141	430
Case-04	393	779	387	817	1209	430
Case-05	461	950	489	817	1277	327

H.5.3. 2.4 m toe water level

Case ID	X ₁₂ [mm]	X ₁₃ [mm]	X ₂₃ [mm]	X ₂₄ [mm]	X ₁₄ [mm]	X ₃₄ [mm]
Case-01	161	450	289	839	1000	550
Case-02	222	510	289	839	1060	550
Case-03	281	569	289	839	1119	550
Case-04	339	628	289	839	1178	550
Case-05	397	686	370	839	1236	410

H.6. Nearshore profile C shallow water probe spacings

H.6.1. 1.6 m toe water level

Case ID	X ₁₂ [mm]	X ₁₃ [mm]	X ₂₃ [mm]	X ₂₄ [mm]	X ₁₄ [mm]	X ₃₄ [mm]
Case-01	132	340	208	868	1000	660
Case-02	179	387	208	868	1047	660
Case-03	225	434	208	868	1094	660
Case-04	271	480	208	868	1140	660
Case-05	317	530	213	868	1186	656

H.6.2. 2.0 m toe water level

Case ID	X ₁₂ [mm]	X ₁₃ [mm]	X ₂₃ [mm]	X ₂₄ [mm]	X ₁₄ [mm]	X ₃₄ [mm]
Case-01	142	370	228	858	1000	630
Case-02	194	421	228	858	1051	630
Case-03	244	472	228	858	1102	630
Case-04	295	523	228	858	1153	630
Case-05	345	580	235	858	1203	623

H.6.3. 2.4 m toe water level

Case ID	X ₁₂ [mm]	X ₁₃ [mm]	X ₂₃ [mm]	X ₂₄ [mm]	X ₁₄ [mm]	X ₃₄ [mm]
Case-01	152	400	248	848	1000	600
Case-02	207	456	248	848	1056	600
Case-03	262	510	248	848	1110	600
Case-04	316	565	248	848	1165	600
Case-05	370	619	248	848	1219	600

H.7. Nearshore profile D deep water probe spacings

H.7.1. 1.6 m toe water level

Case ID	X ₁₂ [mm]	X ₁₃ [mm]	X ₂₃ [mm]	X ₂₄ [mm]	X ₁₄ [mm]	X ₃₄ [mm]
Case-01	140	350	210	860	1000	650
Case-02	191	401	210	860	1051	650
Case-03	241	451	210	860	1101	650
Case-04	291	500	210	860	1150	650
Case-05	340	550	210	860	1200	650

H.7.2. 2.0 m toe water level

Case ID	X ₁₂ [mm]	X ₁₃ [mm]	X ₂₃ [mm]	X ₂₄ [mm]	X ₁₄ [mm]	X ₃₄ [mm]
Case-01	151	370	219	849	1000	630
Case-02	207	426	219	849	1056	630
Case-03	262	480	219	849	1110	630
Case-04	316	535	219	849	1165	630
Case-05	370	950	580	849	1219	269

H.7.3. 2.4 m toe water level

Case ID	X ₁₂ [mm]	X ₁₃ [mm]	X ₂₃ [mm]	X ₂₄ [mm]	X ₁₄ [mm]	X ₃₄ [mm]
Case-01	161	450	289	839	1000	550
Case-02	222	510	289	839	1060	550
Case-03	281	569	289	839	1119	550
Case-04	339	628	289	839	1178	550
Case-05	397	686	289	839	1236	550

H.8. Nearshore profile D shallow water probe spacings

H.8.1. 1.6 m toe water level

Case ID	X ₁₂ [mm]	X ₁₃ [mm]	X ₂₃ [mm]	X ₂₄ [mm]	X ₁₄ [mm]	X ₃₄ [mm]
Case-01	121	320	199	879	1000	680
Case-02	164	363	199	879	1043	680
Case-03	206	405	199	879	1085	680
Case-04	248	447	199	879	1127	680
Case-05	290	489	199	879	1169	680

H.8.2. 2.0 m toe water level

Case ID	X ₁₂ [mm]	X ₁₃ [mm]	X ₂₃ [mm]	X ₂₄ [mm]	X ₁₄ [mm]	X ₃₄ [mm]
Case-01	133	350	217	867	1000	650
Case-02	180	398	217	867	1048	650
Case-03	227	445	217	867	1095	650
Case-04	274	491	217	867	1141	650
Case-05	321	538	217	867	1188	650

H.8.3. 2.4 m toe water level

Case ID	X ₁₂ [mm]	X ₁₃ [mm]	X ₂₃ [mm]	X ₂₄ [mm]	X ₁₄ [mm]	X ₃₄ [mm]
Case-01	143	380	237	857	1000	620
Case-02	195	432	237	857	1052	620
Case-03	247	483	237	857	1103	620
Case-04	298	534	237	857	1154	620
Case-05	348	585	237	857	1205	620